Check for updates

View Article Online
View Journal

Materials Advances

Accepted Manuscript

This article can be cited before page numbers have been issued, to do this please use: K. L. Ngai, *Mater. Adv.*, 2026, DOI: 10.1039/D6MA00279J.

This is an Accepted Manuscript, which has been through the Royal Society of Chemistry peer review process and has been accepted for publication.

Accepted Manuscripts are published online shortly after acceptance, before technical editing, formatting and proof reading. Using this free service, authors can make their results available to the community, in citable form, before we publish the edited article. We will replace this Accepted Manuscript with the edited and formatted Advance Article as soon as it is available.

You can find more information about Accepted Manuscripts in the Information for Authors.

Please note that technical editing may introduce minor changes to the text and/or graphics, which may alter content. The journal's standard Terms & Conditions and the Ethical guidelines still apply. In no event shall the Royal Society of Chemistry be held responsible for any errors or omissions in this Accepted Manuscript or any consequences arising from the use of any information it contains.

ROYAL SOCIETY OF CHEMISTRY

rsc.li/materials-advances

View Article Online
DOI: 10.1039/D6MA00279J

Materials Advances

REVIEW

Relaxation and Diffusion Dynamic and Thermodynamic Properties in Amorphous Materials are Universal

K. L. Ngai*

Istituto per i Processi Chimico-Fisici del CNR, Largo Bruno Pontecorvo 3, I-56127 Pisa, Italy

Open Access Article. Published on 04 June 2026. Downloaded on 6/5/2026 12:04:33 AM.
This article is licensed under a Creative Commons Attribution 3.0 Unported Licence.

Materials Advances Accepted Manuscript

Abstract

The physical structures and chemical compositions of amorphous materials in the liquid and the glassy states are extremely diverse even restricted to a specific class. Therefore, it would be incredible if someone ever suggests the relaxation and diffusion properties of amorphous materials are universal. Nevertheless, the eminent condensed matter physicist P. W. Anderson did just that. As cited by the editors in their call for papers of this themed collection on Amorphous Materials, Anderson once observed that "*Randomness and disorder could result in generic properties that are utterly different from those of merely somewhat impure regular materials*". His observation was not baseless because previously the existence of universality was anticipated in a theory of relaxation and diffusion based on classical chaos published by the present author in 1979. Since then, experimental data and simulation results collected in widely different amorphous materials over the past 47 years have provided indisputable evidences of the universal properties as predicted by the theory, currently known as the Coupling Model (CM). Part of the findings prior to 2022 have been reviewed in *Prog. Mater. Sci.* 2023, **139**, 101130. The current review is focused on the new data emerging after 2022 as well as relevant older data not considered before. Altogether, the evidences extracted from the data reaffirm the universality of relaxation and diffusion properties in diverse amorphous materials and in accord with the predictions of the CM.

1. Introduction

In physics, when someone claims a property is universal in widely different classes of materials, likely it is met with skepticism. I am making this claim for relaxation and diffusion in amorphous materials in this review as the title shows. The same claim was made 47 years ago in 1979 when I published the theoretical paper [1] entitled "Universality of low-frequency fluctuation, dissipation and relaxation properties of condensed matter. I" in *Comments Solid State Phys.* 1979, **9**, 127. The claim of universality caught the attention of P.W. Anderson and aroused his interest in relaxation and diffusion of complex systems. He invited me to Princeton University for a private

View Article Online
DOI: 10.1039/D6MA00279J

Open Access Article. Published on 04 June 2026. Downloaded on 6/5/2026 12:04:33 AM.
This article is licensed under a Creative Commons Attribution 3.0 Unported Licence.

discussion in 1982. In 1984, he published with others the paper [2] entitled "Models of Hierarchically Constrained Dynamics for Glassy Relaxation, *Phys. Rev. Lett*. 1984, **53**, 958. My 1979 paper was cited by them and they alluded my claim by the statement: "… and most recently Ngai,[4] have collected many examples, the latter proposing that it occurs in a very wide range of phenomena and materials." The title of their paper implies that relaxation of glassy materials is universal even though that word was not used. The editors of this themed collection on Amorphous Materials cited from Anderson the statement: "*Randomness and disorder could result in generic properties that are utterly different from those of merely somewhat impure regular materials*". The use of the words "generic properties" means that Anderson also expected universal properties in amorphous materials. However, the nature and the specifics of the generic/universal properties he intimated remains for others to discover. Moreover, the pertinent question following his suggestion is whether randomness and disorder alone can cause the generic/universal properties to be discovered years after he made the suggestion?

Their paper by Anderson and coworkers generate a lot of interest in the physics community on relaxation in complex systems. The enthusiasm of the physics community on the subject led to the workshops organized by Anderson held at the Institute of Physics at Univ. of California, Santa Barbara in 1984, and the Aspens Institute of Physics in the few years later, and I was invited by him to present my progress in plenary talks. In 1986, the discovery of high-temperature superconductor was made by Bednorz and Müller. The excitement generated by the discovery in this mainstream research area led many condensed matter physicists including Anderson to focus their research efforts exclusively on high temperature superconductors. Although in 1995 Anderson still considered the research on generic properties of amorphous materials important by making the statement [3] often quoted by others: "The deepest and most interesting unsolved problem in solid state theory is probably the theory of the nature of glass and the glass transition." After 1986, I was left alone to continue the pursuit in the discovery of universal relaxation and diffusion properties in amorphous materials with guidance by the generally applicable predictions of the theory [1] and later developments [4,5,6,7,8,9.10], commonly known in the literature as the Coupling Model (CM). The universal properties unveiled from experiments and simulations in the intermediate period up to 2010 was published in the monograph [10] entitled "*Relaxation and Diffusion in Complex Systems*, Springer, NY (2011). A lot more and different universal properties revealed in the period from 2010 to 2022 were published in the very extensive review with universality reemphasized by its title "Universal Properties of Relaxation and Diffusion in Complex Materials: *Originating from Fundamental Physics and Rich Applications*". [11] It has 293 figures of experimental data of widely different amorphous materials demonstrating the various universal properties. Most of 293 figures are composed of two or more subfigures. The voluminous amount of data from experiments and simulations rigorously established the various universal properties, and consistency with the predictions of the CM.

Due to rapid growth in the research and applications of amorphous materials in the last four years, many new phenomena and properties of relaxation and diffusion have been uncovered in amorphous materials. There are also older data not studied before but becomes relevant. The present review pays especial attention to the new data since 2022, and also those older data, with the purpose to demonstrate again conformation to the universal properties found in many amorphous materials. As requested by the editor in the sections to follow, clarifications are made in the following Sections of the novelty and scope of the present Review relative to previous

Materials Advances Accepted Manuscript

View Article Online
DOI: 10.1039/D6MA00279J

Open Access Article. Published on 04 June 2026. Downloaded on 6/5/2026 12:04:33 AM.
This article is licensed under a Creative Commons Attribution 3.0 Unported Licence.

Materials Advances Accepted Manuscript

publications. Featured are new data published after 2022, and older data not considered before and analyzed for the first time to verify the universal properties and relation to the predictions of the CM.

The focus of the current review is on three ubiquitous and interdependent processes constituting the dynamic and thermodynamic properties of amorphous materials, and transpiring in the relaxation spectrum over broad time/frequency range. Ordered in time, the three are the caged dynamics, the incipient (secondary) relaxation, and the terminal (primary) relaxation. For glass-forming materials, the latter two processes are the primitive relaxation of the CM [10,11,12,13] combined with the Johari-Goldstein β-relaxation [14,15,16,17], and the structural α-relaxation. An interesting attribute to reveal herein is that the universal properties of any one of the three processes are correlated with the universal properties of the other two. Also shown are the universal properties of the three processes found in structural relaxation of molecular and polymeric glass-formers having exact analogues in plastic crystals with the centers of mass of molecules forming a regular crystalline lattice but the orientations of the molecules are disordered, and in the ionic conductivity relaxation of ionic liquids, glasses, and crystals. The parameter characterizing the extent or size of a universal property of any one of the three processes depends on the chemical and physical structure of the material. This structure-property relationship is intriguing and challenging to understand. The parameter has been identified with the anharmonicity of the interaction potential [5,6,7,8,9,10,11,12,18,19,20]. It correlates with the coupling parameter *n* of the CM of the amorphous materials, which is also the fractional exponent of the Kohlrausch-Williams-Watts (KWW) correlation function, [21,22,23,24,25,26]

$$\varphi(t) = \exp\left[-(t/\tau_\alpha)^{1-n}\right] \quad (1)$$

of the terminal structural or ionic conductivity relaxation. Shown also herein, is the coupling parameter *n* having correlation with some macroscopic property of amorphous materials such as the Poisson's ratio, which is important in applications. The universal properties are fundamental and impactful on the theory of glass transition and deserve emphasis in the current review. An example is the invariance of the shape of the structural α-relaxation or the ionic conductivity relaxation to change of thermodynamic conditions by varying pressure and temperature over large ranges while the relaxation time is kept constant. The astonishing phenomena unexpected and unexplainable by conventional theories of glass transition, like the configurational entropy model of Adam-Gibbs, naturally demands an explanation by any other viable theories of the present times. Surprisingly, as of now no theory except the CM has given an explanation to this and the other universal properties. In the following sections, the outstanding issues raised in the above are discussed in conjunction with some recent and past experimental data as examples, and explanations are given from the predictions of CM. For each universal property, experimental data from radically different kinds of amorphous materials are chosen to show its presence, and bring home the point that it is truly remarkable. As recommended by a reviewer, alternative theoretical frameworks and perspectives are acknowledged, as well as points of contention and controversies with and misunderstanding by others throughout the years in demonstrating the existence of the universal properties claimed by the CM.

2. *T-P* Invariance of α-relaxation dispersion at constant $\tau_\alpha(P,T)$

View Article Online
DOI: 10.1039/D6MA00279J

Open Access Article. Published on 04 June 2026. Downloaded on 6/5/2026 12:04:33 AM.
This article is licensed under a Creative Commons Attribution 3.0 Unported Licence.

2.1. Experimental evidences

Pressure and temperature can be varied in the study of the dynamics of the structural α-relaxation or the ion conductivity α-relaxation of materials by dielectric relaxation. The relaxation time τ_α at ambient pressure can be maintained the same at elevated pressures P by raising the temperature T. Remarkably, found in different classes of materials, the frequency dispersion of the structural α-relaxation or the ionic conductivity α-relaxation is invariant to changes of P and T at constant τ_α.[11] Fig.1 shows examples from three molecular glass-formers, (KDE), propylene carbonate (PC) [11,27], and the pharmaceutical ROY [11,28], and the plastic crystal pentachloronitrobenzene [11,29]. Fig. 2 shows examples from polymers, poly(vinyl acetate) PVAc, poly (methyltolyl siloxane) (PMTS), poly(phenyl glycidyl ether)-*co*-formaldehyde (PPGE), and poly(oxybutylene) (POB).[11,27] In all cases the loss peak proper is well fitted by the Fourier transform of the Kohlrausch function [21,22] in Eq.1, first done by Williams and Watts (WW) [23]. With the KWW fit identified with the contribution from the α-relaxation, the universal property is restated as invariance of β_K to changes of P and T at constant τ_α of the α-relaxation or isochronal superpositioning of the α-relaxation function.

The data shown in Figs.1 and 2 were published before 2022. Since then, there are other data showing the isochronal superpositioning of the α-relaxation. An example is the one published in 2026 from dielectric data in amorphous binary mixtures composed of nifedipine (NIF) and acetylated maltose (acMAL) under ambient and high-pressure conditions.[30] The frequency dispersion of the α-process is invariant to variations of T and P at constant $\tau_\alpha(P,T)$ as shown in Fig.3a for the NIF-acMAL 1:3 m/m binary mixture. Moreover, manifesting as an excess wing on the high-frequency flank of the α-relaxation peak in the loss spectra of neat NIF, the secondary β-relaxation emerges with the addition of acMAL. High-pressure dielectric measurements and physical aging confirmed the CM prediction of the β-relaxation time $\tau_\beta(P,T)$ is approximately the same as the primitive relaxation time $\tau_0(P,T)$ of the CM as shown in Fig.3b and to be discussed together with other examples in Section 3.2. The result unequivocally identified the intermolecular Johari-Goldstein (JG) origin of this secondary relaxation in NIF. Moreover, there is isochronal superpositioning of α- and β-relaxation times as shown in Fig.3a and 3b, and found in many other glass-formers to be demonstrated Section 3.1.

Materials Advances Accepted Manuscript

View Article Online
DOI: 10.1039/D6MA00279J

Open Access Article. Published on 04 June 2026. Downloaded on 6/5/2026 12:04:33 AM.
This article is licensed under a Creative Commons Attribution 3.0 Unported Licence.

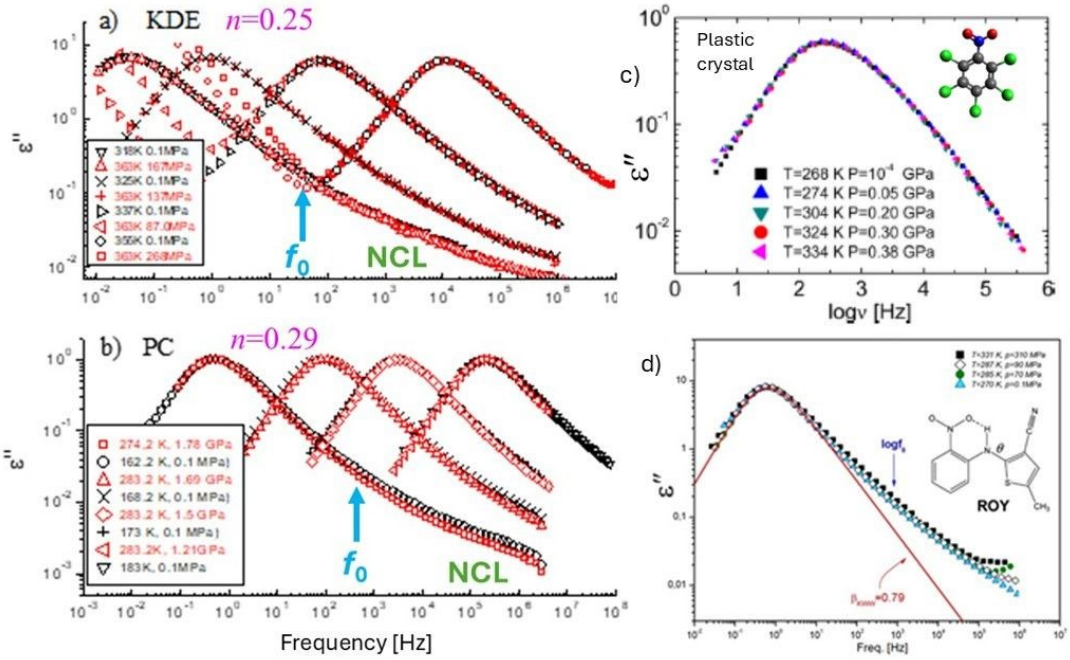

Fig.1. Dielectric loss data at various combinations of T and P to demonstrate the invariance of the dispersion of the α-relaxation at constant α-loss peak frequency. (a) cresolphthalein-dimethyl-ether (KDE). (b) Propylene carbonate (PC). (c) The plastic crystal, pentachloronitrobenzene. (d) the pharmaceutical, ROY. Figures reproduced from Ref.[11] with permission from Elsevier.

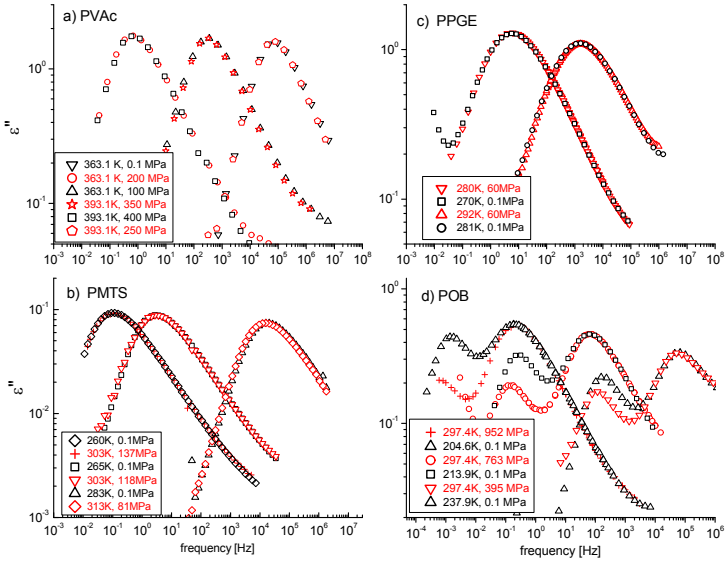

1.

Fig. 2. $\varepsilon''(f)$at various combinations of T and P to demonstrate the invariance of the dispersion of the α-relaxation at constant α-loss peak frequency. a) poly(vinylacetate) (PVAc); b) poly(methyltolylsiloxane) (PMTS). c) poly(phenyl glycidyl ether)-*co*-formaldehyde (PPGE); d) poly(oxybutylene) (POB). Figures reproduced from Ref.[11] with permission from Elsevier.

Materials Advances Accepted Manuscript

View Article Online
DOI: 10.1039/D6MA00279J

Open Access Article. Published on 04 June 2026. Downloaded on 6/5/2026 12:04:33 AM.
This article is licensed under a Creative Commons Attribution 3.0 Unported Licence.

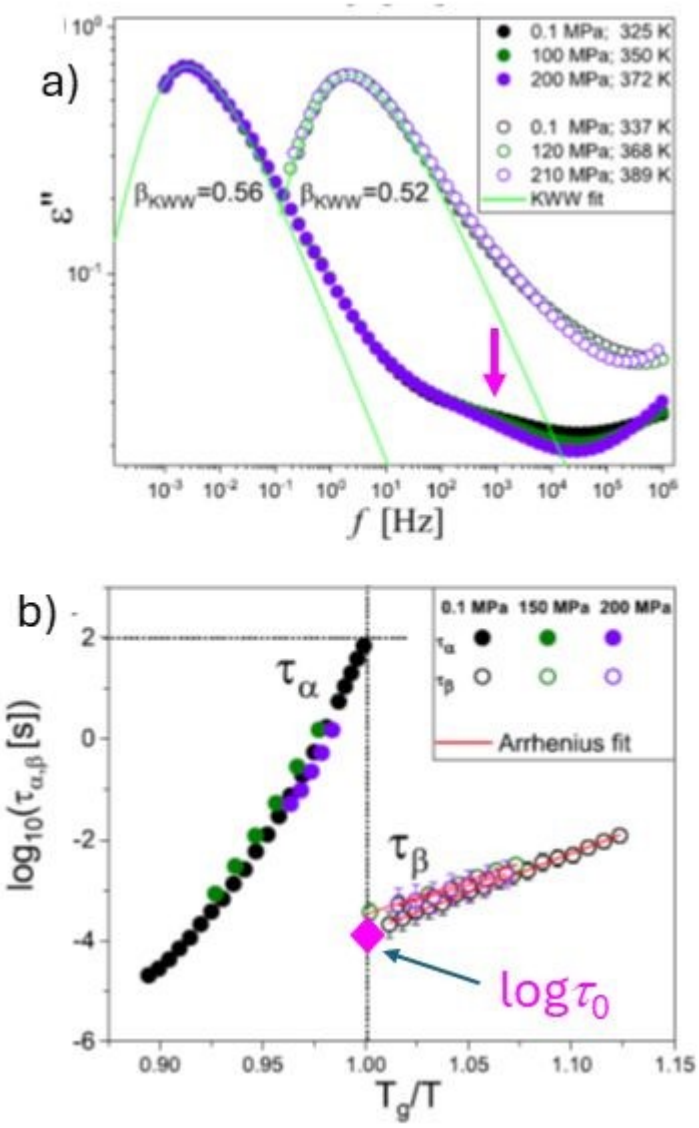

Fig. 3. (a) Comparison of dielectric loss spectra of the NIF-acMAL 1:3 m/m binary mixture at different T and P combinations close to and above T_g. Solid green lines represent Fourier transforms of the KWW functions (Eq.1) with values of β_{KWW}=(1-n) indicated. (b) Dependences of $\log_{10}\tau_\alpha$ and $\log_{10}\tau_\beta$ vs. T_g/T at indicated pressures of the system. Solid red lines denote Arrhenius fits. The magenta diamond locates the value of logarithm of the primitive relaxation time τ_0 of the CM. Data adopted from Ref.30 and reused with permission from Elsevier.

2.2 CM explanation

Materials Advances Accepted Manuscript

View Article Online
DOI: 10.1039/D6MA00279J

Open Access Article. Published on 04 June 2026. Downloaded on 6/5/2026 12:04:33 AM.
This article is licensed under a Creative Commons Attribution 3.0 Unported Licence.

The invariance of $\beta_K(T,P) \equiv [1\text{-}n(T,P)]$ to changes of P and T has been explained by the Coupling Model (CM) [11] by its other signature equation written to include pressure and temperature dependences as,

$$\tau_\alpha(T,P) = [(t_c)^{-n(T,P)}\tau_0(T,P)]^{1/[1-n(T,P)]}. \quad (2)$$

For a given material, t_c depends solely on the interaction potential and is a constant. The value of the expression on the right-hand-side of Eq.(2) depends on two independent variables, $\tau_0(T,P)$ and $n(T,P)$, with entirely different physical origins. The former is a relaxation time, and the latter determines the degree of deviation of the correlation function from exponential time dependence. If $\tau_0(T,P)$ and $n(T,P)$ are not invariant, then their variations have to be synchronized to maintain constant value of $\tau_\alpha(T,P)$ on the left-hand-side of Eq.(2) on varying T and P over wide ranges. However, synchronization of the variations of $\tau_0(T,P)$ and $n(T,P)$ is impossible because they are independent physical quantities. Thus, from its Eq.(2), the CM anticipates that the Kohlrausch exponent $\beta_K(T,P)$ as well as $\tau_0(T,P)$ to be invariant to changes of T and P while $\tau_\alpha(T,P)$ is kept constant. Conventional theories based on configurational entropy S_c and free volume V_f are at odds with the property because these theories normally have no prediction of the frequency dispersion of the α-relaxation, and predict that it will not change by the large variations of T and P that keep $\tau_\alpha(T,P)$ constant.

The CM Eq.(2) was instrumental in explaining the universal property of the isochronal superposition of the α-relaxation function or invariance of $\beta_K(T,P) \equiv [1\text{-}n(T,P)]$, and several other properties to follow. It was the consequence of the crossover of the correlation function from exp-(t/τ_0) to exp $[-(t/\tau)^{1-n}]$ at t_c, which was derived in models based on classical chaos arising from anharmonic interactions.[1,4-12] The crossover had been observed by neutron scattering and simulations in polymers, molecular glass-formers, metallic alloys, and ionic conductors [11], and most recently in a molten salt $Ca_{0.4}K_{0.6}(NO_3)_{1.4}$ in Refs.[31] and compared with the CM prediction in Ref.[32] published in 2025 The Q-dependent intermediate scattering functions $I(Q, t)$ are shown in Fig. 4a with $t_c \approx 0.5$ ps same as that in Fig. 4b found by simulations much earlier.[33] Since the chalcogenide glasses [34,35] are of current interests, particularly those are phase change materials (PCM), new analysis of the intermediate coherent scattering function $F(Q,t)$ of selenium on the time-of-flight spectrometer Mibemol at Q=1.8 Å^{-1} by Rufflé and Longeville [36] at 573 K is shown and analyzed in Fig. 5a. These are older data re-analyzed here for the first time to show the crossover was observed in a different amorphous material. In order to bring out the time dependences of the two steps, the data were replotted as log(-ln $F(Q,t)$) vs. log$t$. The slope of the short time regimes related to vibrations has slope $\beta \approx 2$. After that, log(-ln$F(Q,t)$) have slope $\beta \approx 1$ and then $\beta \approx 0.47$ after at about 1 ps. The results are equivalent to $F(Q,t)$ has the exp $(-t/\tau_0)$ dependence before $t_c \approx 1$ ps, and the exp $[-(t/\tau_\alpha)^{1-n}]$ dependence with (1-n) ≈ 0.47, in support of the validity of the CM for selenium and its application such as Eq.(2). The same analysis is performed on the more recent molecular dynamic simulation data of the phase change material GeTe at 500 K from Sosso et al. [37] as shown in Fig. 5b with the same results. This is older data re-analyzed here for the first time to show the crossover was observed in another amorphous material.

Materials Advances Accepted Manuscript

View Article Online
DOI: 10.1039/D6MA00279J

Open Access Article. Published on 04 June 2026. Downloaded on 6/5/2026 12:04:33 AM.
This article is licensed under a Creative Commons Attribution 3.0 Unported Licence.

The CM explanation by Eq.(2) of the isochronal superposition of the α-relaxation function or invariance of $\beta_K(T,P) \equiv [1\text{-}n(T,P)]$ requires the primitive relaxation time $\tau_0(T,P)$ to be invariant also. Therefore, a critical test of the CM explanation of isochronal superposition in any material is to find support from experiment of the invariance of $\tau_0(T,P)$. Support comes from the fact established in Ref.[12] and Ref.[13] that the primitive relaxation is the precursor of the Johar-Goldstein (JG) β-relaxation, and their relaxation time are approximately the same, *i.e.*, $\tau_0(T,P) \approx \tau_\beta(T,P)$. By virtue of this relation, the CM explanation of the invariance of $\beta_K(T,P)$ is accompanied by invariance of $\tau_\beta(T,P)$. In glass-formers where the JGβ relaxation is resolved and $\tau_\beta(T,P)$ determined, the simultaneous invariance of $\beta_K(T,P)$ and $\tau_\beta(T,P)$ can be verified. This is the case of the NIF-acMAL 1:3 m/m binary mixture in Fig.3, and in Fig.8 to be introduced later in Section 3. If the JGβ relaxation is not resolved in glass-formers as those in Fig.1, it is responsible for the excess wing on the high frequency flank of the α-loss peak. The isochronal superpositioning of the excess wing in KDE, PC, and ROY verifies the invariance of $\tau_\beta(T,P)$.

Some glass-formers with hydrogen bonding such as glycerol[11,38] and sorbitol[39] do not obey isochronal superposition of the α-relaxation function with smaller $\beta_K(T,P)$ values at higher temperature and elevated pressure. This is illustrated for sorbitol[38] in the inset in Figure 6, where the KWW fit at P = 1.8 GPa requires $(1\text{-}\beta_{KWW}) = n(T,P) = 0.60$, which is larger than 0.52 at ambient pressure (P=0.1 MPa). Correspondingly, the ratio $\tau_\beta(T,P)/\tau_\alpha(T,P)$ or $\tau_0(T,P)/\tau_\alpha(T,P)$ increases for any chosen value of $\tau_\alpha(T,P)$ as shown in the main part of Fig.6. The concurrent failures of both isochronal superposition and invariance of $\tau_0(T,P) \approx \tau_\beta(T,P)$ in glycerol and sorbitol are consistent with the CM Eq.(2). This is because if $\beta_{KWW}(T,P)$ is not invariant at constant $\tau_\alpha(T,P)$ in Eq.(2), then it requires that $\tau_0(T,P) \approx \tau_\beta(T,P)$ is also not invariant.

Several hydrogen-bonded materials, including ibuprofen, RS-ketoprofen [39], D-glucose [40], and the strongly hydrogen-bonded ternidazole (TDZ) drug (3-(2-methyl-5-nitroimidazol-1-yl)-propan-1-ol) [41], have the frequency dispersion of the α-relaxation invariant to changes of P and T at constant τ_α. These are hydrogen bonded materials, and yet they show isochronal superposition of the α-loss peak to changes of T and P as shown before in figures in the 2023 review [11]. The JGβ relaxation is not resolved in the cases of ibuprofen and RS-ketoprofen [39] and appears the excess wing is unchanged in relation to the α-loss peak to support invariance of $\tau_0(T,P) \approx \tau_\beta(T,P)$. The isochronal superposition of the α-relaxation spectra is shown in Fig.7(a). and invariance of $\tau_0(T,P) \approx \tau_\beta(T,P)$ of TDZ is shown in Fig.7(b) where the JGβ relaxation is resolved [41]. One value of $\tau_0(T,P)$ is calculated by Eq.(2) to show it is in good agreement with $\tau_\beta(T,P)$.

The isochronal superposition of the α-relaxation function or spectrum to variations of T and P at constant $\tau_\alpha(T,P)$ is also predicted for the "strongly correlating liquids" defined by strong correlations between thermal fluctuations of the potential energy, U, and the virial W (i.e., U and W are proportional with an invariant proportionality constant).[43,44] The correlations are perfect

Materials Advances Accepted Manuscript

View Article Online
DOI: 10.1039/D6MA00279J

Open Access Article. Published on 04 June 2026. Downloaded on 6/5/2026 12:04:33 AM.
This article is licensed under a Creative Commons Attribution 3.0 Unported Licence.

for particles interacting with an inverse power law potential, and hold in systems with intermolecular potentials dominated by van der Waals interactions.[45,46] However, this identification of strongly correlating liquids in the isomorph theory is not generally applicable to real materials.[47] Hydrogen-bonded materials and liquids having dipolar interactions [47] show deviations in the correlation of W and U. However, the hydrogen bonded ibuprofen, RS-ketoprofen, D-glucose, and TDZ show isochronal superposition property. So is the highly polar cresolphthalein-dimethyl-ether (KDE) in Fig.1a. The correlation of W and U is not valid for metallic alloys either, but isochronal superposition holds.[48,49] Found also in the simulations of these metallic alloys is the crossover of the correlation function from exponential to stretched exponential time dependence at $t_c \approx 0.2$ ps. This validates the CM Eq.(2), and thus the CM explanation of the isochronal superposition based on Eq.(2) continues to hold for the metallic alloys.

Except for the CM and the isomorph theory, no other theory past or current have paid attention to this isochronal superposition property. The negligence to consider this generic property is puzzling because isochronal superpositioning involves extensive variations of T and P, which corresponds to wide-ranging changes of thermodynamic condition, and yet the α-relaxation function remains the same. Hence, any theory based on thermodynamic parameters, including specific volume and entropy, is required to check for consistency with this remarkable property. Otherwise, validity of the theory is in doubt.

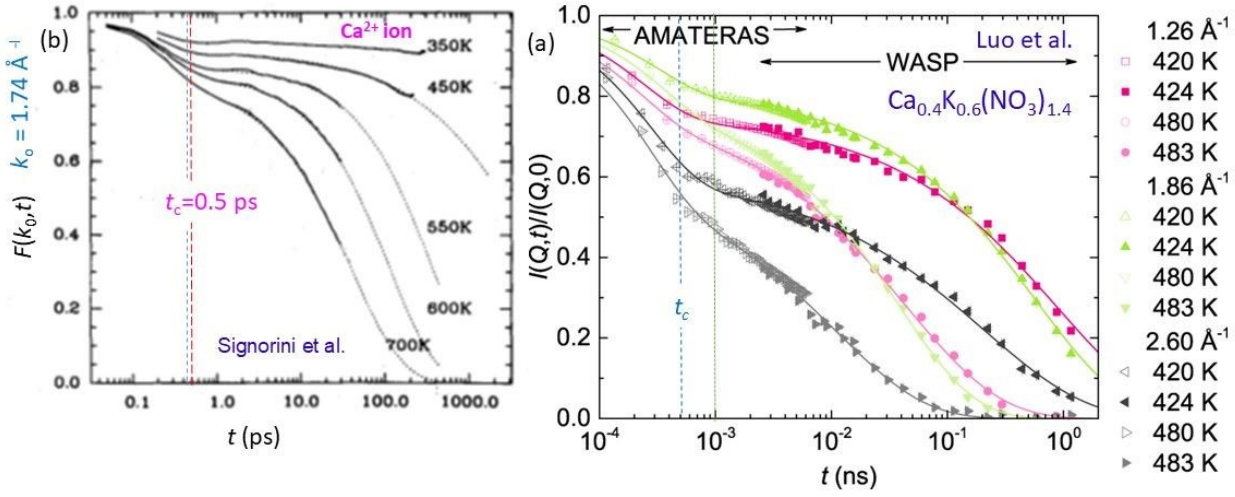

Fig. 4. (a) . Crossover of the correlation function from exponential to stretched exponential time dependence at $t_c \approx 0.5$ - 1.0 ps (blue and green dotted lines) verified by the normalized intermediate scattering function $I(Q,t)$ of CKN using wide-angle neutron spin-echo spectroscopy technique by Luo *et al*. [31]. Reprinted with permission from Luo *et al.*, Nat. Commun. **13**, 2092 (2022). Copyright 2022 Authors, licensed under a Creative Commons Attribution (CC BY) license. (b) The temperature dependence of $F(k_o,t)$ for Ca^{2+} ions for k_o = 1.74 Å^{-1} from Signorini et al.[33] Reused with permission from AIP.

Materials Advances Accepted Manuscript

View Article Online
DOI: 10.1039/D6MA00279J

Open Access Article. Published on 04 June 2026. Downloaded on 6/5/2026 12:04:33 AM.
This article is licensed under a Creative Commons Attribution 3.0 Unported Licence.

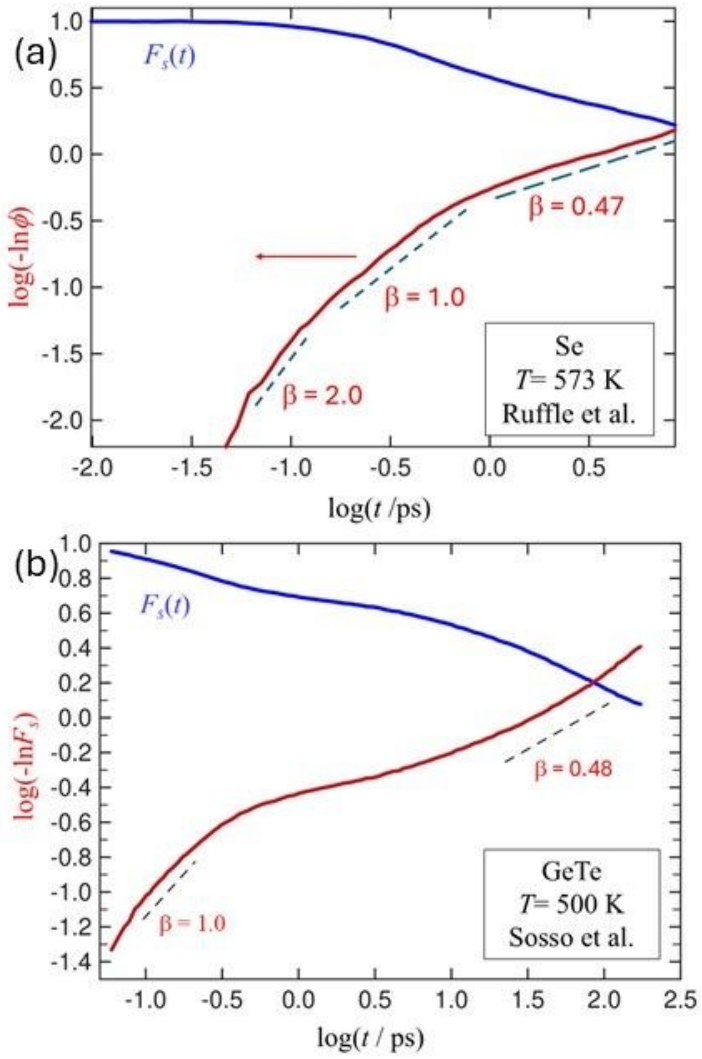

Fig. 5. Temperature dependence of the normalized intermediate scattering function $F_s(t)$ and replotted as log(-ln $F_s(t)$) vs log$t$. (a) Selenium at Q=1.8 Å^{-1} measured on Mibemol from Ref.[36] (b) GeTe at 500 K calculated at q = 2.1 Å^{-1}, from Ref.[37].

Materials Advances Accepted Manuscript

View Article Online
DOI: 10.1039/D6MA00279J

Open Access Article. Published on 04 June 2026. Downloaded on 6/5/2026 12:04:33 AM.
This article is licensed under a Creative Commons Attribution 3.0 Unported Licence.

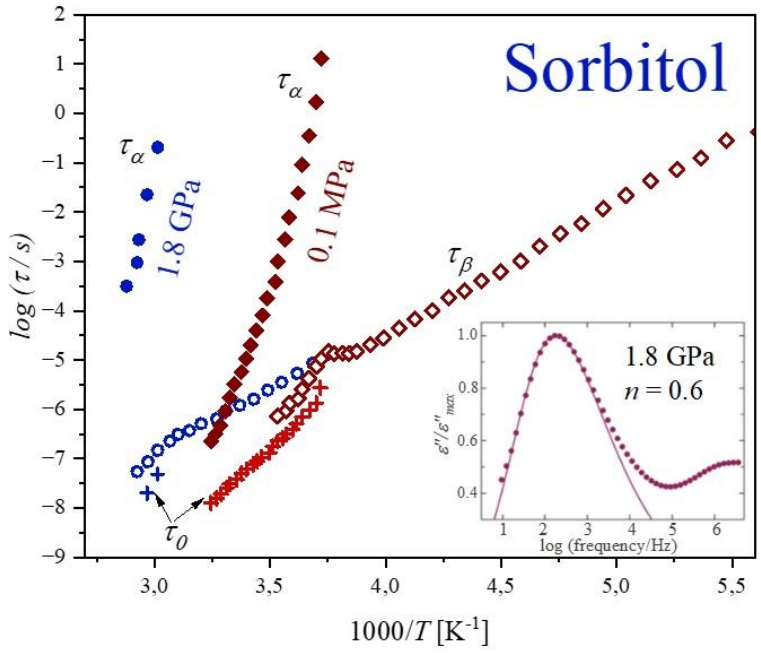

Fig. 6. Isobaric α-relaxation times $\tau_\alpha(T,P)$ at 0.1 MPa, 587.5 MPa, and 1.8 GPa pressure, along with the corresponding JG β-relaxation times $\tau_\beta(T,P)$ at the same pressures for sorbitol. The plus signs (blue) and (red) are the calculated values of $\tau_0(T,P)$ at 1.8 GPa and 0.1 MPa respectively. Inset: Normalized dielectric loss spectrum of sorbitol at P=1.8 GPa and T=343 K. The line is the fit by the Fourier transform of Eq.(2) with n=0.60. At P=0.1 MPa the width of the α-loss peak is narrower and the KWW fit has smaller n=0.52. Data taken from Ref.[39] and plotted as a new figure.

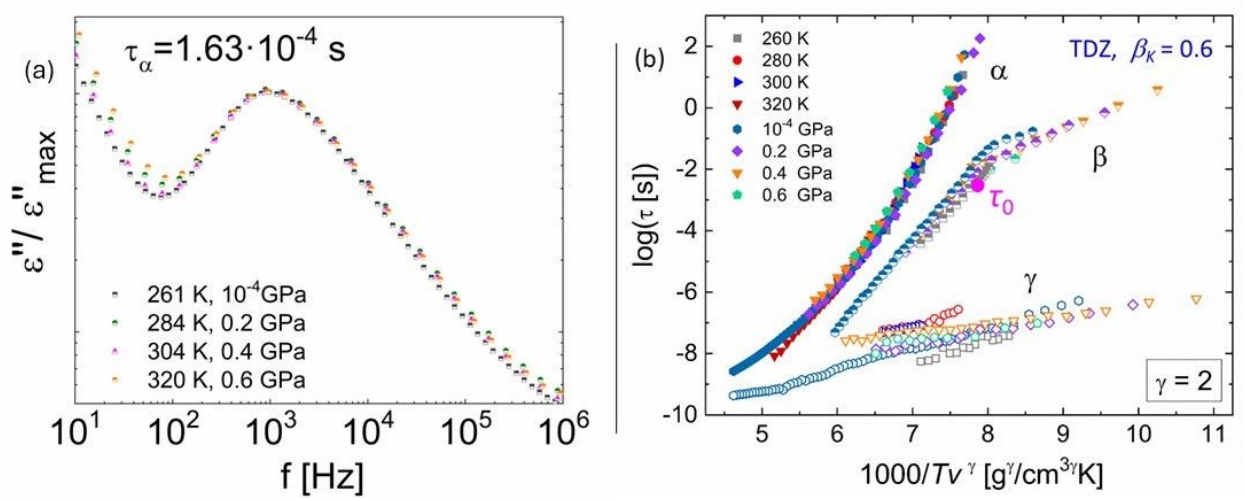

Fig. 7. Series of dielectric loss spectra of ternidazole (TDZ) for two sets of different pressure and temperature conditions, corresponding to the same α-relaxation time $\tau\alpha = 1.63 \times 10^{-4}$ s. Data from Ref.[42] redrawn as a new figure courtesy of Michela Romanini. (b) Thermodynamic scaling plot

Materials Advances Accepted Manuscript

View Article Online
DOI: 10.1039/D6MA00279J

of the relaxation times of all three dynamic processes in TDZ, as function of the quantity $1000/TV^{\gamma}$ with $\gamma = 2$ (V is the specific volume calculated for each (P,T) pair by means of the experimental equation of state. Representative error bars are indicated. Data are from Ref.[42] and replotted as a new figure.

3. *T-P* Invariance of $\tau_\beta(P,T)$ at constant $\tau_\alpha(P,T)$, and $\tau_\beta(P,T) \approx \tau_0(P,T)$

3.1. Experimental and simulation data

Out of the varieties of secondary relaxations considered by Johari and Goldstein in the 1970s [14,15,16], a special class of them was identified in 1989 [12,13] to be related to the primitive relaxation of the CM. Like the primitive relaxation, secondary relaxation belonging to this special class should be present in all glass-formers, and should have strong connection to the structural α-relaxation in properties. Some of the secondary relaxations considered by Johari and Goldstein themselves [14,15,16] are intramolecular in origin with no connection to the α-relaxation, and do not belong to the special class. Traditionally, in the literature all secondary relaxations are called Johari-Goldstein (JG) relaxation. In order to distinguish the secondary relaxations in the special class found [12,13], a different name or nomenclature should be chosen such as JG*x*. Notwithstanding, this choice was not done for the sake of honoring the contributions from these two colleagues. Thus, whenever I use the term, Johari-Goldstein β-relaxation of JGβ relaxation herein and elsewhere, it stands for secondary relaxation in the special class. [10,11,12,13]

The $\varepsilon''(f)$ data in some of the materials in Figs.1 and 2 at higher frequencies are in excess of the KWW fit. The excess wing is due to the contributions from the universal Johari-Goldstein (JG) β-relaxation [11-17], which is unresolved. The superposition of the entire spectra at different combinations of P and T implies the unresolved faster process bears some invariance relation to the α-relaxation to be revealed when the JGβ relaxation is resolved in other materials. Shown in Figs.6a and 6b are two examples from dielectric spectra of quinaldine in tristyrene [50] and cyano-benzene in tristyrene [51]. The data exhibit not only the P-T invariance of $\beta_K(T,P)$ of the α-relaxation, but also another universal property, which is the invariance of $\tau_\beta(P,T)$ at constant $\tau_\alpha(P,T)$. The two properties combined becomes the co-invariance of $\tau_\alpha(T,P)$, $\tau_\beta(T,P)$, and $\beta_K(T,P)$ to variations of T and P while either $\tau_\alpha(T,P)$ or $\tau_\beta(T,P)$ is kept constant. One can recall Fig.3 showing the co-invariance in the NIF-acMAL 1:3 m/m binary mixture.

Molecular dynamics simulations of a model polymers by Bedrov and Smith [52] found the same property as shown in Fig.9 for different combinations of T and P. An example of recent data are the dielectric loss spectra of the NIF-acMAL 1:3 m/m binary mixture at different T and P combinations. The data presented before in Fig.3a also reveal the same property. Moreover, in all cases the primitive relaxation time $\tau_0(T,P)$ is nearly the same as $\tau_\beta(T,P)$ as shown in the figure by the corresponding frequencies, $f_0 \approx f_\beta$.

Surprisingly, neither the isochronal superposition of the α-relaxation function discussed in Section 2 nor the JGβ relaxation was considered in conventional [53] and present-day [54,55,56,57,58,59,60,61,62] theories of glass transition. Naturally, these theories have no explanation of the generic property of co-invariance of $\tau_\alpha(T,P)$, $\tau_\beta(T,P)$, and $\beta_K(T,P)$ to variations of T and P

Open Access Article. Published on 04 June 2026. Downloaded on 6/5/2026 12:04:33 AM.
This article is licensed under a Creative Commons Attribution 3.0 Unported Licence.
Materials Advances Accepted Manuscript

View Article Online
DOI: 10.1039/D6MA00279J

Open Access Article. Published on 04 June 2026. Downloaded on 6/5/2026 12:04:33 AM.
This article is licensed under a Creative Commons Attribution 3.0 Unported Licence.

while either $\tau_\alpha(T,P)$ or $\tau_\beta(T,P)$ is kept constant. The CM is the only one having offered an explanation.

Figs.8c and 8d are the same property for ion conductivity relaxation in two ionic liquids $[Si\text{-}Mim]^+[BF4]^-$ [63] and procainamide HCl [64] to be discussed later in subsection 3.6. This property is for cooperative diffusion of ions and has no connection to glass transition, and yet the same property of co-invariance holds for $\tau_{\sigma\alpha}(T,P)$, $\tau_{\sigma\beta}(T,P)$, and $\beta_{\sigma K}(T,P)$ to variations of T and P while either $\tau_{\sigma\alpha}(T,P)$ or $\tau_{\sigma\beta}(T,P)$ is kept constant. No theory of ionic conductivity relaxation has explained the property except the CM. [11,63]

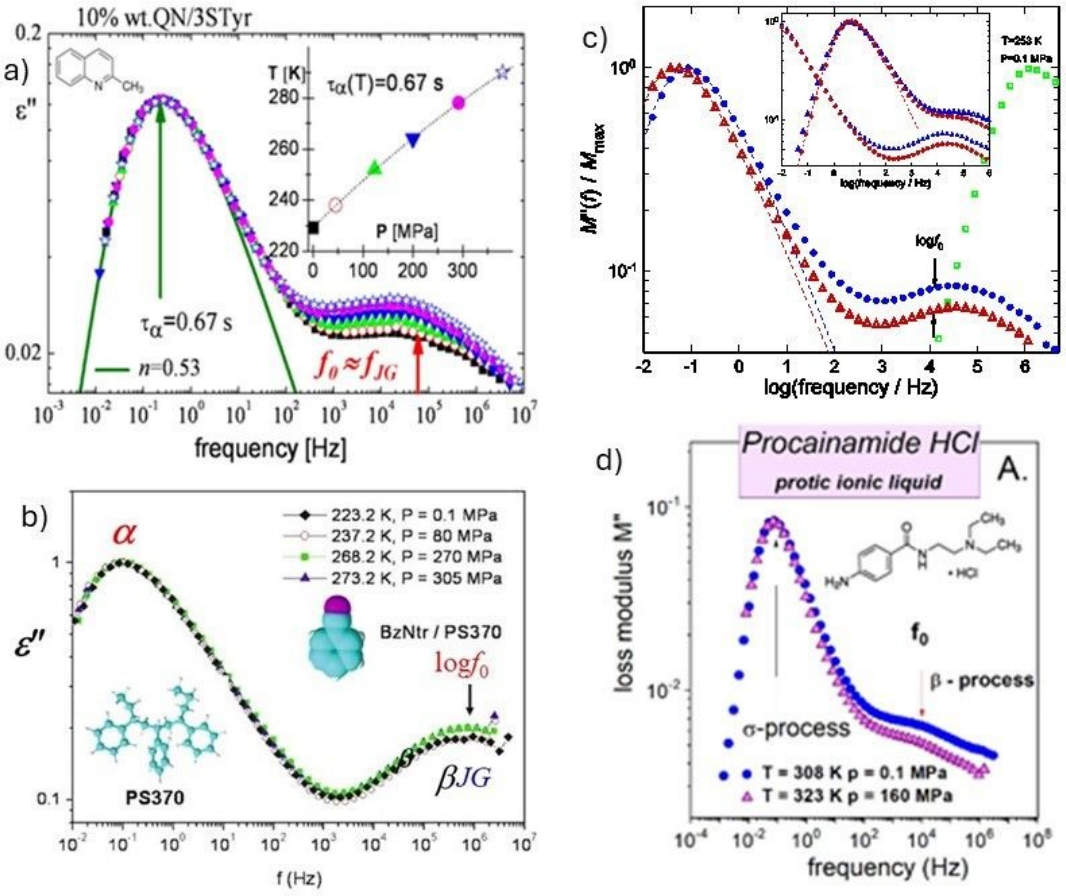

Fig. 8. *T*-*P* superposition of loss spectra with arrow to indicate the calculated primitive f_0 to compare with f_β of JGβ: (a) for 10% QN in tristyrene measured for different *T* and *P* combinations but the same τ_α= 0.67 s. The line is KWW fit with (1-*n*) = 0.53. (b) CNBz/PS370 (X_M=0.1). (c) Normalized *M*″(*f*) spectra of $[Si\text{-}Mim]^+[BF4]^-$ at different combinations of *P* and *T* to show co-invariance of τ_α, τ_β, and *n* at constant τ_α. Red open triangles (*P*=600 MPa, *T*=253 K). Blue circles (*P*=0.1 MPa, *T*=213 K). Green open squares (*P*=0.1 MPa, *T*=253 K). Blue and red lines are KWW fits with *n*=0.43. The inset show co-invariance at two more constant values of τ_α. The arrows indicate the locations of the primitive f_0. (d) Same for the ionic liquid. Figures are from Ref.[11] and reproduced with permission from Elsevier.

Materials Advances Accepted Manuscript

View Article Online
DOI: 10.1039/D6MA00279J

Open Access Article. Published on 04 June 2026. Downloaded on 6/5/2026 12:04:33 AM.
This article is licensed under a Creative Commons Attribution 3.0 Unported Licence.

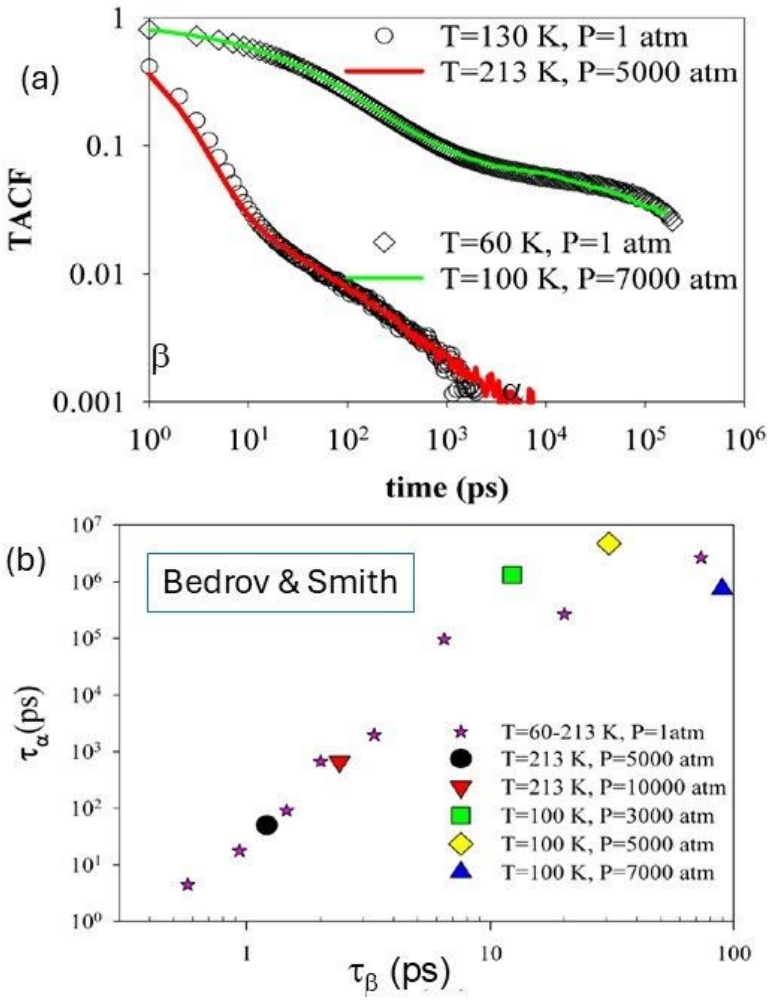

Fig. 9 (*a*) Comparison of torsional autocorrelation function (TACF) of bead-necklace model for polymer with bond length $l = 1.5$Å ($\sigma/l = 2.7$) obtained at $T = 130$ K and $P = 1$ bar with that at $T = 213$ K and $P = 5000$ bar, and at $T = 60$ K and $P = 1$ bar with that at $T = 100$ K and $P = 7000$ bar. (*b*) Correlation between relaxation times for α- and β-processes as obtained from simulations of melts with $l = 1.5$Å ($\sigma/l = 2.7$) at various thermodynamic conditions.[52] Figures courtesy of D. Bedrov.

3.2. $\tau_\beta(P,T) \approx \tau_0(P,T)$ explains co-invariance of $\tau_\alpha(T,P)$, $\tau_\beta(T,P)$, and $\beta_K(T,P)$

By virtue of the universal property 2, i.e. invariance of $\beta_K(T,P) \equiv [1\text{-}n(T,P)]$ to changes of P and T at constant $\tau_\alpha(T,P)$, it follows that $\tau_0(T,P)$ in Eq.(2) is also invariant. Thus, if $\tau_0(T,P)$ is approximately the same as $\tau_\beta(T,P)$, one has the explanation of the co-invariance of $\tau_\alpha(T,P)$, $\tau_\beta(T,P)$, and $\beta_K(T,P)$ to variations of T and P while $\tau_\alpha(T,P)$ is kept constant. This approximate relation

$$\tau_0(T,P) \approx \tau_\beta(T,P) \qquad (3)$$

Materials Advances Accepted Manuscript

View Article Online
DOI: 10.1039/D6MA00279J

Open Access Article. Published on 04 June 2026. Downloaded on 6/5/2026 12:04:33 AM.
This article is licensed under a Creative Commons Attribution 3.0 Unported Licence.

is expected since both the primitive and the JGβ relaxations are local processes. It had been verified in hundreds of glass-formers of various kinds, whether the JGβ relaxation is resolved or not [10,11] By contrast, mainstream theories of glass transition usually do not consider the JGβ relaxation, and make no attempt to account for the value of $\tau_\beta(T,P)$ and its properties. For the materials in Figs.5a and 5b, the primitive relaxation time $\tau_0(P,T)$ calculated via Eq.(2) from $\tau_\alpha(P,T)$ with the known values of t_c= 2 ps and $\beta_K(T,P)$ is approximately the same as the $\tau_\beta(T,P)$, as shown via their corresponding frequencies in the figures.

3.3. Chalcogenides $\tau_\beta(P,T) \approx \tau_0(P,T)$

The JGβ relaxation has never been found in the chalcogenides, $Ge_aAs_bSe_c$, in the past.[65,66,67,68]. Hence, no one can verify Eq.(3), and may even doubt the existence of the JGβ relaxation in $Ge_aAs_bSe_c$. One has to wait till 2026 to see reports of the observation of the JGβ relaxation by experiments in glasses of $GeSe_3$ by Baglioni et al. [34], and As_2Se_3 by Umair et al. [35] The $GeSe_3$ samples studied is in the high-enthalpy glassy states produced by rapid thermal quenching from the melt or by X-ray irradiation of the solid glass. The two methods enhance structural disorder and make possible the observation of the JGβ relaxation by fast-scanning calorimetry as an exothermic signal below $T_{g\alpha}$. In the case of As_2Se_3, a fast-quenched sample from the melt shows clear evidence of the JGβ relaxation deep in the glassy state.

Plotted in Fig. 10 against T_g/T with T_g = 498 K by Baglione et al. [34], are JGβ enthalpy relaxation times $\tau_\beta(T)$ of the two $GeSe_3$ glasses subjected to the rapid thermal quenching from the melt and X-ray irradiation. The α-relaxation times $\tau_\alpha(T)$ were obtained as the ratio of shear viscosity to shear elastic modulus from data given in Ref.[69]. Baglioni et al. performed additional experiment to observe the effect of probing rate r on the calorimetric trace of irradiated glasses**.** Differential thermograms over the temperature range from 380 to 760 K of glasses quenched at 10 K s^{-1} and irradiated at room temperature for 100 s, were probed at the probing rates r ranging from 300 to 8000 K. From the results of this experiment, they were able to obtain $\tau_\alpha(T)$ and $\tau_\beta(T)$ from reciprocal of the probe rate r near and above T_g = 498 K as shown in Fig.10. Details of the procedure was given in Ref.[34]. Thus, the JGβ relaxation is unveiled for the first time in $GeSe_3$ together with its relaxation times $\tau_\beta(T)$ having the Arrhenius temperature dependence of $\tau_\beta(T) = \tau_{\beta\infty}\exp(E_\beta/RT)$ in the glass with E_β = 1.01 ± 0.02 eV and $\tau_{\beta\infty}$ = 0.5 ± 0.4 ps or $\log(\tau_{\beta\infty}/s)$ = - 12.3. The ratio, E_β/RT_g, has the value of 24 ± 1, consistent with those values commonly associated with the JGβ relaxation of many glasses.[70,71,72,73] The finding of the JGβ relaxation in $GeSe_3$ by rapid quenching and X-ray irradiation is due to the increase of its relaxation strength by the increased enthalpy of the glass. This implies that the JGβ relaxation exists in nominal $GeSe_3$ glass but its weak relaxation strength makes it difficult to be observed. To test the relation, $\tau_\beta(T) \approx \tau_0(T)$, generally found in JGβ relaxation in many glass-formers for $GeSe_3$, Eq.(2) is used to calculate $\tau_0(T)$. The value of 0.64 for $(1\text{-}n)\equiv\beta_{KWW}$, or n=0.36 of $GeSe_3$ was determined by stress relaxation by Böhmer and Angell.[62] In the absence of neutron scattering data to determine t_c for $GeSe_3$, it is assumed to be 1 ps, the same as in selenium and GeTe (see Figs.5a and 5b). The $\tau_0(T)$ calculated from $\tau_\alpha(T)$ by Eq.(2) at several temperatures above T_g are represented by the yellow star symbols in Fig.8. There are good agreements between the $\tau_0(T)$ calculated and $\tau_\beta(T)$ from experiment.

Another check for consistency is by applying the equation derived from the CM Eqs.(1), (2), and (3) in Ref.[12] that relates $T_{g\beta}/T_{g\alpha}$ to $n(T_{g\alpha})$ and $\tau_{\beta\infty}$. If t_c=1 ps, the relation is given by

Materials Advances Accepted Manuscript

View Article Online
DOI: 10.1039/D6MA00279J

$$\frac{T_{g\beta}}{T_{g\alpha}} = 1 - \frac{(15.0)n(T_{g\alpha})}{-\log\tau_{\beta\infty} + 3}\,. \qquad (4)$$

Here, $T_{g\beta}$ and $T_{g\alpha}$ are defined as the temperatures at which $\tau_\beta(T_{g\beta})$ and $\tau_\alpha(T_{g\alpha})$ are equal to 10^3 s, and $\tau_{\beta\infty}$ is the prefactor of the Arrhenius dependence $\tau_{\beta\infty}\exp(E_{a\beta}/kT)$ of $\tau_\beta(T)$. In Ref.[12], where t_c=2 ps, the factor (15.0) in Eq.(4) was replaced by (14.7). Plotted in Fig.11 is $T_{g\beta}/T_{g\alpha}$ versus $n(T_{g\alpha})$ for four judicious choices, 10^{-12}, 10^{-13}, 10^{-14}, and 10^{-15} s of $\tau_{\beta\infty}$. In the present case of $GeSe_3$, defined by $\tau_\beta(T_{g\beta})$=10^3 s and $\tau_\alpha(T_{g\alpha})$=10^3 s, the values of $T_{g\beta}$ and $T_{g\alpha}$ are determined by the data of $\tau_\beta(T)$ and $\tau_\alpha(T)$ in Fig.10. The values are 332 K and 498 K respectively, and hence $T_{g\beta}/T_{g\alpha}$=0.667. In Fig. 11, the horizontal line representing $T_{g\beta}/T_{g\alpha}$=0.667 intersects the lines calculated according to Eq.(4) with the choice of 10^{-12} s at n=0.34, and 10^{-13} s at n=0.36. These pairs of values of $\tau_{\beta\infty}$ and n are consistent with the experimental values of $10^{-12.3}$ s, and n = (1- β_{KWW}) = 0.36 from Baglioni et al., and thus the consistency reaffirms the validity of Eq.(4) derived from the CM specifically for the chalcogenides.

For rapidly quenched As_2Se_3, the values of the relaxation time, $\tau_c(T)$, obtained with enthalpy relaxation by Umair et al. [35] are plotted against the reciprocal of the annealing temperature T_a in Fig. 12, and compared with the structural α-relaxation times, $\tau_s(T)$. The latter were obtained as the ratio η/G_∞ of the shear viscosity η, [74,75] and the shear modulus G_∞.[76] Added are some values of $\tau_s(T)$ from an unpublished photon correlation experiment. Umair et al. fitted the $\tau_c(T)$ data to an Arrhenius temperature dependence: $\tau_c(T) = \tau_{c\infty}\exp(E_\beta/RT)$ with E_β= 1.1 ± 0.2 eV and $\tau_{c\infty}$=0.3 ± 1.0 ps, or $\log(\tau_{c\infty}/s)$ = -12.5 s. As remarked by Umair et al., the value of $\tau_{c\infty}$ is consistent with that expected for the inverse of a vibrational angular frequency. The ratio, E_β/RT_g, has the value of 26.7 ± 1.0, which is consistent with the empirical criterion used to identify the JG relaxation in various glasses. Thus, by fast quenching, the relaxation strength of the JGβ relaxation of As_2Se_3 making it easier to be detected in enthalpy relaxation, as found before in other fast quenched glasses by calorimetry [68,72,73] and dynamic mechanical spectroscopy. [76]

In Fig.11, the horizontal line is drawn to have log(relaxation time/s) = 3. The two temperatures $T_{g\alpha}$ and $T_{g\beta}$ of As_2Se_3 are determined operationally by the intersections of the line with $\log\tau_s(T)$ data and the Arrhenius line representing $\log\tau_c(T)$ respectively. The value of $T_{g\beta}/T_{g\alpha}$ obtained is 0.79. This experimental value of $T_{g\beta}/T_{g\alpha}$ can be used in conjunction with Eq.(4) to determine the (1-n)≡β_{KWW} of As_2Se_3, which is not known previously. Revisiting Fig.11 and the plots of $T_{g\beta}/T_{g\alpha}$ versus n for the four choices, 10^{-12}, 10^{-13}, 10^{-14}, and 10^{-15} s, of $\tau_{\beta\infty}$, it can be seen the dotted line representing of $T_{g\beta}/T_{g\alpha}$=0.79 intersects the curve for $\log(\tau_{c\infty}/s)$ = -12.5 (not shown) at n=0.22 as indicated by the arrow. The value of n is slightly increased to 0.26 if $\log(\tau_{c\infty}/s)$ = -15. With the value of n=0.22 determined and t_c=1 ps, Eq.(2) is used to calculate the primitive relaxation time $\tau_0(T)$ from the experimental $\tau_\alpha(T)$ or $\tau_s(T)$ in Fig.12 at two temperatures near $T_{g\alpha}$. The results of $\tau_0(T)$ shown by black closed circles are in good agreement with the Arrhenius dependence used to fit the $\tau_c(T)$ data deep in the glassy state, and thus the relation $\tau_0(T) \approx \tau_\beta(T)$ is verified for As_2Se_3. The $\tau_0(T)$ calculated with n=0.26 are slightly shorter.

Open Access Article. Published on 04 June 2026. Downloaded on 6/5/2026 12:04:33 AM.
This article is licensed under a Creative Commons Attribution 3.0 Unported Licence.

Materials Advances Accepted Manuscript

View Article Online
DOI: 10.1039/D6MA00279J

Open Access Article. Published on 04 June 2026. Downloaded on 6/5/2026 12:04:33 AM.
This article is licensed under a Creative Commons Attribution 3.0 Unported Licence.

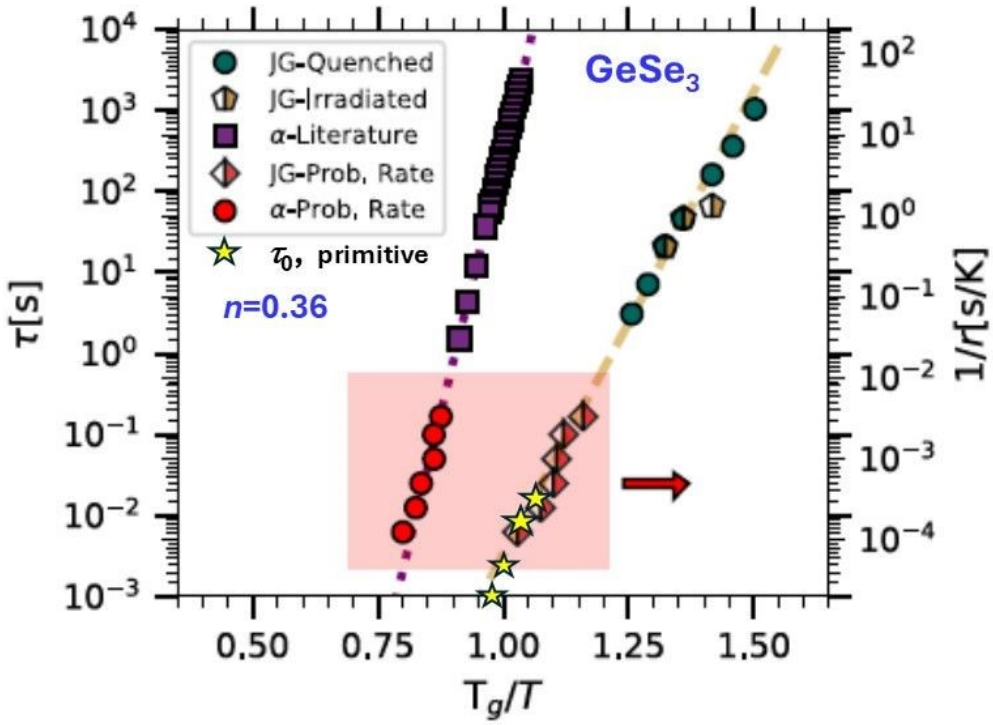

Fig. 10. Left *y* axis: enthalpy relaxation times for the low-temperature tail/shoulder for $GeSe_3$ glasses quenched at 20,000 K s^{-1} (green circles) and glasses quenched at 10 K s^{-1} and then irradiated at room temperature for 150 s (half-filled golden pentagons). The probing rate was 2,000 K s^{-1} in all cases. Literature data for the structural relaxation time (purple squares). Right *y* axis: inverse probing rate as a function of the inverse T_g-scaled temperature at which (1) the enthalpy recovery peak in the thermograms and (2) the exothermic shoulder in the differential thermograms show the largest slope (red-filled circles and half-filled rhombuses, respectively). The shaded area emphasizes all data corresponding to the right axis to enhance readability. The dotted and dashed lines are linear fits to the literature data for the structural relaxation and to the enthalpy relaxation data for the quenched glasses, respectively. The right *y* axis is shifted vertically by a factor of 50 with respect to the left *y* axis in order to match the data obtained as a function of the probing rate (right *y* axis) with the extrapolation of the structural relaxation and the enthalpy relaxation times (left *y* axis). The yellow stars are the primitive relaxation times $\tau_0(T)$ calculated by using the CM Eq.(2). Figure taken from Ref.[34] and reused with permission from Elsevier.

Materials Advances Accepted Manuscript

View Article Online
DOI: 10.1039/D6MA00279J

Open Access Article. Published on 04 June 2026. Downloaded on 6/5/2026 12:04:33 AM.
This article is licensed under a Creative Commons Attribution 3.0 Unported Licence.

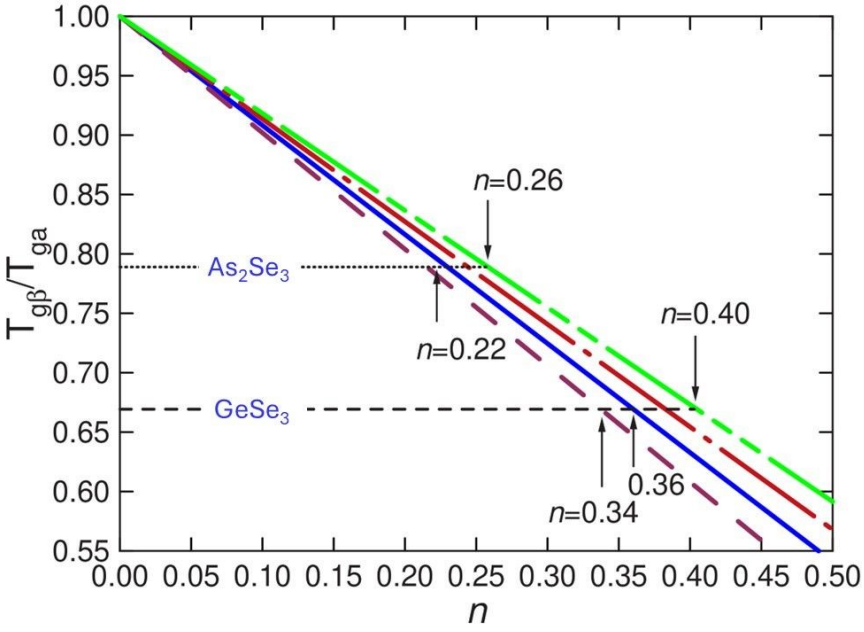

Fig. 11. Plot of $T_{g\beta}/T_{g\alpha}$ versus $n(T_{g\alpha})$ for four judicious choices, 10^{-12}, 10^{-13}, 10^{-14}, and 10^{-15} s of $\tau_{\beta\infty}$. The dashed line for $GeSe_3$, corresponding to $T_{g\beta}/T_{g\alpha}$=0.667 intersects the plots at values of n consistent with the independently determined value of n=0.34. The dotted line for As_2Se_3 corresponding to $T_{g\beta}/T_{g\alpha}$ = 0.79 is used to determine the values of n within the range from 0.22 to 0.26.

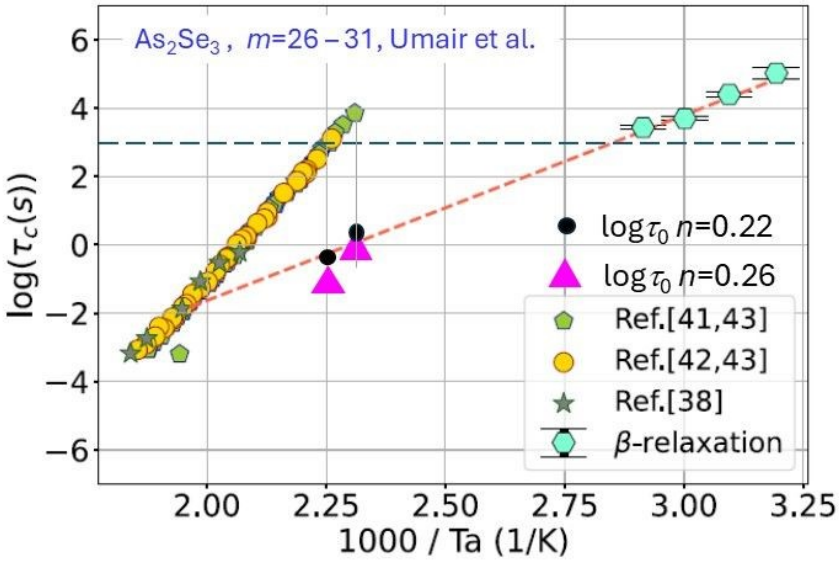

Fig. 12. Activation plot for As_2Se_3. The characteristic enthalpy relaxation time (τ_c) is reported as a function of the reciprocal of the annealing temperature. Values for the structural relaxation time (circles and pentagons) for the α-relaxation are also reported as computed from literature viscosity and shear modulus data. Additional values of τ_s are from photon correlation experiments (★). The dashed line is the (extrapolated) Arrhenius temperature dependence of τ_c.

Materials Advances Accepted Manuscript

View Article Online
DOI: 10.1039/D6MA00279J

The black circles and magenta triangles are the primitive relaxation times $\tau_0(T)$ calculated by using the CM Eq.(2). Figure taken from Ref.[35] and reused with permission from Elsevier.

3.4. Time-Domain Interferometry (TDI) verifying $\tau_\beta(P,T) \approx \tau_0(P,T)$

Besides dielectric spectroscopy commonly used to verify Eq.(3) as shown in Fig.5, there are other techniques including the microscopic quasi-elastic scattering experiments with time-domain interferometry (TDI) based on synchrotron radiation [77,78,79,80,81,82,83,84]. The analyses of the experimental TDI data by the CM have verified Eq.(3) microscopically in OTP in Ref. [85], polybutadiene (PBD) in Ref. [85], glycerol in Ref. [86], 1-propanol in Refs.[85,87], 5-methyl-2-hexanol (5M2H) in Refs.[85,82], cumene in Ref.[11], and $Ca_{0.4}K_{0.6}(NO_3)_{1.4}$ (CKN) in Ref. [32,84]. An example of TDI data of $\tau_\beta(q,T)$ at several q values of the monohydric alcohol, 5-methyl-2-hexanol, are shown in Fig.13a together with the $\tau_\beta(T)$ and the primitive $\tau_0(T)$ calculated via Eq.(2) from $\tau_\alpha(T)$ and (1-n), as shown in Fig.13b. In this figure, the JGβ relaxation is resolved in the dielectric and light scattering spectra. There are good agreements between the three relaxation frequencies, $1/[2\pi\tau_\beta(q,T)]$ from TDI, $f_0=[2\pi\tau_0(T)]$ calculated by Eq.(2), and the JGβ loss peak frequency from both dielectric and dynamic light scattering. Similar results and agreements were found for TDI data of OTP [85], PBD [85], glycerol [86], 1-propanol [85,87], and CKN [32]. The 2025 TDI $\tau_\beta(q,T)$ data of CKN obtained by Saito et al. [60] are reproduced in Fig. 14, and compared well with the values of $\tau_0(T)$ calculated via Eq.(2) in the CM explanation paper[32] also published in 2025. In the same figure are $\tau_\alpha(T)$ from neutron scattering from Luo et al. [31] at several Q values together with that from impulsive stimulated light scattering (ISLS)[89,90], dielectric spectroscopy[91], dynamic light scattering [92,93]. The calculated $\tau_0(T)$ are in good agreement with Brillouin scattering data which measures the primitive relaxation as in other materials including $ZnCl_2$,[94] polyisoprene and atatic polypropylene.[95] The TDI $\tau_\beta(q,T)$ data of glycerol will be shown in Fig.38a later to compare with $\tau_0(T)$ calculated from the $\tau_\alpha(T)$ of bulk glycerol, and $\tau_\alpha(T)$ of glycerol confined in 1.16 nm spaces.

The TDI data of JGβ relaxation and the relation of its relaxation time to that of the α-relaxation found in polymeric and molecular glass-formers with and without hydrogen bonding have not been considered by the current theories of glass transition [54,55,56,57,58,59,60,61,62]. In view of the strong connections in properties found by experiments and simulations between the two relaxations and demonstrated by the microscopic TDI experiments, the task of solving the glass transition problem is incomplete without addressing the JGβ relaxation.

Open Access Article. Published on 04 June 2026. Downloaded on 6/5/2026 12:04:33 AM.
This article is licensed under a Creative Commons Attribution 3.0 Unported Licence.

Materials Advances Accepted Manuscript

View Article Online
DOI: 10.1039/D6MA00279J

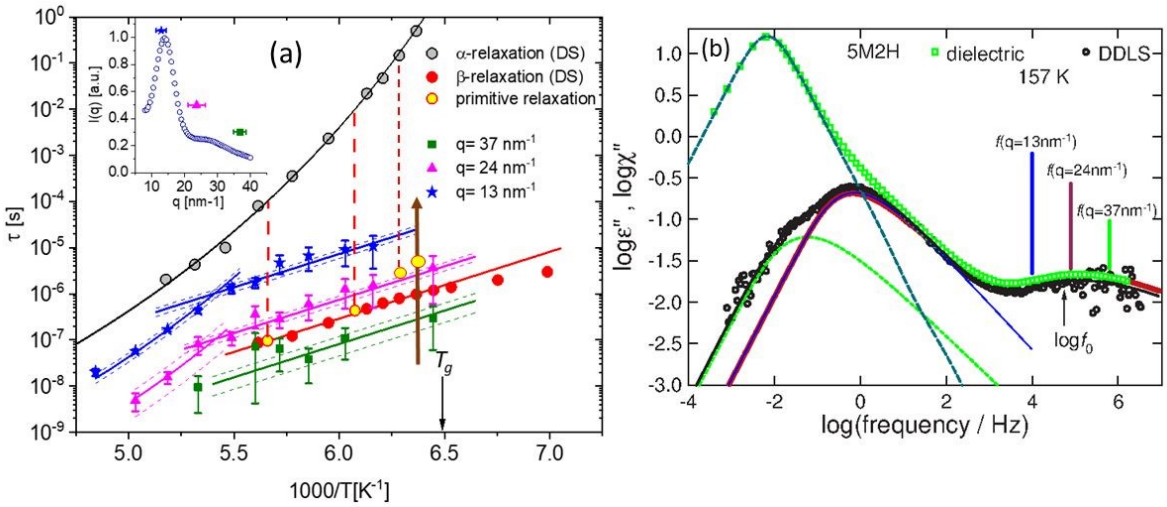

Fig. 13. (a) *T*-dependence of the relaxation times measured by TDI at three different q-values, and by DS. The primitive τ_0 predicted by CM at several temperatures (yellow circles). Inset: diffuse scattering pattern of 5M2H at T=187.6 K, with the q values and the corresponding ranges covered in the TDI measurements. (b) Direct comparison of dielectric (green squares) and DDLS data of 5M2H (black circles), and black line is fit at 157 K. The blue line is the KWW fit to α-relaxation for both dielectric and DDSL data with $n = 0.44$. Vertical lines show locations of $f(q)$ from TDI at 157 K in (a). Figures reproduced from Ref.[11] with permission from Elsevier.

Open Access Article. Published on 04 June 2026. Downloaded on 6/5/2026 12:04:33 AM.
This article is licensed under a Creative Commons Attribution 3.0 Unported Licence.

Materials Advances Accepted Manuscript

View Article Online
DOI: 10.1039/D6MA00279J

Open Access Article. Published on 04 June 2026. Downloaded on 6/5/2026 12:04:33 AM.
This article is licensed under a Creative Commons Attribution 3.0 Unported Licence.

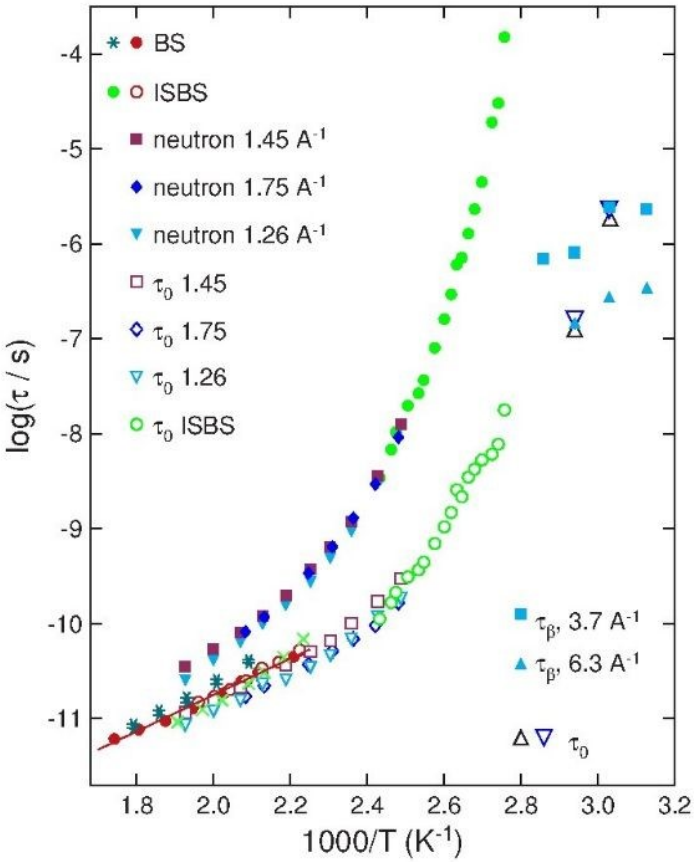

Fig. 14. Brillouin scattering $\tau_{BS}(T)$ and $\tau_{ISBS}(T)$ are much shorter than the neutron $\tau_{\alpha}(T)$ at four different Qs over the same temperature range was also found for CKN. This general anomaly can be quantitatively explained by CM in the calculated $\tau_0(T)$ by Eq.(4) from neutron $\tau_{\alpha}(T)$. For all three Qs, the calculated $\tau_0(T)$ are nearly the same as $\tau_{BS}(T)$ and $\tau_{ISLS}(T)$ below T_g. The neutron data at Q=1.26, 1.45, and 1.75 Å^{-1} are from Luo *et al.* [31]. The short ISLS relaxation times data (open red circles) at temperatures above 455 K are from Ref.[90]. The longer time ISLS data (green closed circles) at temperatures below 411.1 K are from Ref.[89] and the green open circles are the corresponding primitive relaxation times $\tau_0(T)$ calculated. The Brillouin scattering relaxation time $\tau_{BS}(T)$ data of CKN from Pavlatou et al. [94] and Li *et al.* [95] are represented by filled red circles and green ∗ respectively. The pale blue squares and triangles represent the $\tau_{\beta}(T)$ from TDI study at 3.7 and 6.3 Å^{-1} respectively from Saito et al. [84]. The black open downward and upward pointing purple open triangles represent $\tau_0(T)$ calculated by Eq.(2) with β_{α}=0.43, $\tau_{\alpha}(T)\approx$ 1 s and 10^3 s respectively, and two possible values of 1 ps and 0.5 ps for t_c. Figure reproduced from Ref.[31] with permission from AIP

3.5. Amorphous Ice $\tau_{\beta}(P,T) \approx \tau_0(P,T)$

The relaxation and diffusion of amorphous ice and water are difficult to study experimentally due to polyamorphism and the polyamorphs including amorphous solid water (ASW), hyperquenched glassy water (HGW), low density liquid water (LDL), and high density liquid water (HDL). Nevertheless, the studies by many contributors to name a few

Materials Advances Accepted Manuscript

View Article Online
DOI: 10.1039/D6MA00279J

Open Access Article. Published on 04 June 2026. Downloaded on 6/5/2026 12:04:33 AM.
This article is licensed under a Creative Commons Attribution 3.0 Unported Licence.

[96,97,98,99,100,101,102,103,104,105,106] over the last five decades have finally provide enough data for a critical CM analysis of the caged dynamics, JGβ relaxation, and α-relaxation of these four polyamorphs with results published in 2026.[107] The essential results are briefly summarized as follows. All polyamorphs have smaller coupling parameter n or larger β_{KWW} as expected from the small size of water molecule. Evidences come from dielectric spectra of LDL and HGW, and those of LDL are shown in Fig.15a at four temperatures 128 – 151 K and in Fig.15b at 142 K. The high frequency flank of the α-loss peak has slope = 0.82 at frequency ranges that should correspond to the exponent $(1-n)=\beta_{KWW}$ of the KWW function in Eq.(1). The primitive relaxation frequency ν_0 of LDL calculated via Eq.(2) with $(1-n) = 0.82$ for four temperatures are shown by the thinner arrows. The thicker arrows at 5 temperatures in (a) and (b) combined indicate the probable locations of the JGβ relaxation frequencies ν_β suggested by the inflection in the frequency dependence of the $\varepsilon''(\nu)$ data. There is good agreement between ν_0 and ν_β. The same properties of the JGβ and α-relaxation as well as the property, $\nu_0 \approx \nu_\beta$, were found from the dielectric loss data of HGW.

The JGβ and α relaxation times, $\tau_\beta(T)$ and $\tau_\alpha(T)$, of the four polyamorphs are represented in Fig.16 by closed and open symbols respectively. For comparison, the relaxation times of water confined in various nanometer spaces, $\tau_{conf}(T)$, [108,109,110,111] are shown. Nano-confined water is not the same as the amorphous ices, and hence $\tau_{conf}(T)$ need not be exactly the same as $\tau_\beta(T)$. Nevertheless, the two are not very different. Later in Section 4 where caged dynamics is considered, one can see the caged dynamics in amorphous ices exhibit the same properties of coupling to the JGβ and the α-relaxation as other glass-formers.

Materials Advances Accepted Manuscript

View Article Online
DOI: 10.1039/D6MA00279J

Open Access Article. Published on 04 June 2026. Downloaded on 6/5/2026 12:04:33 AM.
This article is licensed under a Creative Commons Attribution 3.0 Unported Licence.

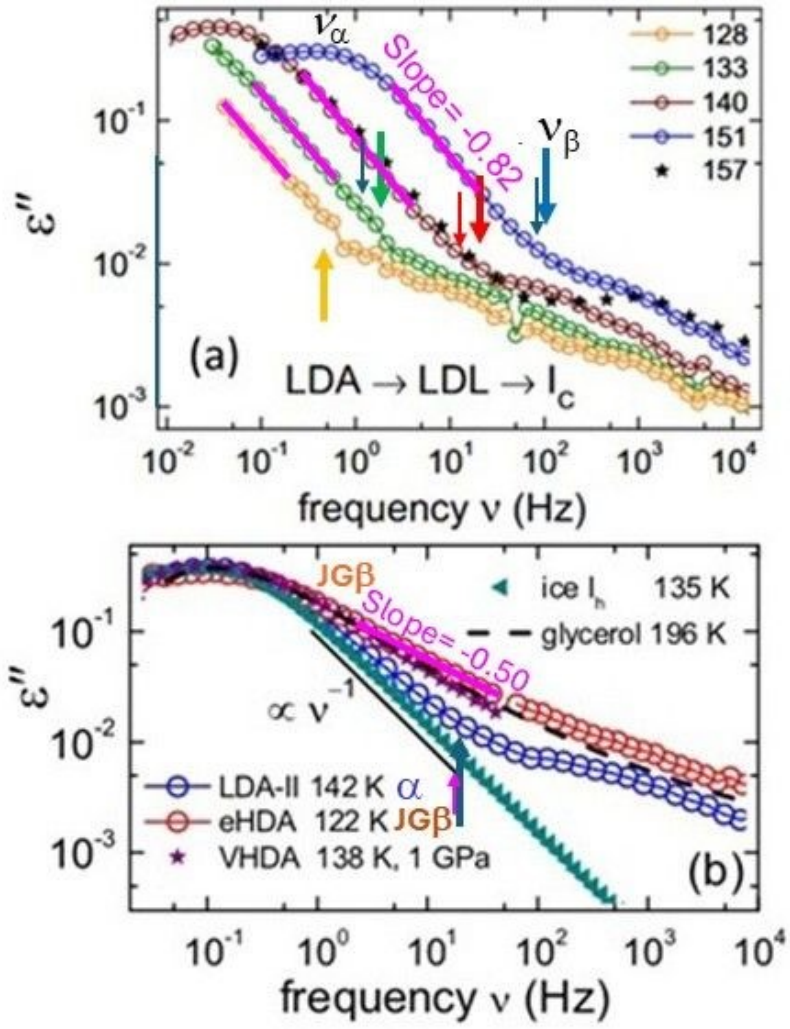

Fig. 15. Dielectric loss spectra of LDL are plotted in (a) as connected open symbols for several temperatures (from Amann-Winkel et al. [98]), and in (b) at 142 K only (from Ref.[99]). (b) Consider only the LDA-II data for this review, and ignore the other data of eHDS and VHDA. The spectra are normalized to their peak amplitudes. The loss peaks are identified with the α-relaxation. Added are the thicker arrows indicating the probable location of the JGβ relaxation frequencies at 5 temperatures in (a) and (b) combined. The thick magenta lines in (a) with slope = 0.82 are fits to the slopes of LDA and LDL data at frequency ranges that should correspond to the exponent $(1\text{-}n)=\beta_K$ of the KWW function with its Fourier transform fitting the α-loss peak. The primitive relaxation frequency ν_0 of LDL calculated via Eq.(1) with $(1\text{-}n)$ = 0.82 for four temperatures are shown by the thinner arrows. Figures (a) and (b) are adopted respectively from Ref.[98] and Ref.[99], and reused with permission from Proc. Natl. Acad. Sci. U. S. A. and APS.

Materials Advances Accepted Manuscript

View Article Online
DOI: 10.1039/D6MA00279J

Open Access Article. Published on 04 June 2026. Downloaded on 6/5/2026 12:04:33 AM.
This article is licensed under a Creative Commons Attribution 3.0 Unported Licence.

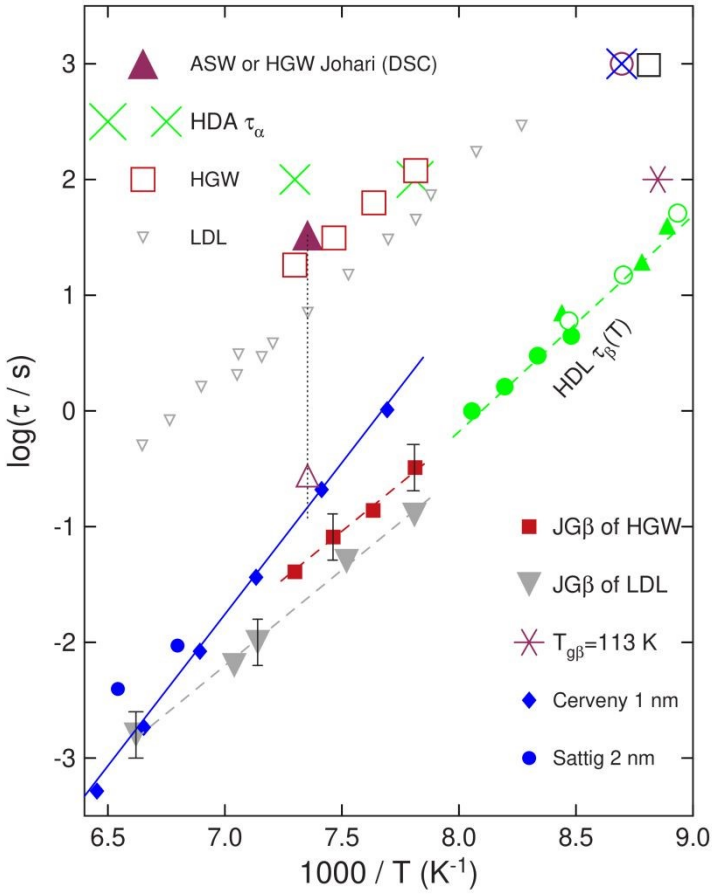

Fig. 16. Plotted are the dielectric and calorimetric relaxation times of ASW, HGW, LDL, and HDL. The legends of the data are given in the figure, and the source is illustrated in the text. Smaller grey ∇ are dielectric α-relaxation times of LDL from Ref.[98] and Ref.[106] respectively. Green and larger symbols are the dielectric (•,o) and calorimetric (▲) relaxation times of HDL from Ref.[98] identified by them as τ_α, but reinterpreted in Ref.[101] as the JGβ relaxation times τ_β. The larger and smaller green × are $\tau_\alpha(T_{g,\mathrm{HDA}})$=100 s at $T_{g,\mathrm{HDA}}$ =128 K and 137 K of HDA at ambient pressure deduced by extrapolation of high pressure volumetric and calorimetric data respectively. The lone and large red ✳ represents the JGβ relaxation times τ_β of ASW and HGW assumed with the value of 100 s at its $T_{g\beta}$ ~ 113 K determined from the NCL crossover. The broken arrow indicates it. Added are the JGβ relaxation times τ_β of HGW (red large ■) and LDL (grey large ▼), and the relaxation times of nano-confined water from adiabatic calorimetry (⊗, □) from Oguni et al.[108,109] in upper right corner, dielectric (♦)[110] and NMR (•)[111] studies.

3.6. Ionic conductivity relaxation, $\tau_{\sigma\beta}(P,T) \approx \tau_{\sigma 0}(P,T)$

The CM has the prediction for ion conductivity relaxation. It is given by the analogues of Eqs.(1)-(3), where the primary conductivity (σ) relaxation time $\tau_{\sigma\alpha}(P,T)$ replaces $\tau_\alpha(P,T)$, the secondary conductivity relaxation $\tau_{\sigma\beta}(T,P)$ replaces $\tau_\beta(T,P)$ of the JGβ relaxation, the primitive conductivity $\tau_{\sigma 0}(P,T)$ replaces $\tau_0(P,T)$, and $n_\sigma(P,T)$ replaces $n(P,T)$. All the properties mentioned in the above

Materials Advances Accepted Manuscript

View Article Online
DOI: 10.1039/D6MA00279J

for structural relaxation are found generally in conductivity relaxation spectra of ionic liquids including $\tau_{\sigma\beta}(P,T) \approx \tau_{\sigma 0}(P,T)$, as shown before by [Si-MIm]$^+$[BF4]$^-$ from Ref.[63] in Fig.8(c), and procainamide HCl in Fig.8(d) from Ref.[64]. The CM Eq.(2) for ion conductivity relaxation can be recast as

$$\log \tau_{\sigma\alpha}(T,P) - \log\tau_{\sigma 0}(T,P) = [1-\beta_{\sigma K}(T,P)]\log[\tau_{\sigma\alpha}(T,P)/t_c]. \quad (5)$$

The invariance of $\beta_{\sigma K}(T,P)$ to variations of P and T at constant $\tau_{\sigma\alpha}(P,T)$ can be proven in the same way as for structural relaxation in Section 2.1. By this fact, Eq.(5) immediately requires the invariance of $\tau_{\sigma 0}(P,T)$. On combining this result with $\tau_{\sigma 0}(P,T) \approx \tau_{\sigma\beta}(T,P)$, one has derived from the CM the universal property of T-P co-invariance of $\tau_{\sigma\beta}(T,P)$ and $\beta_{\sigma K}(T,P)$ at constant $\tau_{\sigma\alpha}(P,T)$ for ion conductivity relaxation.

The universal properties of ionic liquids are reinforced by the CM analyses in 2024 and 2025 [112,113] of data from two recent studies of ionic liquids.[114,115,116,117] In Ref.[114], ambient and high pressures dielectric measurements of a supercooled acidic ionic liquid and its mixture with water found the presence of the primary and the secondary conductivity relaxations. The T-P co-invariance of $\tau_{\sigma\beta}(T,P)$ and $\beta_{\sigma K}(T,P)$ at constant $\tau_{\sigma\alpha}(P,T)$ were found as shown by an example in Fig.17a. The property, $\tau_{\sigma 0}(P,T) \approx \tau_{\sigma\beta}(T,P)$, is verified in Fig.17b for the dried sample and the aqueous mixture.

The experimental studies of the phosphonium ionic liquids containing the cation $[P_{666,14}]^+$ and anions of different sizes and shapes by various authors have brought out a wealth of remarkable properties of ionic conductivity relaxation and structural relaxation. [115,116,117] The emphasis is on the liquid-liquid transition (LLT) from liquid 1 (L1) to liquid 2 (L2) effected by either lowering temperature to cross the transition temperature T_{LL} or by elevating pressure past the transition pressure P_{LL}. The LLT originates from structural reorganization as observed by spectroscopy and calorimetry. The dynamics of the ionic conductivity relaxation in L1 and L2 are different and the LLT from L1 to L2 causes abrupt increase in the temperature (pressure) dependence of the isobaric (isothermal) ionic conductivity relaxation times $\tau_\sigma(T,P)$ after crossing T_{LL} (P_{LL}). Remarkably, accompanying this behavior of $\tau_\sigma(T,P)$, there is the abrupt increase in the width of the frequency dispersion or $n_\sigma(T,P) \equiv [1-\beta_{\sigma KWW}(T,P)]$. For phosphonium liquids composed of some other anions showing no abrupt change of $\tau_\sigma(T,P)$, so does $\beta_{\sigma KWW}(T,P)$. These strong correlations found between $\tau_\sigma(T,P)$ and $n(T,P)$ indicate the two are dependent and possibly the former is linked to or determined by the latter. The possibility is fulfilled in the Coupling Model explanation of the dynamic and thermodynamic properties of ionic conductivity relaxation.[11] Eq. (5) captures the dependences of $\tau_\sigma(T,P)$ on $[1-\beta_{\sigma KWW}(T,P)]$. The CM Eq.(5) is applied to the experimental data of the phosphonium ionic liquids. An example from [P666,14][TCM] is shown in Fig.18. The application reveals quantitatively the primitive relaxation times $\tau_{0\sigma}(T,P)$ in Eq.(5). The results verify the absence in $\tau_{0\sigma}(T,P)$ of any abrupt increase on crossing T_{LL} or P_{LL} unlike $\tau_\sigma(T,P)$. This attribute of $\tau_{0\sigma}(T,P)$ comes from the local and single ion nature of the primitive relaxation, making it insensitive to the change of interionic interaction by the structural reorganization in the LLT. Thus, the dynamics of ionic conductivity relaxation in L1 and L2 and the changes involved in the LLT have an explanation from the CM.

Also observed in the phosphonium ionic liquids in either L1 or L2 is the invariance of the frequency dispersion of the conductivity relaxation or $\beta_{\sigma KWW}(T,P)$ to variations of T and P while keeping $\tau_\sigma(T,P)$ constant. This is shown for the case of $[P_{666,14}]$[TCM] in the top panel of Fig.18.

Open Access Article. Published on 04 June 2026. Downloaded on 6/5/2026 12:04:33 AM.
This article is licensed under a Creative Commons Attribution 3.0 Unported Licence.

Materials Advances Accepted Manuscript

View Article Online
DOI: 10.1039/D6MA00279J

As another connection between $\tau_\sigma(T,P)$ and $\beta_{\sigma KWW}(T,P)$, this co-invariance property is general and found in other kinds of ionic liquids. The inorganic molten salt, $0.4Ca(NO_3)_2$-$0.6KNO_3$ (CKN), is in stark contrast in structures and ion type with the organic ionic liquids discussed in Figs.8c, 8d, 17, and 18. Nevertheless, the invariance of $\beta_{\sigma KWW}(T,P)$ at constant $\tau_\sigma(T,P)$ is found over a range of $\tau_\sigma(T,P)$ was found [118] and shown in Fig.19.

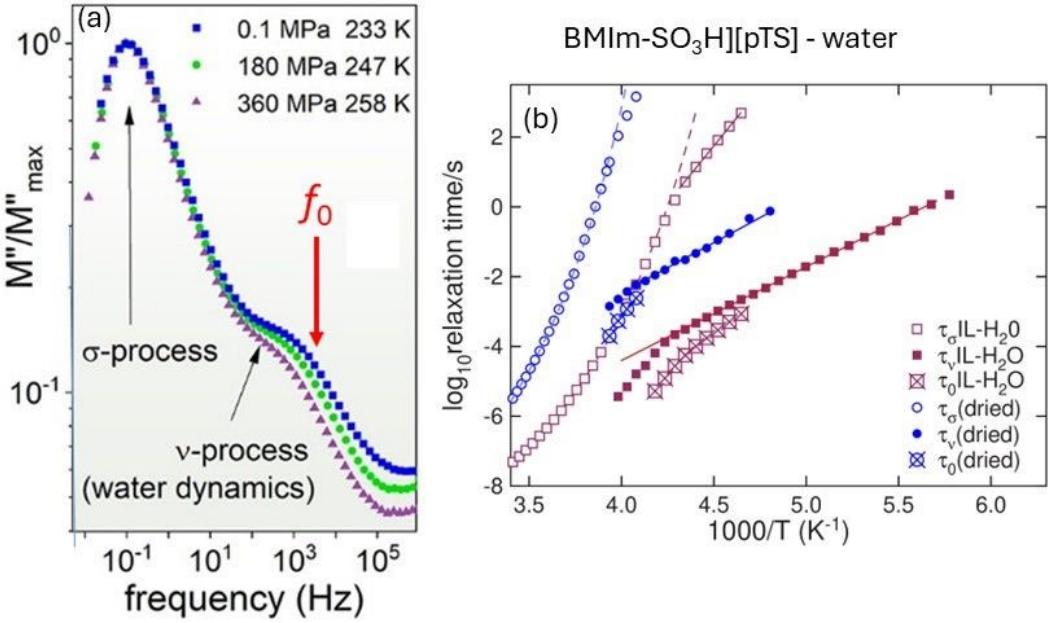

Fig. 17. (a) Representative normalized electric modulus $M''(f)$ data of the primary (σ) and secondary (ν) conductivity relaxations in the IL–water mixture measured at different combinations of T and P. The figure serves to demonstrate the shape of the primary conductivity relaxation as well as the ratio of the two relaxation times τ_σ and τ_ν are invariant to large changes of thermodynamic condition. The red arrow indicates the location of the primitive conductivity relaxation frequency f_0 calculated by the Coupling Model equation (5). Figure taken from Ref.[90] and reused with permission from PCCP. (b) Relaxation map showing the temperature variations of the conductivity relaxation times $\tau_\sigma(T)$ and $\tau_\nu(T)$ of the IL–water and the dried sample at ambient pressure. Dashed lines are the VFT fits (above T_g) and solid lines are Arrhenius fits (below T_g) fits of dielectric experimental data. The primitive relaxation times $\tau_0(T)$ are calculated by the CM Eq.(5). Figures taken from Ref.[114] and reused with permission from PCCP.

Open Access Article. Published on 04 June 2026. Downloaded on 6/5/2026 12:04:33 AM.
This article is licensed under a Creative Commons Attribution 3.0 Unported Licence.

Materials Advances Accepted Manuscript

View Article Online
DOI: 10.1039/D6MA00279J

Open Access Article. Published on 04 June 2026. Downloaded on 6/5/2026 12:04:33 AM.
This article is licensed under a Creative Commons Attribution 3.0 Unported Licence.

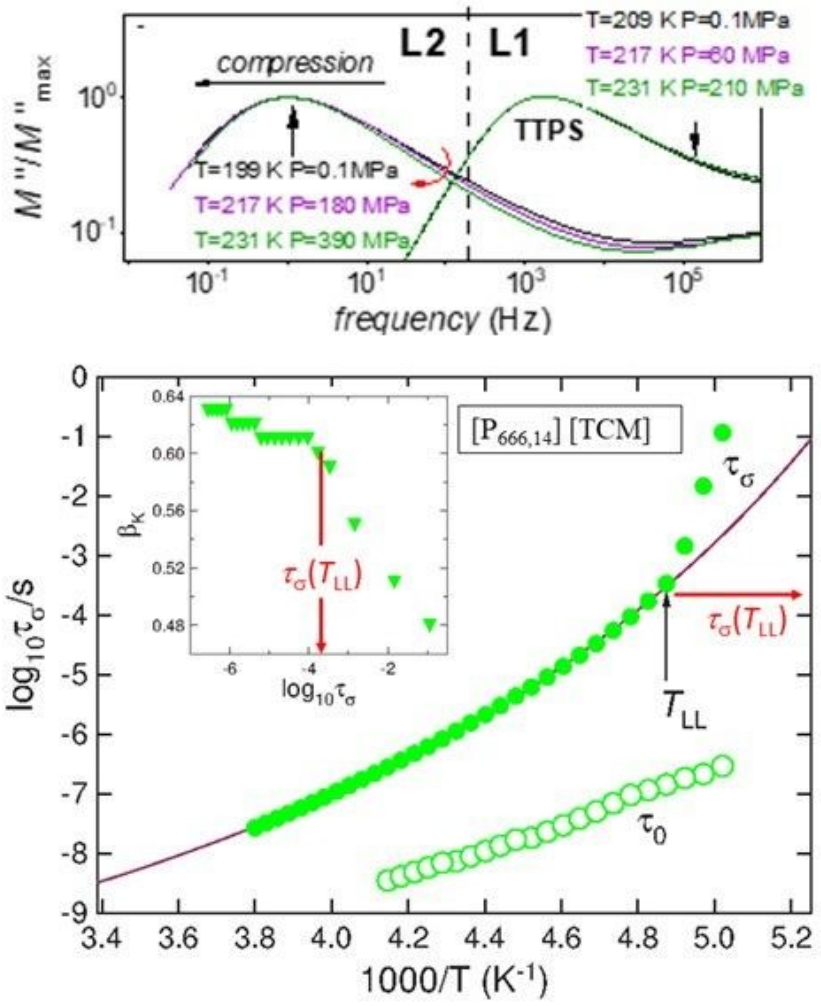

Fig. 18. (Top) The representative M''(f) spectra of $[P_{666,14}][TCM]$ recorded at various T-P conditions however at the same τ_σ superimposed to each other in liquid 1 and liquid 2, respectively. Note that time temperature pressure superposition (TTPS) rule is valid. (Bottom) The data of the conductivity relaxation times $\tau_\sigma(T,P_a)$ of $[P_{666,14}]^+[TCM]^-$ from Ref.[91] are shown by closed squares. The solid line denotes the fit of data at higher temperatures by the VFT function. An abrupt increase of $\tau_\sigma(T,P_a)$ from the VFT fit starts at T_{LL} of the liquid-liquid transition. The horizontal red arrow indicates $\tau_\sigma(T_{LL},P_a)$, the conductivity relaxation time at T_{LL}. The open squares are the primitive conductivity relaxation times $\tau_{\sigma 0}(T,P_a)$ calculated by Eq.(5) using $\tau_\sigma(T,P_a)$ and $\beta_{\sigma KWW}(T,P_a)$ from experiment. The inset is the plot of $\beta_{\sigma KWW}(T,P_a)$ versus $\tau_\sigma(T,P_a)$ to demonstrate the onset of the abrupt decrease of $\beta_{\sigma KWW}(T,P_a)$ occurs at about the *same* $\tau_\sigma(T_{LL},P_a)$ depicted by the horizontal and vertical arrows in the main part of the figure and the inset respectively. The temperature dependence of the conductivity relaxation times $\tau_\sigma(T,P_a)$ changes from one VFT law to another one at the T_{LL} = 204 K. Figure taken from Ref.[112] and reused with permission from PCCP.

Materials Advances Accepted Manuscript

View Article Online
DOI: 10.1039/D6MA00279J

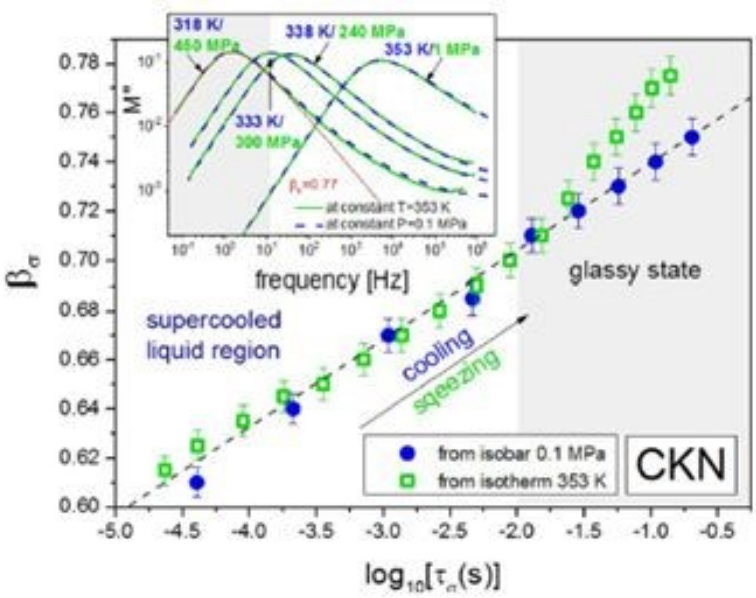

Fig. 19. Conductivity α-relaxation on T and P in the molten salt, $0.4Ca(NO_3)_2$-$0.6KNO_3$ (CKN). At constant conductivity relaxation time $\tau_{\sigma\alpha}$, the entire conductivity relaxation spectra obtained at widely different combinations of T and P superpose almost perfectly in the supercooled liquid state as shown by the same Kohlrausch exponent β_σ at the same $\tau_{\sigma\alpha}$. The inset shows some representative electric modulus data and the fit by the Kohlrausch function. Figure reproduced from Ref.[118] by permission from APS.

3.7. Polymers

To demonstrate co-invariance of $\tau_\alpha(T,P)$, $\tau_\beta(T,P)$, and $\beta_K(T,P)$ to variations of T and P at constant $\tau_\alpha(T,P)$ in polymers, the example from diglycidyl ether of bisphenol-A (DGEBA) with M_w=380 g/mol is chosen.[119] Shown in Fig. 20a are $\tau_\alpha(T,P)$ and $\tau_\beta(T,P)$, at two different pressures, P_1=0.1 MPa and P_2=400 MPa. When $\tau_\alpha(T_1,P_1)$ and $\tau_\alpha(T_2,P_2)$ have the same value of 100 s, it can be seen from Fig.17a that $\tau_\beta(T_1,P_1)$ and $\tau_\beta(T_2,P_2)$ also have the same value. Invariance of $\beta_K(T,P)$ at constant $\tau_\alpha(T,P)$ was demonstrated in Fig.51 of Ref.[11]. Molecular dynamics simulations of a model polymers found the same property by Bedrov and Smith [52], as shown before in Fig.9.

Open Access Article. Published on 04 June 2026. Downloaded on 6/5/2026 12:04:33 AM.
This article is licensed under a Creative Commons Attribution 3.0 Unported Licence.

Materials Advances Accepted Manuscript

View Article Online
DOI: 10.1039/D6MA00279J

Open Access Article. Published on 04 June 2026. Downloaded on 6/5/2026 12:04:33 AM.
This article is licensed under a Creative Commons Attribution 3.0 Unported Licence.

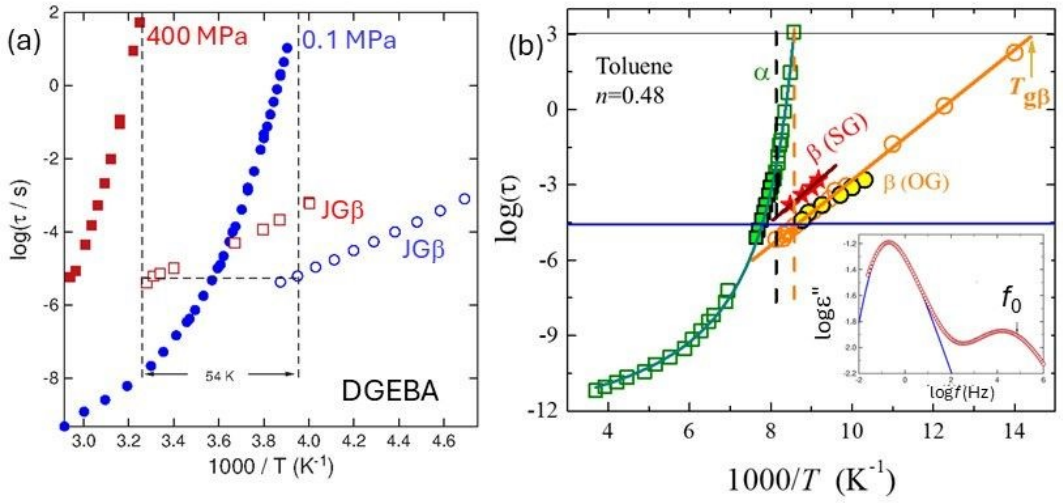

Fig. 20. (a) $\log \tau_\alpha$ and $\log \tau_\beta$ of DGEBA in isobaric condition vs 1000/T. The difference in T_g is 54 K, which is matched by the separation of $\log \tau_\beta$ (dashed line).[119] (b) $\log \tau_\alpha$ and $\log \tau_\beta$ of ordinary glass (open symbols), and the relaxation times for the vapor-deposited samples (solid symbols). Added are the two vertical lines located at $1000/T_g$ and $1000/T_{on}$. Inset: $\varepsilon''(f)$ of toluene, KWW fit with n=0.48, and the calculated value of the primitive frequency f_0. Figure reproduced from Ref.[119] with permission from PCCP.

3.8. Ultrastable glass

Instead of elevating pressure to change the thermodynamic condition of a glass-former to verify the co-invariance o $\tau_\alpha(T,P)$, $\tau_\beta(T,P)$, and $\beta_K(T,P)$ to variations of T and P at constant $\tau_\alpha(T,P)$, we [119,120] have compared the ordinary glass (OG) with the ultrastable glass (USG) formed by vapor deposition at their respective glass transition onset temperatures $T_{\text{on,OG}}$ and $T_{\text{on,USG}}$. By definition, the structural α-relaxation times at these two temperatures, $\tau_\alpha(T_{\text{on,OG}})$ and $\tau_\alpha(T_{\text{on,USG}})$, have the same value. Thus, the purported universal co-invariance property can be tested by comparing $\tau_\beta(T_{\text{on,OG}})$ with $\tau_\beta(T_{\text{on,USG}})$. Such data are available for the JGβ relaxations of toluene [121], etoricoxib, and telmisartan [122]. In all three cases, the value of $\tau_\beta(T_{\text{on,OG}})$ is the same as $\tau_\beta(T_{\text{on,USG}})$, and co-invariance of τ_α and τ_β to change of thermodynamic condition of the glass at constant τ_α is verified by comparing OG with USG. Fig.20b shows the case of toluene, and Fig.21 for etoricoxib, and telmisartan. The CM relation, $\tau_0(T) \approx \tau_\beta(T)$, is verified in toluene above T_g as shown by an example in the inset of Fig.20b from the dielectric loss spectrum at 119 K with f_α=0.2 Hz from Ref. [123] and the Kohlrausch fit with exponent (1-n)=0.52. The calculated primitive frequency $f_0=(1/2\pi\tau_0)$ is about the same as the peak frequency $f_\beta=(1/2\pi\tau_\beta)$.

Like toluene, the JGβ relaxation of etoricoxib and telmisartan, becomes *slower* in the USG than in OG. Studied also in Ref.[122] are the secondary relaxations in USG and OG glasses of β-D-maltose octa-acetate, carvedilol, and celecoxib. Known before from their properties in the supercooled liquid state, these secondary relaxations do not belong to the class of JGβ relaxations [12,13], and have no connection to the α relaxation in properties. Unsurprisingly, they behave differently from JGβ relaxation in β-D-maltose octa-acetate, carvedilol, and celecoxib by becoming *faster* in the USG than in the OG [122]. It is worthwhile to note that we [122] distinguished

Materials Advances Accepted Manuscript

View Article Online
DOI: 10.1039/D6MA00279J

Open Access Article. Published on 04 June 2026. Downloaded on 6/5/2026 12:04:33 AM.
This article is licensed under a Creative Commons Attribution 3.0 Unported Licence.

the JGβ relaxation from the intramolecular non-JGβ relaxation [12,13] when considering the changes from OG to USG. On the other hand, others like Kasting et al. [124] did not do so and considered all of them together as well as Berthier and Ediger in Ref.[58].

Although the studies of the change of the secondary relaxation from OG to USG are widely publicized in publications, [59,120,121,122,124] no explanation of the experimental findings has been given by others. Apparently, the only explanation of the USG and OG data is that given by the CM [119,120,122]. Notwithstanding, Berthier and Ediger (BE) [50] was concerned with the CM explanation by the statement: *"... the timescale τ_β measured experimentally decreases with the aging time for a number of systems (Refs.64 and 67), whereas the structural relaxation presumably increases instead, suggesting that care is needed to relate τ_β to τ_α in an unambiguous manner*.". The systems BE referred to in their Ref. 67 (corresponding to Ref.[122] herein) are β-D-maltose octa-acetate, carvedilol, and celecoxib. As mentioned before and explained already in Ref.[122], the secondary relaxations in these three glass-formers are intramolecular and non-JGβ relaxations. Unlike the true JGβ relaxations[12,13] of toluene, etoricoxib, and telmisartan, they have no connection to and correlation with the α relaxation in properties and thus their relaxation times can behave differently than toluene, and become faster in SG than in OG. Thus, the concern of the CM explanation by BE is not real.[125] The other point related to their Ref.64 was resolved in Ref.[125] and is not duplicated here.

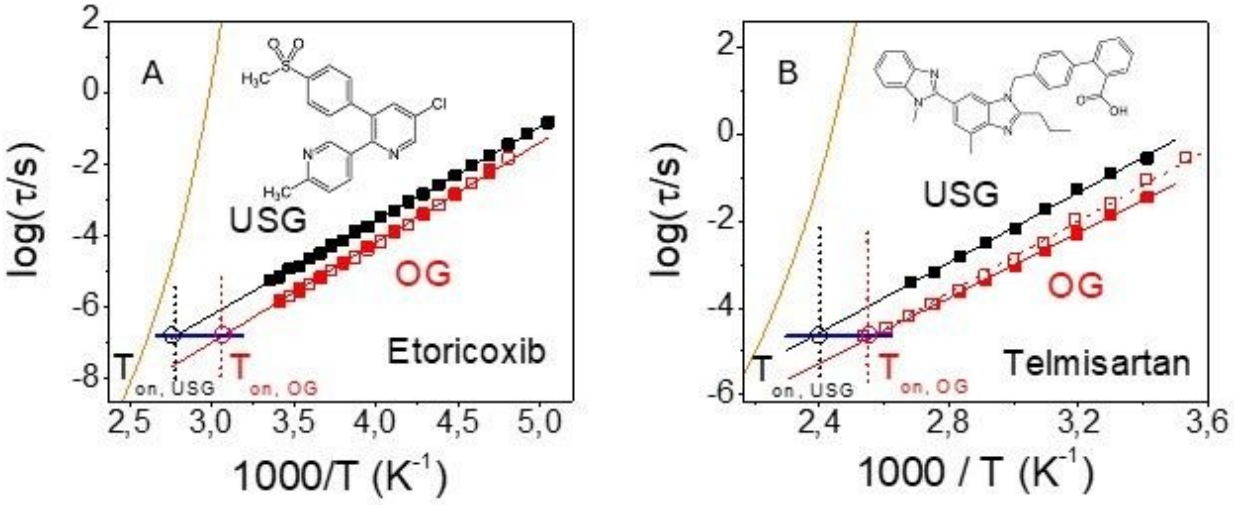

Fig. 21. Relaxation map of relaxation time of the analysed JGβ relaxations in etoricoxib and telmisartan in Fig.21. Back and red closed symbols correspond to the USG and the OG obtained after transformation of the USG and subsequent cooling down, respectively. The red open points and the orange VFT fit to the structural α-relaxation. The black and red circles indicate the values of the JGβ relaxation times at $T_{on,USG}$ and $T_{on,OG}$. The horizontal blue line helps to show the invariance of the JGβ relaxation time at T_{on} for these materials. The structure of each molecule is depicted. Figure reproduced from Ref.[122] with permission from PCCP.

Materials Advances Accepted Manuscript

View Article Online
DOI: 10.1039/D6MA00279J

Open Access Article. Published on 04 June 2026. Downloaded on 6/5/2026 12:04:33 AM.
This article is licensed under a Creative Commons Attribution 3.0 Unported Licence.

3.9. TV^{γ}-scaling originates from the primitive relaxation/JG β relaxation.

Thermodynamic scaling of the τ_α or viscosity and diffusion coefficient of glass-forming liquids at various T and P means the data conform to a single function of the product variable TV^{γ}, where V is the specific volume and γ is a material specific constant. From the co-invariance of $\tau_\alpha(T,P)$, $\tau_0(T,P) \approx \tau_\beta(T,P)$, and $\beta_K(T,P)$ to variations of T and P at constant $\tau_\alpha(T,P)$, it follows immediately that τ_α and $\tau_0 \approx \tau_\beta$ as well as β_K are all functions of TV^{γ} with the same γ. This general property was verified by experiments and simulations in many molecular, polymeric, and metallic glass-formers. [11,42,126,127,128] Examples from strongly hydrogen-bonded ternidazole drug (3-(2-methyl-5-nitroimidazol-1-yl)-propan-1-ol), TDZ for short [42] was presented before in Fig.7b for a different purpose. Here, poly(methyl methacrylate)[128] and phenylphthalein-dimethyl ether (PDE) [127] are shown in Fig.22a and Fig.22b. Since the primitive/JGβ relaxation transpire in times before the α-relaxation, causality requires that TV^{γ}-scaling of τ_α originates from that of τ_0 and τ_β [11,126,127]. This conclusion is supported by γ being related to the slope of the repulsive part of the intermolecular potential. Thus, this fundamental and pivotal role played by the JGβ relaxation should not be ignored in solving the glass transition problem.

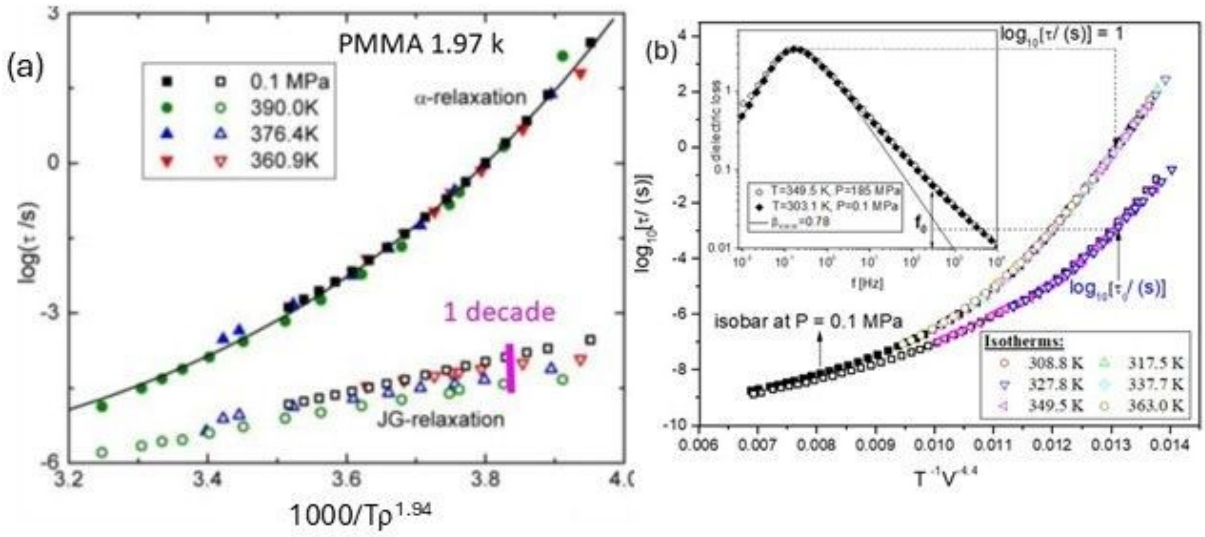

Fig. 22. (a) Density scaling plots of the PMMA relaxation times for the α (filled symbols) and JG (open symbols) processes. The solid line is fit with γ = 1.94. Despite the uncertainties of the relaxation times obtained in fitting the spectra, the scatter of τ_β is less than 1 decade as indicated by the short vertical line. Figure reproduced from Ref. [126] by permission from ACS. (b) The inset shows perfect superpositioning of ε'' spectra of PDE at 2 combinations of P and T for a constant τ_α. The primitive $f_0=1/2\pi\tau_0$ calculated is indicated by the arrow. Consequently, TV^{γ}-scaling of τ_α as well as τ_0 hold as shown. Figures from Ref.[11] reused with permission from Elsevier.

Materials Advances Accepted Manuscript

View Article Online
DOI: 10.1039/D6MA00279J

Open Access Article. Published on 04 June 2026. Downloaded on 6/5/2026 12:04:33 AM.
This article is licensed under a Creative Commons Attribution 3.0 Unported Licence.

Materials Advances Accepted Manuscript

4. Coupling of Caged Molecule Dynamics to JGβ and α Relaxations

4.1. Change of *T*-dependence of caged dynamics at $T_{g\beta}$ and $T_{g\alpha}$

At early times all molecules are confined within cages determined by the intermolecular potential. This is the caged dynamics regime. At temperatures below or slightly above the glass transition temperature $T_{g\alpha}$ effected by the structural α relaxation, the caged dynamics is the only process that can be observed if probed at times much shorter than the relaxation times of the important Johari-Goldstein β-relaxation (ignoring the inconsequential intramolecular relaxation such as from the methyl group in molecules and polymers). Shown in Fig.23a are terahertz dielectric loss as a function of temperature of sorbitol, trehalose, and bovine serum albumin (BSA).[11] In Fig. 23b are the mean square displacement $<u^2>$ from neutron scattering of trehalose compares with the THz data.[11] In all cases, the caged dynamics probed changes temperature dependence on crossing the JGβ glass transition temperature $T_{g\beta}$ and $T_{g\alpha}$.

In Fig.23c are the dielectric loss tangent of amorphous solid water at 1 kHz [96,97,107] with the inset showing the adiabatic calorimetry data of water confined in 1.1 nm silica-gel pores[108,109]. The $T_{g\beta}$ at 113 K observed by adiabatic calorimetry is shown in the inset, and $T_{g\alpha}$ at 136 K was determined by DSC [96,97]. These older data are reconsidered in the light of the secondary glass transition from the JGβ relaxation in the CM, and are analyzed for the first time in 2026 to show the universal property of the coupling of caged dynamics to the JGβ and α relaxations in water.[107]

In Fig. 23d are the $<u^2>$ from neutron scattering of the polymer, polyethylene terephthalate (PET), plotted together with the dielectric relaxation times $\tau_\beta(T)$ and $\tau_\alpha(T)$ reaching 10^3 s to determine $T_{g\beta}$ and $T_{g\alpha}$ respectively. Generally observed is the change in the temperature dependence of the caged dynamics on crossing the glass transition temperatures $T_{g\beta}$ and $T_{g\alpha}$ of the JGβ and α relaxations. The value of $T_{g\beta}$ can be determined directly by adiabatic calorimetry [108,109,129] and o-Ps lifetime τ_3 as a function of temperature in positron annihilation lifetime spectroscopy (PALS) [130,131]. The calorimetric data are shown in Fig.23c for water, and in Fig. S1 for cumene[132] in Supplementary Materials (SM) together with the $<u^2>$ data from neutron scattering. The PALS results are shown for 1,4 polybutadiene and poly(methyl methacrylate) in Figs.S2 and S3(a) of SM, and the dielectric loss data at 10 GHz of the latter is shown in Fig, S3(b) of SM.

Fig.24a show the internal friction $Q^{-1}(T)$ at 0.4 MHz contributed by the caged dynamics in $Pd_{42.5}Ni_{7.5}Cu_{30}P_{20}$ metallic glass. [133,134] The changes of $Q^{-1}(T)$ are observed at two temperatures,[133] which are indeed $T_{g\beta}$ and $T_{g\alpha}$ as supported by the isothermal mechanical and modulated DSC relaxation times $\tau_\beta(T)$ and $\tau_\alpha(T)$ of the same metallic alloy reaching 100 s at these temperatures in Fig.24b.[134] The metallic alloy data in Fig.24 are older, but the analysis given here to reveal the changes of the caged dynamics at $T_{g\beta}$ is new.

From the examples given, the change of caged dynamics in its temperature dependence on crossing the glass transition temperatures $T_{g\beta}$ and $T_{g\alpha}$ of the JGβ and α relaxations were found in drastically different amorphous materials, including polymers,[135] biomolecules,[136] molecules with and without hydrogen bonds [137,138,139], metallic glasses, and amorphous water[107]. Previously, these properties of caged dynamics have not been considered in the chalcogens and chalcogenides. In the following subsection, the neutron scattering data of two such materials published in the past are revisited to reveal the properties. Thus, the coupling of the caged

View Article Online
DOI: 10.1039/D6MA00279J

dynamics to to the JGβ and α relaxations is another universal property predicted by the CM. None of the current theories of glass transition [54,55,56,57,58,59,60,61,62] have considered these ubiquitous properties found experimentally. The Mode Coupling Theory (MCT) [54] did considered the caged dynamics in terms of its non-ergodicity parameter but JGβ relaxation is absent in MCT.

Open Access Article. Published on 04 June 2026. Downloaded on 6/5/2026 12:04:33 AM.
This article is licensed under a Creative Commons Attribution 3.0 Unported Licence.

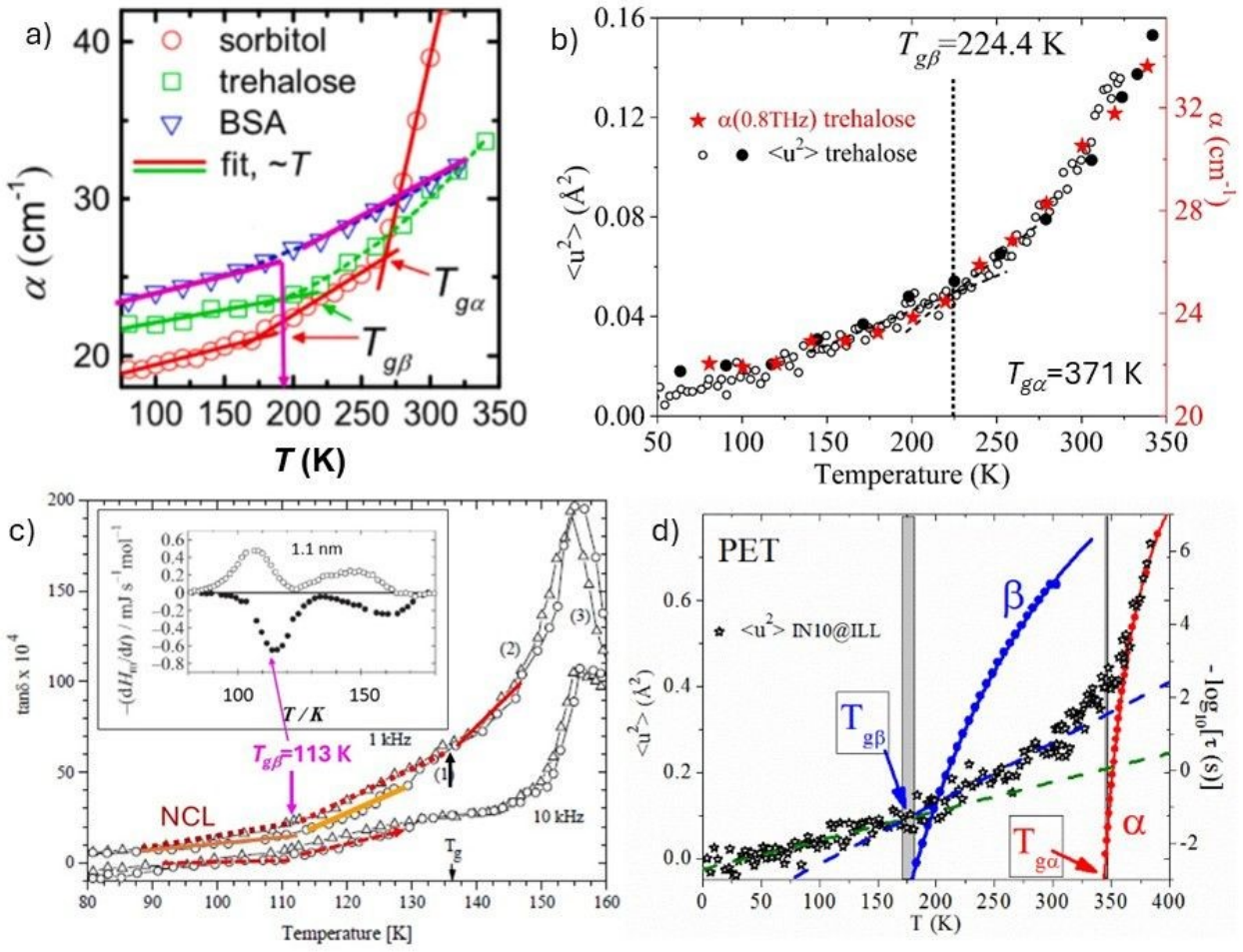

Fig. 23. Experimental data as a function of temperature showing changes of the temperature dependence of the caged dynamics at $T_{g\beta}$ and $T_{g\alpha}$. (a) Terahertz absorption of sorbitol (T_g ≈268 K), trehalose (T_g ≈385 K), and BSA.[11] (b) 0.8 THz absorption (stars) and $<u^2>$ from neutron scattering of trehalose (•).[11] (c) Isochronal dielectric loss data of amorphous solid water at 1 kHz from Ref.[11]. (d) Mean square displacement, $<u^2>$, of amorphous PET (open black stars) as measured at the IN10 spectrometer by Sanz and co-workers. The blue and red circles are dielectric relaxation times $\tau_\beta(T)$ and $\tau_\alpha(T)$ reaching 10^3 s at $T_{g\beta}$ and $T_{g\alpha}$ respectively. Figure reproduced from Ref.[11] with permission from Elsevier.

Materials Advances Accepted Manuscript

View Article Online
DOI: 10.1039/D6MA00279J

Open Access Article. Published on 04 June 2026. Downloaded on 6/5/2026 12:04:33 AM.
This article is licensed under a Creative Commons Attribution 3.0 Unported Licence.

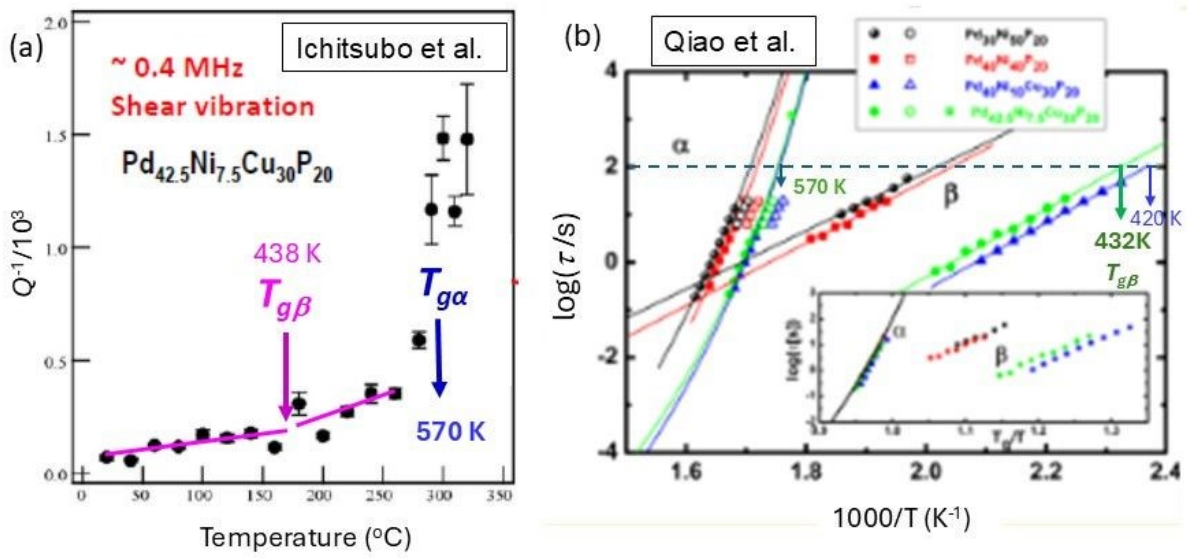

Fig. 24. (a) Temperature dependence of internal friction Q^{-1} of $Pd_{42.5}Ni_{7.5}Cu_{30}P_{20}$ metallic glass ($T_{g\alpha}$≈575 K) measure at 0.4 MHz. [133] This figure is taken from the presentation given by T. Ichitsubo on May 10, 2010 at KITP, Univ. California, Santa Barbara, and was made available from the KITP website. (b) $\log\tau_\alpha$ and $\log\tau_\beta$ of four metallic glass formers determining the respective $T_{g\alpha}$ and $T_{g\beta}$. The solid symbols are from the analysis of the isothermal mechanical spectra. The corresponding open symbols were obtained from the modulated DSC measurements. The solid lines are the best fit to the VFT and Arrhenius equations. The star symbol for $Pd_{42.5}Ni_{7.5}Cu_{30}P_{20}$ was obtained from aging measurements. Inset: Fragility plot for the four metallic glass formers. Figure is reproduced from Ref.[134] and reused with permission from ACS publishing.

4.2. Selenium and $Ge_{0.033}As_{0.033}Se_{0.934}$

Buchenau and Zorn [140,141] measured $<u^2(T)>$ of selenium from neutron time-of-flight spectra on the spectrometer IN6 at ILL in Grenoble, and the data are shown in Fig.25. The data at temperatures below $T_{g\alpha}$ = 305 K is scanty. This is because these authors were not interested in the caged dynamics and had a different purpose in mind when acquiring the $<u^2(T)>$ data. Guided by these past experiences in analyzing $<u^2(T)>$ data observed the change of T-dependence of $<u^2(T)>$ at $T_{g\beta}$ and $T_{g\alpha}$, the change of $<u^2(T)>$ of selenium first at 165 ± 10 K, with large uncertainty is identified with $T_{g\beta}$. The second change of $<u^2(T)>$ at $T_{g\alpha}$ =305 K is clearly seen. The ratio $T_{g\beta}/T_{g\alpha}$ falls within the range 0.54 ± 0.03.

Mechanical spectroscopy applied to selenium by Böhmer and Angell [67,68] was not able to detect the JGβ relaxation and determine its $T_{g\beta}$. In order to test whether $T_{g\beta}$ of selenium is 165 ± 10 K or not, help comes from the CM Eq.(4) with $T_{g\beta}$ and $T_{g\alpha}$ are defined by $\tau_\beta(T_{g\beta})$ and $\tau_\alpha(T_{g\alpha})$ equal to 10^3 s, and $\tau_{\beta\infty}$ is the prefactor of the Arrhenius dependence $\tau_{\beta\infty}\exp(E_{a\beta}/kT)$ of $\tau_\beta(T)$. The value of $n(T_{g\alpha})$ for selenium can be deduced by the relation $(1\text{-}n)\equiv\beta_{KWW}$ from the β_{KWW} value given by Böhmer and Angell [67,68]. However, two different values of β_{KWW} near $T_{g\alpha}$, 0.42 and 0.50, were given by them, corresponding to 0.58 and 0.50 for the values of $n(T_{g\alpha})$. Plazek [142]

Materials Advances Accepted Manuscript

View Article Online
DOI: 10.1039/D6MA00279J

Open Access Article. Published on 04 June 2026. Downloaded on 6/5/2026 12:04:33 AM.
This article is licensed under a Creative Commons Attribution 3.0 Unported Licence.

gave the value of $n(T_{g\alpha})$=0.53 from fitting creep compliance data.[143] The value of $\tau_{\beta\infty}$ for selenium is not known. Since $\tau_\beta(T) \approx \tau_0(T)$ and $\tau_0(T)$ is the relaxation time of non-cooperative process, the size of the prefactors $\tau_{0\infty} \approx \tau_{\beta\infty}$ is comparable to the reciprocal of some vibrational frequency. In Fig.26 plotted is $T_{g\beta}/T_{g\alpha}$ versus $n(T_{g\alpha})$ for four judicious choices, 10^{-12}, 10^{-13}, 10^{-14}, and 10^{-15} s of $\tau_{\beta\infty}$. Within the uncertainties of values of $0.50 \le n(T_{g\alpha}) \le 0.55$, and $10^{-15} \le \tau_{\beta\infty} \le 10^{-12}$ s, the values of $T_{g\beta}/T_{g\alpha}$ determined ranges from 0.465 to 0.59. For the most probable values of $n(T_{g\alpha})$=0.53 and $\tau_{\beta\infty}$ =10^{-13} or 10^{-14} s, the plot in Fig.26 yields $T_{g\beta}/T_{g\alpha}$ values of 0.51 and 0.54, in agreement with values within the range of 0.54 ± 0.03 determined independently by the change in temperature dependence of neutron $\langle u^2(T)\rangle$ from caged dynamics data in Fig.25. This agreement supports $T_{g\beta}$ of selenium is 165 ± 10 K.

The chalcogenide, $Ge_{0.033}As_{0.033}Se_{0.934}$, with composition close to Se studied by mechanical spectroscopy by Böhmer and Angell [67] was also investigated using neutron scattering measurements by Russina et al.[144], with energy resolution of 0.072 meV and over a Q range up to 2.03 Å^{-1}. Shown in Fig.27 is the temperature dependence of the elastic scattering intensity $S^{el}(Q, E=0)$. Since $S^{el}(Q, E=0)$ is the same as exp-$[\langle u^2(Q,T)\rangle Q^2/3]$, the change in temperature dependence of the logarithm of the former reflects the change of $\langle u^2(Q,T)\rangle$ from caged dynamics. It can be seen from Fig.27 that $\langle u^2(Q,T)\rangle$ changes at $T_{g\alpha}$ = 334 K The detection of the change at $T_{g\beta}$ is rendered difficult by the scarcity of data points below $T_{g\alpha}$. Despite the difficulty, the data at higher Q values of 1.95 Å^{-1} and 1.76 Å^{-1}seem to exhibit a change within the range from 180 to 190 K.

If $T_{g\beta}$ has either one of these two values, 180 K or 190 K, the corresponding $T_{g\beta}/T_{g\alpha}$ values are 0.54 and 0.57, which can be tested by using Eq.(4) in the same manner as done for selenium. In the family of $Ge_aAs_bSe_c$, the average coordination number $\langle r\rangle$ is given by the sum $4a+3b+2c$. For $Ge_{0.033}As_{0.033}Se_{0.934}$, its $\langle r\rangle$ is equal to 2.1. Its value of β_{KWW}=0.52 or $n(T_{g\alpha})$ = 0.48 was determined before by Böhmer and Angell [67] and shown in the inset of Fig.27. Plotted in Fig.28 is $T_{g\beta}/T_{g\alpha}$ versus $n(T_{g\alpha})$ for four choices, 10^{-12}, 10^{-13}, 10^{-14}, and 10^{-15} s of $\tau_{\beta\infty}$, as well as 10^{-18} s for contrast. The intersections of the vertical brown line at $n(T_{g\alpha})$=0.48 of the plots with $\tau_{\beta\infty}$ = 10^{-12}, 10^{-13}, 10^{-14}, and 10^{-15} s determine the values of $T_{g\beta}/T_{g\alpha}$ = 0.54, 0.57, 0.59, and 0.62 respectively. These possible values of $T_{g\beta}/T_{g\alpha}$ are consistent with 0.54 and 0.57 deduced from the change in temperature dependence of $\langle u^2(Q,T)\rangle$ of caged dynamics in Fig.27. The agreement supports $T_{g\beta}$ of $Ge_{0.033}As_{0.033}Se_{0.934}$ is somewhere within 180 to 190 K. It is slightly higher than 165 ± 10 K of selenium due to the minor addition of Ge and As. Again, the data from Russina et al.[144], are old but analyzed for the first time to show the universal property of the coupling of caged dynamics to the JGβ and α relaxations in a chalcogenide glass-former.

Materials Advances Accepted Manuscript

View Article Online
DOI: 10.1039/D6MA00279J

Open Access Article. Published on 04 June 2026. Downloaded on 6/5/2026 12:04:33 AM.
This article is licensed under a Creative Commons Attribution 3.0 Unported Licence.

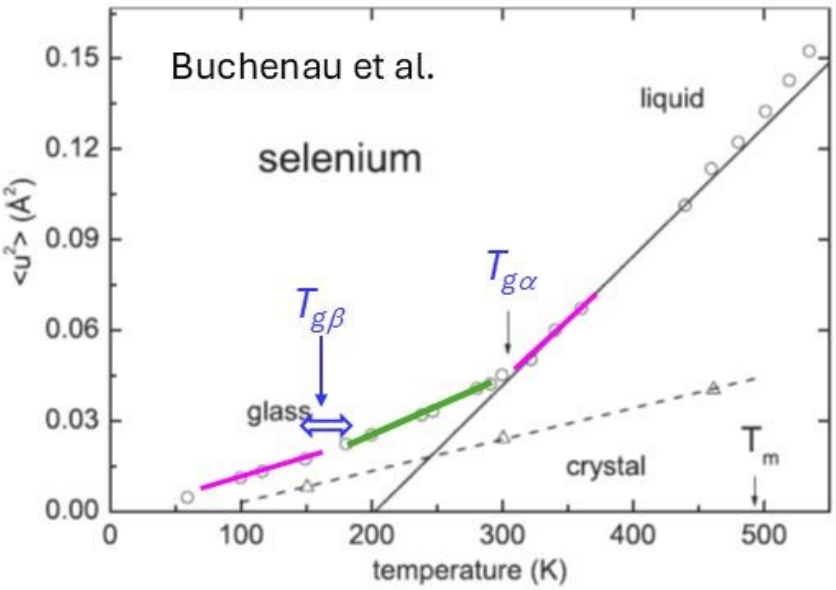

Fig. 25. Mean-square displacements in glassy, liquid and crystalline selenium determined from neutron data for motions with frequencies above 10^{11} Hz. (o) Amorphous, (Δ) crystal. Figure taken from Ref.[140], and reused with permission from Europhys. Lett.

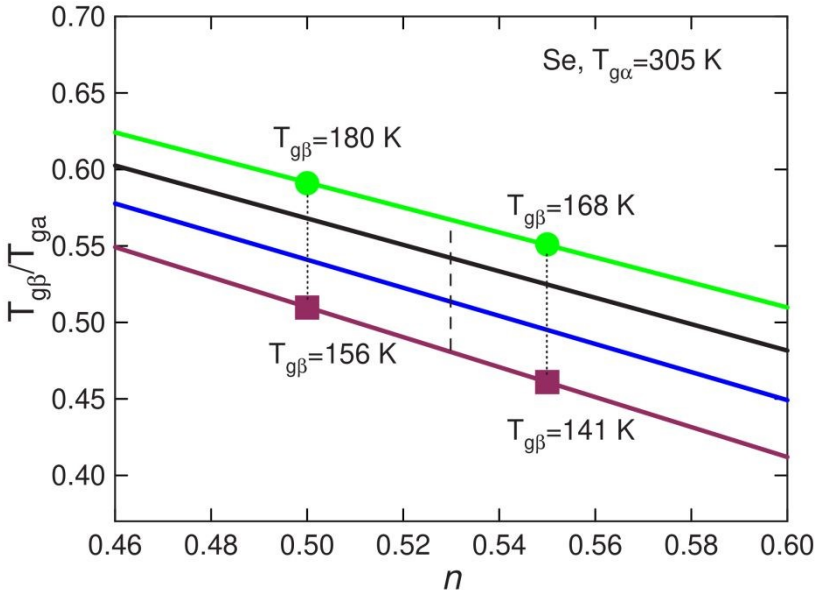

Fig. 26. Plot of $T_{g\beta}/T_{g\alpha}$ versus $n(T_{g\alpha})$ for four judicious choices, 10^{-12}, 10^{-13}, 10^{-14}, and 10^{-15} s of $\tau_{\beta\infty}$. The values of $T_{g\beta}/T_{g\alpha}$ determined for three possible values of n=0.50, 0.53, and 0.55 of selenium are indicated. For the most probable value of n=0.53, $T_{g\beta}$ has values ranging from 147 K to 173 K.

Materials Advances Accepted Manuscript

View Article Online
DOI: 10.1039/D6MA00279J

Open Access Article. Published on 04 June 2026. Downloaded on 6/5/2026 12:04:33 AM.
This article is licensed under a Creative Commons Attribution 3.0 Unported Licence.

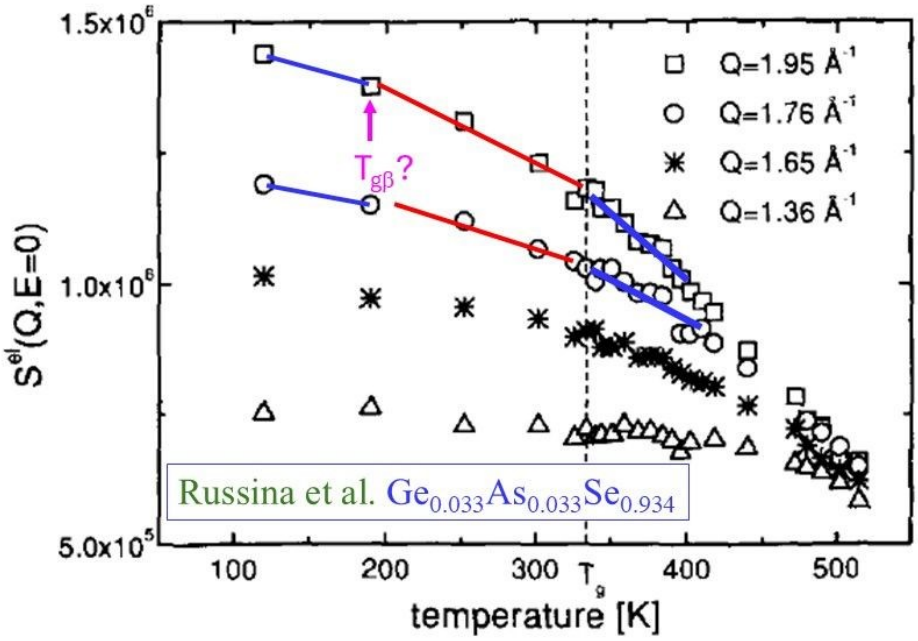

Fig. 27. The temperature dependence of the elastic scattering intensity $S^{el}(Q, E=0)$ of $Ge_{0.033}As_{0.033}Se_{0.934}$ from neutron scattering by Russina et al.[144]. The lines drawn to suggest changes of temperature dependence of caged dynamics at $T_{g\beta}$ and $T_{g\alpha}$.

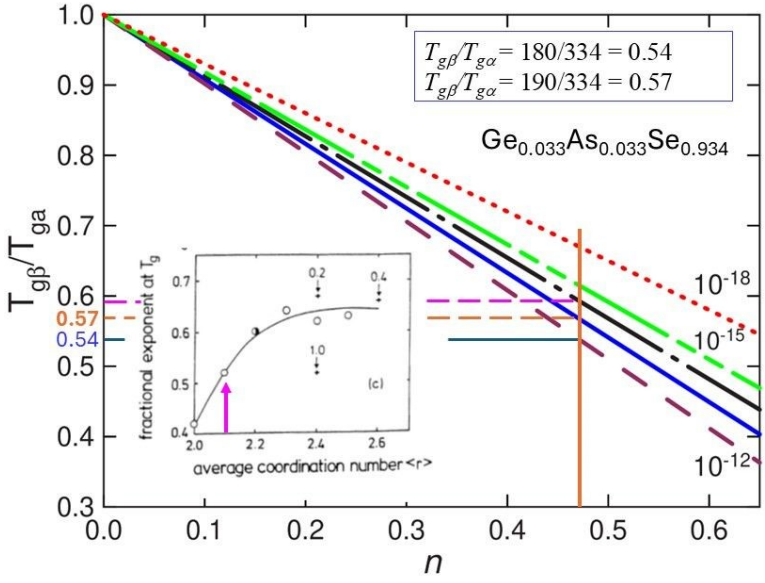

Fig. 28. Plot of $T_{g\beta}/T_{g\alpha}$ versus $n(T_{g\alpha})$ for four judicious choices, 10^{-12}, 10^{-13}, 10^{-14}, and 10^{-15} s, and unlikely choice 10^{-18} s of $\tau_{\beta\infty}$ for $Ge_{0.033}As_{0.033}Se_{0.934}$. The arrow in the inset from Ref.[67] indicates the KWW exponent = 0.52 or n=0.48. The short horizontal lines indicate the possible values of $T_{g\beta}/T_{g\alpha}$=0.54, 0.57, and 0.59.

Materials Advances Accepted Manuscript

View Article Online
DOI: 10.1039/D6MA00279J

Open Access Article. Published on 04 June 2026. Downloaded on 6/5/2026 12:04:33 AM.
This article is licensed under a Creative Commons Attribution 3.0 Unported Licence.

4.3. Termination of caged dynamics by onset of primitive/JGβ relaxation

Another way to verify the coupling of the caged dynamics to the JGβ/primitive is by observing at fixed temperature the termination of the caged dynamics regime at some time of the order of τ_0 due to the onset of the primitive/JGβ relaxation. The time dependence of the mean square displacement $<r^2(t)>$ from the caged dynamics is a power law $\propto t^{\gamma}$, with γ positive and significantly smaller than one. The termination is observed by the change from $<r^2(t)> \propto t^{\gamma}$ to $<r^2(t)> \propto t^{1-n}$ with (1-n) being the exponent of the KWW function in Eq.(1) at time near $\tau_0 \approx t_{\alpha 2,\max}$. The latter is the time at which the non-Gaussian parameter $\alpha_2(t)$ is maximum [11]. At still longer times, $<r^2(t)> \propto t^{1-n}$ changes to $<r^2(t)> \propto t^{1.0}$ of free diffusion. The terminal cooperative α relaxation time τ_α is quantitatively related to $\tau_0 \approx \tau_\beta$ by the CM Eq.(3) involving t_c and n. The generality of the coupling of caged dynamics to primitive/JGβ relaxation is manifested in Figs.29a and 29b for colloidal particles from confocal microscopy [145], Fig.29c for $Zr_{50}Cu_{50}$ [49], Fig.30a for CKN [32,84] and Fig.30b for binary L-J particles by simulations [146,147]. The same was found by MD simulations performed on Li ion diffusion in Li metasilicate, Li_2SiO_3 [147] and ionic liquid 1-ethyl-3-methylimidazolium nitrate ($EMIM^+/NO_3^-$).[147] The data of CKN and analysis given are new.

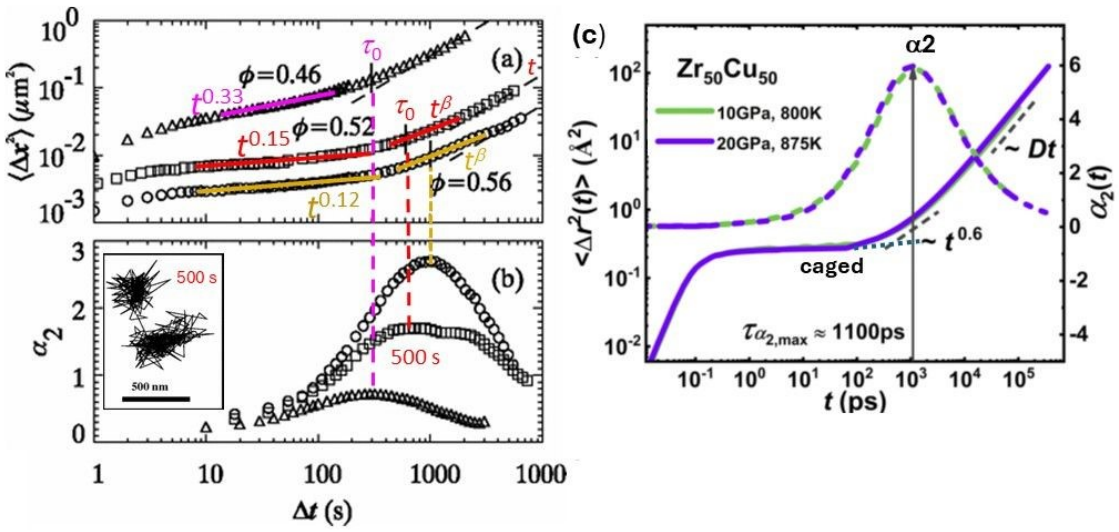

Fig. 29. (a) MSD $<\Delta x^2(\Delta t)>$ for volume fractions ϕ = 0.46, 0.52, and 0.56 in colloidal systems from Ref.[116]. At Δt = 500 s, a typical particle for ϕ = 0.56, shifts position and leaves the cage shown by the inset in (b), and 500 s is identified with τ_0. The lines at short times with slopes γ=0.33, 0.15, and 0.12 indicates t^{γ} dependence of caged particles regime. The lines at long times indicate t^{β} dependence with β= 0.62, The change occurs at ~ τ_0 and also ~ $t_{\alpha 2,\max}$ when the non-Gaussian parameter $\alpha_2(\Delta t)$ assume its maximum shown in (b) and as indicated by the vertical dashed lines. Figure adapted from Ref.[145] and reused with permission from Science. (c) Isochronal superposition of $\Delta r^2(t)$, $\alpha_2(t)$, and $F_s(q,t)$ obtained at various T and P at constant $\tau_{\alpha 2,\max}$ ≈1000 ps for $Zr_{50}Cu_{50}$ from Ref.[49]. Figure from Ref.[49] and reused with permission from AIP.

Materials Advances Accepted Manuscript

View Article Online
DOI: 10.1039/D6MA00279J

Open Access Article. Published on 04 June 2026. Downloaded on 6/5/2026 12:04:33 AM.
This article is licensed under a Creative Commons Attribution 3.0 Unported Licence.

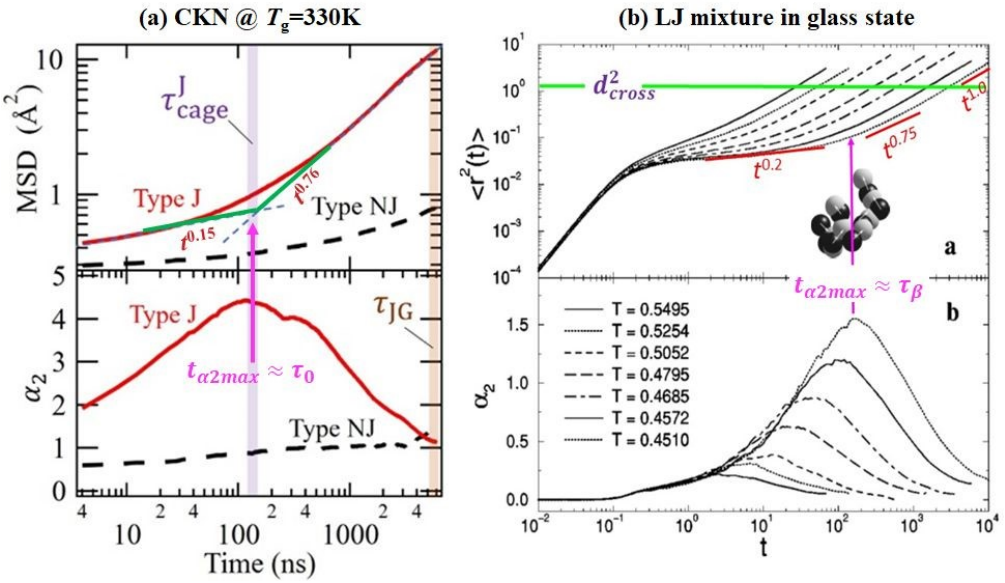

Fig. 30. (a) MD simulations of CKN at 330 K in the glass state [32,84]. The peak of $\alpha_2(t)$ at $t_{\alpha 2,\max}$ corresponds to the time $\sim \tau_0$ when caged dynamics ($t^{0.15}$) is terminated by the onset of the primitive/JGβ relaxation. (b) For the binary LJ mixture, the vertical line indicates the time $t=t^*$ or $t_{\alpha 2,\max}$ at which $\alpha_2(t)$ is maximum for T=0.4510. Note that $t_{\alpha 2,\max}$ is before the subdiffusive $<r^2(t)> \propto t^{0.75}$ regime. Added by the author are the time dependences of the caged particles regime $<r^2(t)> \propto t^{0.2}$, the subdiffusive $<r^2(t)> \propto t^{0.75}$, and the crossover to the Fickian diffusion at $<r^2(t)> = d^2_{cross} \approx 1.25$. The figure is reproduced from Ref.[146], Copyright 1999, APS.

4.4. From caged dynamics to the correlation of Poisson's ratio ν with n

Consideration of caged dynamics is not only important for fundamental understanding of the dynamics, but also has connection to macroscopic properties. An example is its relation to Poisson's ratio. When a material is compressed in one direction, it tends to expand in the two other directions, the Poisson's ratio ν is defined as the ratio between the fraction of expansion divided by the fraction of compression. For isotropic material, ν is related to the infinite frequency bulk and shear elastic constants K_∞ and G_∞ respective by the relation, [148,149,150,151]

$$\nu = \frac{1}{2} - \frac{3}{6K_\infty/G_\infty + 2} \quad (6)$$

In the family of metallic glasses, a clear correlation had been established between the Poisson's ratio ν and plasticity or ductility.[152,153,154,155,156] In the glassy state, the time-dependent density–density correlation function $F(Q,t)$ normalized by the static structure factor $S(Q)$ exhibits a plateau. The plateau appears at times longer than that of the vibration times but shorter than those of the JGβ relaxation and the α-relaxation. The height of the plateau, is referred to in the literature as the Debye-Waller factor $f_0(T)$. The quantity, $1-f_0(T)$, gives the part of the density fluctuations that is frozen or caged in the glassy state, corresponding to the mean-square displacement $<u^2(T)>$

Materials Advances Accepted Manuscript

View Article Online
DOI: 10.1039/D6MA00279J

exclusively contributed by the caged dynamic as shown in Fig.25 for selenium and Fig.27 for $Ge_{0.033}As_{0.033}Se_{0.934}$. There is another relation of f_0 to K_∞/G_∞ given by [148,149],

$$f_0 = \frac{1}{\frac{3K_\infty}{4G_\infty}+1} \quad (7)$$

When combined, the two dependences of ν and f_0 on K_∞/G_∞ leads to the correlation of the Poisson's ratio ν with (1-f_0) of the caged dynamics, which was obtained numerically in Ref.[151] and is given in Fig.31.

Results from molecular dynamics simulations [18,19], quasielastic neutron and dynamic light scattering [156,157,158,159,160], together with the interpretations by the Coupling Model were employed in establishing the correlation between (1-f_0) of caged dynamics and n.[150,151] A simpler way to arrive at the correlation is that both the caged dynamics intensity parameter (1-f_0) and the non-exponentiality parameter n of the α-relaxation are both determined by the anharmonicity of the inter-molecular potential, which governs the dynamics at all times ranging from caged dynamics to the α-relaxation at long times. By combining the two correlations, ν with (1-f_0) and (1-f_0) with n, predicted from theory is the correlation between the Poisson's ratio ν and the parameter n of the structural α-relaxation. The correlation is found in the family of chalcogenide, Ge_xSe_{1-x}, and molecular and polymeric glass-formers.[151] The example from polymers including selenium is shown in Fig.32.

The relation of caged dynamics to the JGβ relaxation and α-relaxation predicted by the CM as discussed in Sections 4.1 and 4.3 was applied successfully in Ref.[150] to explain the interesting correlation found empirically between ductility and Poisson's ratio in materials.[152,153]

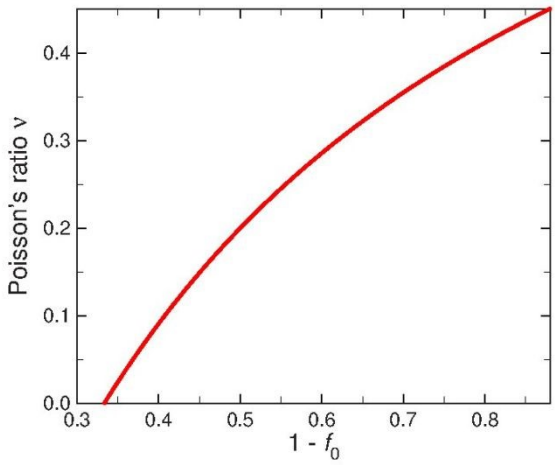

Fig. 31. Plot of Poisson's ratio versus 1-f_0. Figure taken from Ref.[151] and reused with permission from Elsevier.

Open Access Article. Published on 04 June 2026. Downloaded on 6/5/2026 12:04:33 AM.
This article is licensed under a Creative Commons Attribution 3.0 Unported Licence.

Materials Advances Accepted Manuscript

View Article Online
DOI: 10.1039/D6MA00279J

Open Access Article. Published on 04 June 2026. Downloaded on 6/5/2026 12:04:33 AM.
This article is licensed under a Creative Commons Attribution 3.0 Unported Licence.

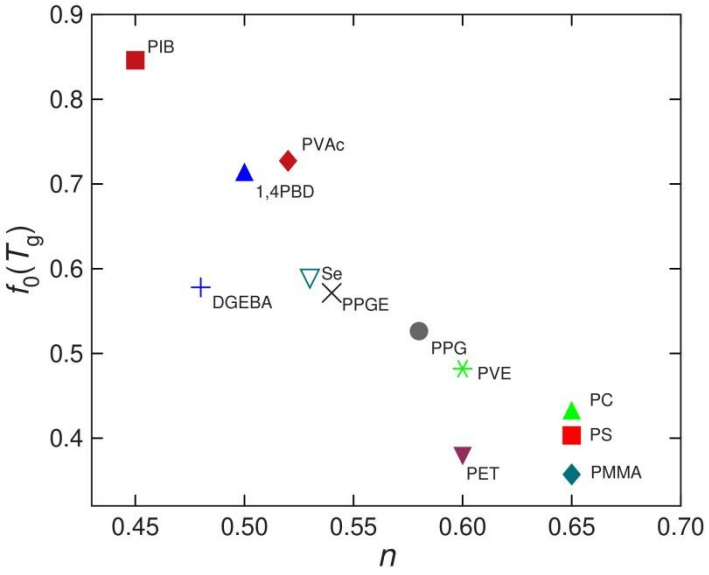

Fig. 32. Plot of $f_0(T_g)$ against the non-exponentiality or coupling parameter n for polymers. Figure taken from Ref.[151] and reused with permission from Elsevier.

Data of molecular, polymeric, and a limited number of Ge_xSe_{1-x} glasses were used to support the correlations established before [151]. Here we include more chalcogenides to enrich the correlations. In Table 1, collected are the parameters, average coordination number <r>, fragility index m, n, and ν of six Ge_xSe_{1-x} glasses. The correlations of all parameters to change of composition is evident. The value of n decreases with increasing Ge fraction. The trend suggests the values of n of $GeSe_2$ and GeSe with Ge fraction larger than Ge_3Se_7 can be smaller than 0.35. From Eqs.(2) and (3), one obtains,

$$\log\tau_\alpha - \log\tau_\beta \approx n\log(\tau_\alpha/t_c), \tag{8}$$

which says the separation between the JGβ relaxation from the α-relaxation is proportional to n. The relaxation map of $GeSe_3$ having n=0.36 in Fig.10 shows that the separation, $\log\tau_\alpha - \log\tau_\beta$, is small. From Eq.(8) and the expected smaller values of n in $GeSe_2$ and GeSe, it follows that the JGβ relaxation is even closer to the α-relaxation than $GeSe_3$ and harder to resolve. This explains why the JGβ contribution to the mechanical loss modulus $E''(T)$ is so weak in strength and close to the α-relaxation in temperature.[161] In contrast, the $E''(T)$ from JGβ relaxation in PCMs including GeTe, $Ge_2Sb_2Te_5$, and AIST are strong. In the glassy state, the JGβ relaxation is dominant in determining the unique dynamic properties of amorphous PCMs such as the presence of rapid local atomic rearrangement of atoms and relation to crystallization.[162]

The correlation of Poison ratio ν with <r> = 2(x + 1) of Ge_xSe_{1-x} glasses in Table 1 were found in other three systems of chalcogenides, (Ge-Sb-Se), (Ge-[66Sb-34As]-[83Se-17Te]), and (Ge-Sb-[60Se-40Te]) from Ref.[163] The correlation was shown in Fig. 6 of Ref.[163]

Materials Advances Accepted Manuscript

View Article Online
DOI: 10.1039/D6MA00279J

Open Access Article. Published on 04 June 2026. Downloaded on 6/5/2026 12:04:33 AM.
This article is licensed under a Creative Commons Attribution 3.0 Unported Licence.

Table 1. Correlations of Poisson ratio ν, and fragility index *m* with n in the family of Ge_xSe_{1-x}

Glass: Ge_xSe_{1-x}	$<r> = 2(x + 1)$	*m*	*n*	Poisson ratio ν
a-Se	2	64	0.53	0.322
$GeSe_9$	2.2	37	0.40*	0.307
$Ge_{15}Se_{85}$	2.3		0.38*	0.295
$GeSe_4$	2.4	30	0.37*	0.286
$GeSe_3$	2.5	27	0.36	0.281
Ge_3Se_7	2.6	26	0.35*	0.264

* Values were obtained from the curve fit in Fig.2c of Böhmer and Angell [41]. Poisson ratio at room temperatures were taken from Refs. [164,165,166]

4.5 Entangled polymer chains analogy. Interestingly, the coupling of caged dynamics to primitive/JGβ relaxation in different kinds of glass-formers illustrated by Figs.23-30 has an analogy in the dynamics of entangled polymer chains interacting with the interchain potential. The analogy was recognized and developed since 2024. According to the Coupling Model applied to this problem [167,168,169,170,171], like all other many-body interacting systems, the relaxation and diffusion of entangled polymer chains with molecular weight *M* should have the universal properties involving the analogues of caged dynamics, primitive/JGβ relaxation, and terminal α relaxation of glass-formers. The analogues are: (*i*) caged chain dynamics with $<r^2(t)> \propto t^{\gamma}$ with γ positive and significantly smaller than one; (*ii*) the termination of $<r^2(t)> \propto t^{\gamma}$ for caged chain dynamics at or near the primitive chain relaxation time $\tau_0(T,M)$ by changing to $<r^2(t)> \propto t^{1-n}$ with (1-*n*) being the exponent of the KWW correlation function of the terminal chain relaxation; (*iii*) Fickian diffusion with $<r^2(t)> = Dt^{1.0}$ starting at $\tau(T,M)$ and at long times, where

$$\tau(T,M) = [(t_c)^{-n}\tau_0(T,M)]^{1/[1-n]} \quad (9)$$

and $t_c \approx 1$ ns to a few ns. [167,168,169,170,171] The M^2-dependence of $\tau_0(T,M)$ on *M* is well known from the Rouse model [172], and hence the prediction of

Materials Advances Accepted Manuscript

View Article Online
DOI: 10.1039/D6MA00279J

$$\tau(T,M) \propto [\tau_0(T,M)]^{1/[1-n]} = M^{\frac{2}{1-n}} [\zeta_0(T)]^{1/(1-n)}, \quad (10)$$

and

$$D \propto M/\tau(T,M) = M^{1-\frac{2}{1-n}} [\zeta_0(T)]^{1/(1-n)}. \quad (11)$$

Critical examination of data from past and recent experiments and simulations [167,168,169,170,171] had verified the predictions. Examples of data from simulations [173], and the field-gradient (FG) and field-cycling (FC) 1H NMR experiments [174,175], are presented in Fig.33 and Fig.34 respectively together with the predictions from the CM of the time dependence of $\langle r^2(t) \rangle$ and the M-dependence of D.[168] For details see Refs. [167,168,169,170,171].

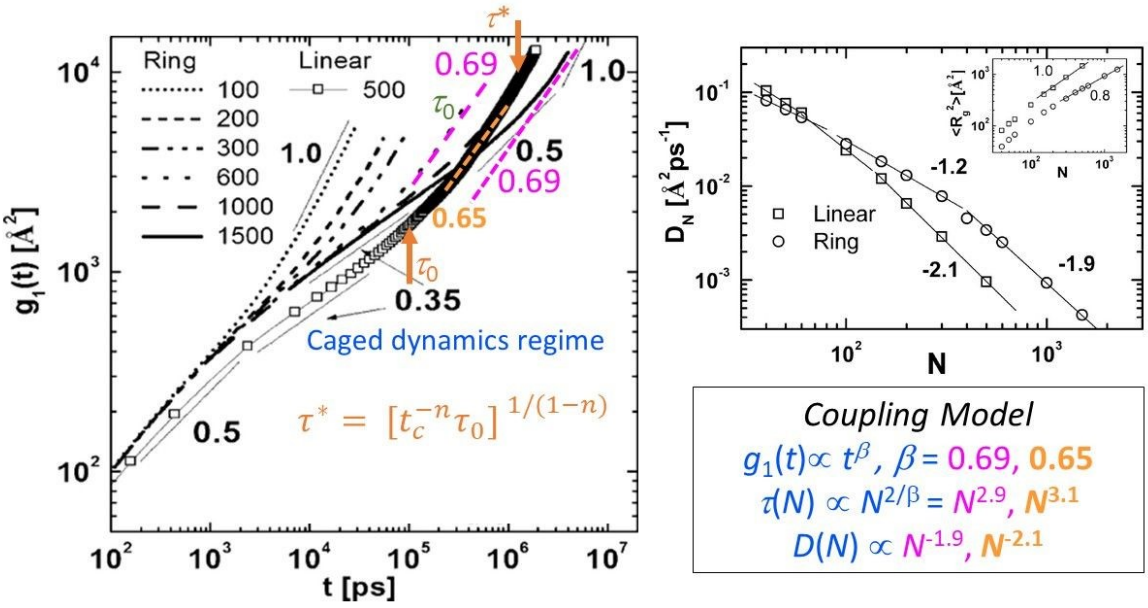

Fig. 33. (Left) Mean-square displacements of monomers $g_1(t)$ for ring (lines) and linear (squares) polyethylene molecules in a melt from Ref. [144]. The limiting slopes are indicated as number and thin lines. (Right) Diffusion coefficients D_N for ring and linear PE molecules in a melt as a function of chain length (the total carbon atom number N). Inset: Scaled center-of-mass mean-square displacements $g_3(t)$ for ring (circles) and linear (diamonds) PE molecules. Figure taken from Ref. [168] and reused with permission from Elsevier.

1.

Open Access Article. Published on 04 June 2026. Downloaded on 6/5/2026 12:04:33 AM.
This article is licensed under a Creative Commons Attribution 3.0 Unported Licence.

Materials Advances Accepted Manuscript

View Article Online
DOI: 10.1039/D6MA00279J

Open Access Article. Published on 04 June 2026. Downloaded on 6/5/2026 12:04:33 AM.
This article is licensed under a Creative Commons Attribution 3.0 Unported Licence.

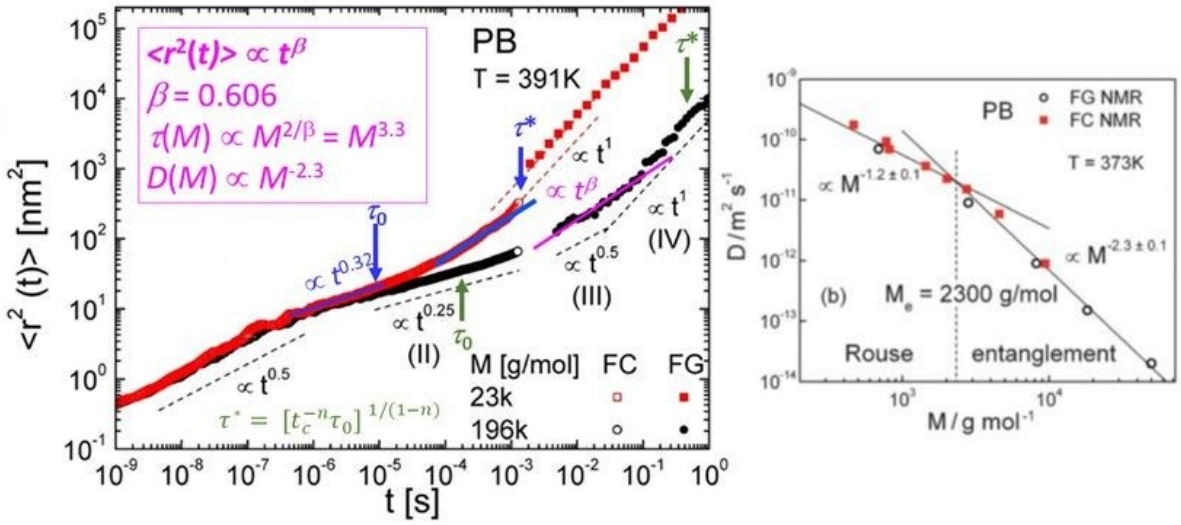

Fig. 34. (Left) MSD of PD196k and PB23 K obtained from FC and FG NMR data at 391 K from Ref.[174]. Dashed lines represent power-laws from tube-reptation theory. The magenta and blue lines $\propto t^{\beta}$ with β=0.606. The inset illustrates the prediction of M-dependence of D by the CM using β=0.606.[174.] (Right) Molar mass dependence of the diffusion coefficient D in polybutadiene (PB) obtained by FC 1H NMR relaxometry and by FG NMR diffusometry from Ref.[175]. Solid lines: power laws with exponents as indicated; the dashed line marks crossover from Rouse to entanglement dynamics at the molar mass close to M_e. Figures are reproduced from Ref.[168] and reused with permission from Elsevier.

5. *T-P* co-invariance of caged dynamics with α and β relaxation at constant τ_α

The strong connections of the caged dynamics to the JGβ and α relaxations suggest it is co-invariant with $\tau_\alpha(T,P)$, $\tau_\beta(T,P)$, and $\beta_K(T,P)$ to changes of P and T at constant $\tau_\alpha(T,P)$. Experiments and simulations have been reexamined to verify this expectation recently and the results were published in 2026.[176]. Exemplified by the nearly constant loss (NCL) in Figs.1a and 1b, the caged dynamics of KDE and propylene carbonate is clearly co-invariant with $\tau_\alpha(T,P)$, $\tau_\beta(T,P)$, and $\beta_K(T,P)$. Neutron scattering experiment by Niss et al. [177] measured the mean square displacements $\langle u^2(T)\rangle$ of cumene at 0.01 MPa and 500 MPa shown in the left panel of Fig.35. The $\langle u^2(T)\rangle$ data measured at all temperatures below and near $T_{g\alpha}$ are entirely contributed by the caged dynamics because the time scale of measurement is nanosecond, and it changes its T-dependence on crossing $T_{g\beta}$ and $T_{g\alpha}$ known from calorimetry. Scaled by the corresponding glass transition temperatures $T_{g\alpha}(P)$, the two sets of $\langle u^2(T,P)\rangle$ data were superposed to form a master curve shown in the right panel of Fig.35. The result verifies the co-invariance of $\tau_\alpha(T,P)$, $\beta_K(T,P)$, and $\langle u^2(T,P)\rangle$ representing the caged dynamics.

The same co-invariance was found in polybutadiene from neutron scattering by Frick et al. [178]. As illustrated by lines drawn in Fig.36a, the $\langle u^2(T,P)\rangle$ contributed by the caged dynamics at ambient pressure changes temperature dependence on crossing $T_{g\beta}$ and $T_{g\alpha}$, showing once more

Materials Advances Accepted Manuscript

View Article Online
DOI: 10.1039/D6MA00279J

Open Access Article. Published on 04 June 2026. Downloaded on 6/5/2026 12:04:33 AM.
This article is licensed under a Creative Commons Attribution 3.0 Unported Licence.

the property considered in Section 4.1. In addition, the $\langle u^2(T,P)\rangle$ at elevated pressures can be scaled to a master curve by taking the thermodynamic glass transition temperature $T_{g\alpha,P}$ at pressure P as a scaling parameter [178]. The master curve is shown in Fig.36b. After scaling $\langle u^2(T,P)\rangle$ by $T_{g\alpha,P}$, the dynamics in the data for different pressures are now compared effectively at some constant value τ_α. The success in obtaining the master curve is equivalent to finding the caged dynamics and all faster JGβ and slower α relaxations in $\langle u^2(T,P)\rangle$ are co-invariant to changes of T and P while τ_α is kept constant.

Another way to verify the co-invariance in the time domain is by molecular dynamics simulations on two metallic alloys $Zr_{50}Cu_{50}$ and $Zr_{50}Cu_{44}Al_6$ at various combinations of T and P to extract the time dependence of the self-intermediate scattering function, $F_s(q,t) = \frac{1}{N}\langle\sum_{i=1}^{N}\exp[\boldsymbol{q}\cdot(\boldsymbol{r}_i(t)-\boldsymbol{r}_i(0))]\rangle$.[49] Here, $\boldsymbol{q}$ is the wavevector corresponding to the first peak position of the structure factor, the MSD, $\langle\Delta r^2(t)\rangle = \frac{1}{N}\langle\sum_{i=1}^{N}[\boldsymbol{r}_i(t)-\boldsymbol{r}_i(0)]^2\rangle$, and the non-Gaussian parameter, $\alpha_2(t) = 3\langle\Delta r^4(t)\rangle/5\langle\Delta r^2(t)\rangle^2-1$. The $\tau_\alpha(T,P)$ is determined from $F_s(q,t)$ at T and P. On varying T and P but keeping $\tau_{\alpha2,\max}(T,P)$ constant, the results of $\langle\Delta r^2(t)\rangle$, $F_s(q,t)$, and $\alpha_2(t)$ for several combinations of T and P are shown in Figs.36c and 36d for $Zr_{50}Cu_{50}$. The plateau in $F_s(q,t)$ or the weak temperature dependence of $\langle\Delta r^2(t)\rangle$ appearing at shorter times is contributed by the caged dynamics, which is terminated by the onset of the primitive/JGβ process identified by the power law $\sim t^{0.6}$ in the figure. The $\alpha_2(t)$ obtained at T and P exhibits a peak at time $\tau_{\alpha2,\max}(T,P)$ shorter than $\tau_\alpha(T,P)$. The former can be taken as a characteristic time of the dynamics faster than the α-relaxation, which include the caged molecules and the JG β relaxation. It can be seen in Figs.36c and 36d that the entire time dependences of the MSD, $\langle\Delta r^2(t)\rangle$ and $F_s(q,t)$, as well as $\alpha_2(t)$ obtained at different pressures with $\tau_{\alpha2,\max}(T,P)$ kept constant obey isochronal superposition. Thus, the time domain simulation data of $Zr_{50}Cu_{50}$ and $Zr_{50}Cu_{44}Al_6$ (not shown) verify the co-invariance of $\tau_\alpha(T,P)$, $\tau_\beta(T,P)$, $\beta_K(T,P)$, and $\Delta_c(T,P)$ of caged dynamics.

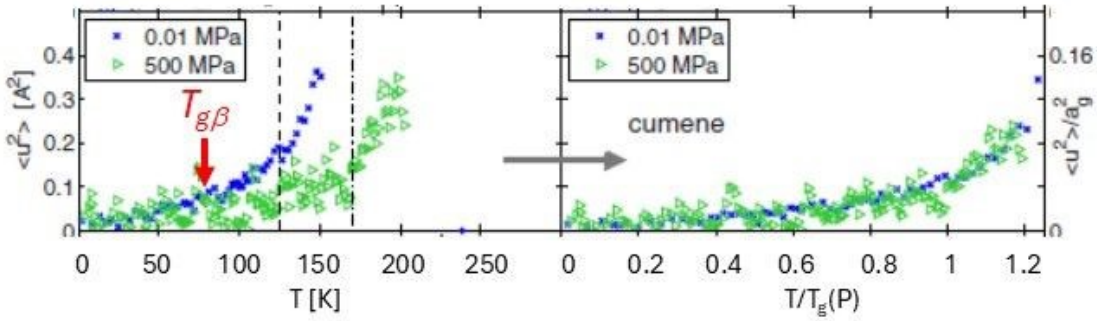

Fig. 35. The MSD of cumene at atmospheric pressure and at 500 MPa. The left-hand-side of the figure shows $\langle u^2(T,P)\rangle$ and temperature on an absolute scale. The dashed lines indicate $T_{g\alpha}$, the dash-dotted lines $T_{g\alpha}$ at high pressure. The temperature scale in the right-hand-side of the figure is scaled by the pressure-dependent $T_g(P)$ and the y-axis is scaled with $a^2 \propto \rho^{2/3}$ evaluated at [$T_g(P)$, P]. Figure adopted from Ref.[177] and reused with permission from APS.

Materials Advances Accepted Manuscript

View Article Online
DOI: 10.1039/D6MA00279J

Open Access Article. Published on 04 June 2026. Downloaded on 6/5/2026 12:04:33 AM.
This article is licensed under a Creative Commons Attribution 3.0 Unported Licence.

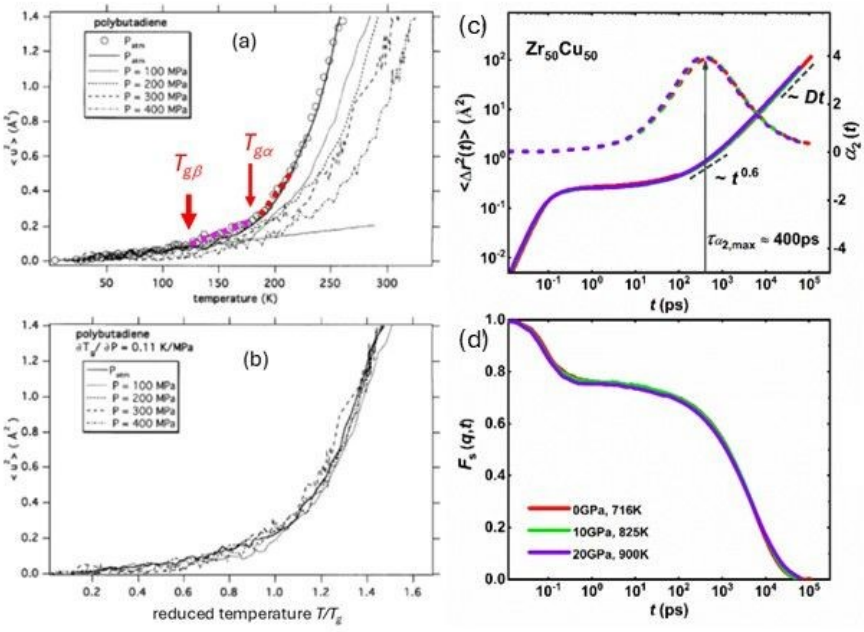

Fig. 36. (a) MSD of polybutadiene as a function of T at different pressures from Ref.[178]. The black straight line corresponds to a linear extrapolation of the low temperature behavior. The magenta and red broken lines bring out the changes of T-dependence of $<u^2(T,P_{atm})>$ at $T_{g\beta}$ and $T_{g\alpha}$. (b) Master curve for the MSD by rescaling data from (a) by a P-dependent shift factor of dT_g/dP=0.11 K/MPa. (c) and (d) Isochronal superposition of $\langle \Delta r^2(t)\rangle$, $\alpha_2(t)$, and $F_s(q,t)$ obtained at various T and P at constant $\tau_{\alpha 2,\max}(T,P) \approx 400$ ps for metallic alloy $Zr_{50}Cu_{50}$. Figures. (a) and (b) adopted from Ref. [178], and Figs. (c) and (d) from Ref.[49] and reused by permission of Elsevier.

6. Reduction of τ_α to $\tau_0 \approx \tau_\beta$ by nano-confinement

The α-relaxation is a cooperative many-body process and dynamically heterogeneous with length scales $\xi_\alpha(T)$ that is material and temperature dependent. The multidimensional ^{13}C solid-state exchange NMR experiment was used to determine $\xi_\alpha(T)$ of dynamic heterogeneities in different glass-formers. The experiment on PVAc at $T = T_g$ +9 K yields $\xi_\alpha(T)$=3.7 nm. [11,179.] Values of $\xi_\alpha(T)$ for glycerol are 1.3 nm for $T = T_g$ +10 K. For OTP, $\xi_\alpha(T)$ ranges from 2.2 nm to 2.9 nm at $T = T_g$ +9 K.[179] The size of $\xi_\alpha(T)$ at T_g can be much larger. Based on these estimates of $\xi_\alpha(T)$ above T_g and its expected monotonic increase with decrease in temperature, it is clear that the α-relaxation is severely modified if confined within spaces with size of the order of nanometers. According to the CM equation, $\tau_\alpha(T) = [(t_c)^{-n(T)}\tau_0(T)]^{1/[1-n(T)]}$, if the size of confinement d_{conf} is smaller than $\xi_\alpha(T)$ the coupling parameter $n(T)$ is reduced to zero, the observed $\tau_{\alpha,conf}(T)$ observed is the primitive relaxation time $\tau_0(T)$ of the bulk material or approximately $\tau_\beta(T)$. Nano-confinement with $d_{conf} < \xi_\alpha(T)$ have been accomplished experimentally in 3- or 2-dimensional spaces of nanometer

Materials Advances Accepted Manuscript

View Article Online
DOI: 10.1039/D6MA00279J

size, at free surface of bulk material, and in supported or free-standing nanometer thin films [11]. In all cases the CM prediction, $\tau_{\alpha,conf}(T)\approx\tau_0(T)\approx\tau_\beta(T)$ had been verified. The following are some examples.

6.1 Poly(methylphenylsiloxane) PMPS

Schönhals et al. [180,181,182] studied PMPS (M_w=1000 g/mol, T_g=212 K) confined in random nanoporous glasses with mean pore dimensions of 2.5 nm, 5.0 nm, 7.5 nm and 20 nm by dielectric spectroscopy, calorimetry, and quasielastic neutron scattering. In all pores, the confined PMPS had faster α-relaxation than the bulk (see Fig.37). When the T-dependence of τ_α is still VFTH-like (bulk or confined in 20 and 7.5 nm pores), the dielectric strength Δε of PMPS decreases with increasing temperature, typical for structural α-relaxation. However, $\tau_{\alpha,conf}(T)$ or $\tau_{\alpha,nano}(T)$ confined in 2.5 nm pores has its T-dependence changed to Arrhenius dependence $\tau_\infty\exp(E_a/k_BT)$. The activation energy E_a is 40 kJ/mol and $\tau_\infty=10^{-12.7}$ s, like those of a primitive/JGβ relaxation. Confirmation comes from the good agreement between τ_0 calculated from τ_α of the bulk polymer at one temperature as shown in the figure. This is confirmed by the accompanying change in the T-dependence of the dielectric relaxation strength $\Delta\varepsilon(T)$ to increasing with increasing temperature (see lower inset), a characteristic of localized molecular motion and all JGβ relaxations.

Neutron scattering experiments were carried out for PMPS.[180,182] The temperature dependence of $\langle r^2\rangle_{eff}$ for bulk PMPS and PMPS confined in 7.5, 5.0 and 2.5 nm pores are shown in the upper inset of Fig.37. On increasing temperature, the first rise of $\langle r^2\rangle_{eff}$ in the vicinity of 100 K is due to the fast methyl group rotation. This is a localized and independent relaxation and therefore it is not much influenced by the confinement. After this step rise, $\langle r^2\rangle_{eff}$ in bulk and confined in 7.5 and 5.0 nm pores, exhibits a slow increase of $\langle r^2\rangle_{eff}$ with temperature contributed by caged dynamics and the second step increase in T-dependence on crossing $T_{g\alpha}$, as other materials in Figs.23,24,25,27. This step increase of $\langle r^2\rangle_{eff}$ is absent in the case of PMPS confined in 2.5 nm because the structural relaxation is converted to the primitive/JGβ relaxation when PMPS is confined in 2.5 nm pores, and the relaxation time $\tau_{\alpha,conf}(T)$ or $\tau_{\alpha,nano}(T)$ is reduced to $\tau_0(T)\approx\tau_\beta(T)$. Therefore, the caged dynamics observed via $\langle r^2\rangle_{eff}$ continues unabated to higher temperatures until $\tau_{\alpha,nano}(T)$ or $\tau_{\alpha,conf}(T)\approx\tau_0(T)\approx\tau_\beta(T)$ becomes comparable to the resolution time of 3 ns of the neutron scattering spectrometer IN16 used. At this temperature, the converted primitive/JGβ relaxation starts to contribute to $\langle r^2\rangle_{eff}$ in addition to the caged dynamics and should be observed as a step increase of $\langle r^2\rangle_{eff}$. Indeed, the step increase was observed at ~ 360 K (upper inset), and it is consistent with the temperature at which the Arrhenius dependence of $\tau_{\alpha,conf}(T)$ of PMPS confined in 2.5 nm pores extrapolated to higher temperatures is close to 3 ns. It is worthwhile to point out $\langle r^2\rangle_{eff}$ of bulk PMPS (upper inset) also has a step increase at T~280 K. This is due to the merged α and JGβ relaxation of bulk PMPS entering the resolution window of IN16 as evidenced by its $\tau_\alpha(T)$ is near 1 - 3 ps at T~280 K in Fig.37.

Thin films of 2600 mol. wt. PMPS with thickness ~1.5 to 2.0 nm intercalated within parallel layers of the inorganic layered silicates were studied by dielectric spectroscopy.[183] The α-

Open Access Article. Published on 04 June 2026. Downloaded on 6/5/2026 12:04:33 AM.
This article is licensed under a Creative Commons Attribution 3.0 Unported Licence.
Materials Advances Accepted Manuscript

View Article Online
DOI: 10.1039/D6MA00279J

Open Access Article. Published on 04 June 2026. Downloaded on 6/5/2026 12:04:33 AM.
This article is licensed under a Creative Commons Attribution 3.0 Unported Licence.

relaxation time $\tau_{\alpha,film}(T)$ is several orders of magnitude shorter than $\tau_{\alpha,bulk}(T)$ of the bulk. The thin film under severe chain confinement suggests the coupling parameter n is reduced to zero throughout the film, and $\tau_{\alpha,film}(T)$ becomes the same as $\tau_0(T)$ calculated from the bulk $\tau_{\alpha,bulk}(T)$ and the KWW exponent $\beta_K(T)$=1-$n(T)$ by Eq.(2). Good agreement between $\tau_{\alpha,film}(T)$ and $\tau_0(T)$ was obtained.[184] Similar large change of $\tau_{\alpha,bulk}(T)$ of bulk poly(ethylene oxide) (PEO) was observed by dielectric spectroscopy when it was transformed to ultrathin films with thickness ~ 1 nm confined within the galleries of hydrophilic silicates, sodium-montmorillonite.[185] The finding was again explained by the agreement between $\tau_{\alpha,film}(T)$ and $\tau_0(T)$.[186] The same was found for freestanding polystyrene thin films with thickness of ~ 22 nm [187] and explained in Fig.169 of Ref.[11].

No other theory of glass transition has attempted to explain quantitatively the experimentally observed $\tau_{\alpha,conf}(T)$ of 2.5 nm thin film[180,181,182] of PMPS or the $\tau_{\alpha,film}(T)$ of 1.5 to 2.0 nm intercalated thin films [183] of PMPS. The CM stands alone in able to explain quantitatively the observed $\tau_{\alpha,conf}(T)$ and $\tau_{\alpha,film}(T)$.

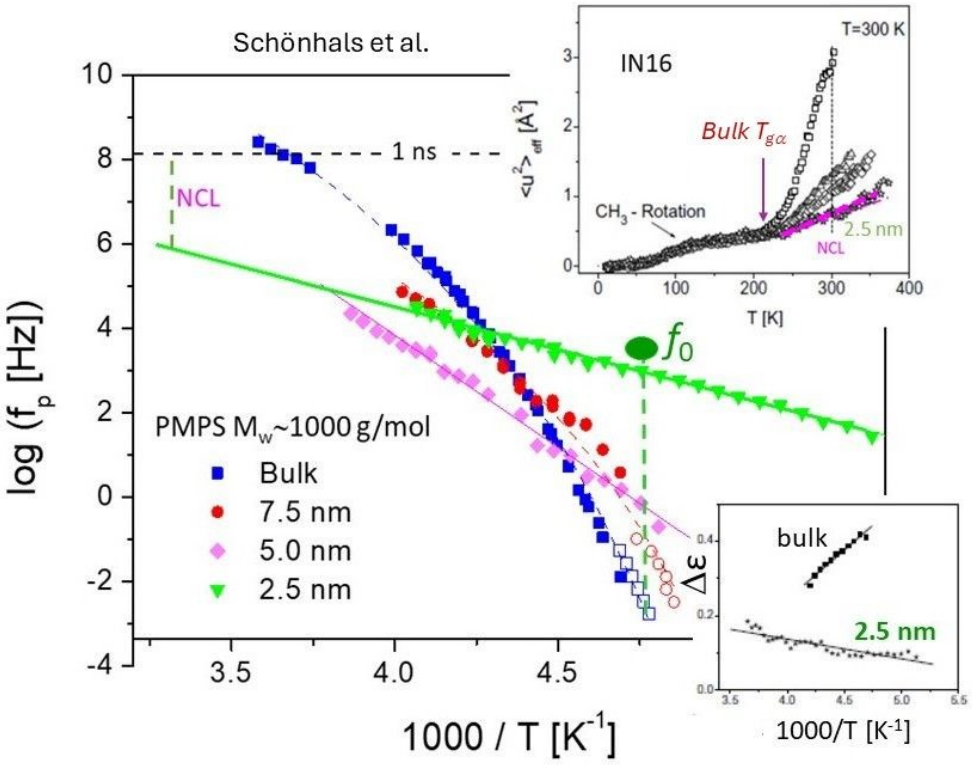

Fig. 37. Relaxation map of PMPS plotting f_p vs. 1/T: (■) bulk, (▲) 7.5 nm, (•) 5 nm, and (□) 2.5 nm. Open-symbols are from TMDSC. Dashed lines are VFT fits. Solid lines are fits by the Arrhenius equation. The primitive f_0 is calculated from f_p at one temperature by the CM. The lower inset shows relaxation strength $\Delta\varepsilon$ vs. 1/T: (■) bulk, (•) 2.5 nm. The difference in T-dependence indicates the α-relaxation becomes the JGβ when confined in 2.5 nm pores. The upper inset presents the T-dependence of $\langle r^2\rangle_{\text{eff}}$ from neutron scattering for the different pore sizes: *open squares* (bulk), *open circles* (7.5 nm), *open diamonds* (5 nm), *open triangles* (2.5 nm). Figures adopted from Ref.[11] and reproduced with permission from Elsevier.

Materials Advances Accepted Manuscript

View Article Online
DOI: 10.1039/D6MA00279J

Open Access Article. Published on 04 June 2026. Downloaded on 6/5/2026 12:04:33 AM.
This article is licensed under a Creative Commons Attribution 3.0 Unported Licence.

Materials Advances Accepted Manuscript

6.2 Glycerol and prilocaine.

Studies of the change in dynamics of molecular glass-formers in nano-confined spaces from that of the bulk were made recently and published in the literature. Examples are the nano-confined glycerol [188] and prilocaine [189] with the quantitative explanations from the CM given in Ref.[190] and Ref.[191] respectively. The data of $\tau_{\alpha,conf}(T)$ or $\tau_{\alpha,nano}(T)$ of glycerol confined in 1.16 nm pore size of zeolitic imidazolate framework (ZIF-8), and prilocaine confined in 1 nm pores of molecular sieves are presented in Figs.38a and 38b respectively. Shown also are the primitive $\tau_0(T)$ calculated from the bulk $\tau_\alpha(T)$ to demonstrate once again verification of the CM prediction of $\tau_{\alpha,conf}(T)\approx\tau_0(T)$ when the condition $d_{conf} < \xi_\alpha(T)$ is satisfied.[190,191] So far, other theories have not attempted to predict quantitatively the structural relaxation time of these two nano-confined glass-formers to compare with the experimentally observed value of $\tau_{\alpha,conf}(T)$.

Included in Fig.38a are results of bulk glycerol from the quasielastic γ-ray scattering experiment using time-domain interferometry (TDI) by Saito et al.[82] They were able to resolve the JGβ relaxation from the α-relaxation in glycerol, and determine its relaxation times $\tau_\beta(q,T)$ at q=31, 41, and 58 nm^{-1}. The α-relaxation times $\tau_\alpha(q,T)$ at q=15 nm^{-1} from TDI are also included in Fig.38a. The TDI time spectra [82] of the α-relaxation at q=15 nm^{-1} were well fitted by the KWW function with $\beta_{\rm KWW}$ consistent with that used to fit the dielectric α loss peak [192]. For example, $\beta_{\rm KWW}$=0.7 at 220 K for both TDI and dielectric. Moreover, as shown in Fig. 38a and in Ref.[86], $\tau_\beta(q,T)$ at q= 41 and 58 nm^{-1} from TDI are nearly the same as $\tau_{\alpha,conf}(T)$ of glycerol confined in 1.16 nm pores of ZIF-8, and the calculated primitive $\tau_0(T)$ is only slightly shorter. Besides these remarkable results, it is important to recognize that while the JGβ relaxation is not resolved by dielectric spectroscopy, it is resolved in the TDI spectra at different q values. Thus, the existence of the JGβ relaxation in glycerol is guaranteed. It is not resolved in isothermal dielectric spectra due to its weaker dielectric strength than that of the α-relaxation, but resolved after aging for five weeks.

The universal presence of the JGβ relaxation acting as the precursor of the structural α-relaxation is predicted by the CM, since the primitive relaxation is a part of it. JGβ relaxation time $\tau_\beta(T)$ approximately the same as $\tau_0(T)$. The latter combined with Eq.(2) leads to the relation,

$$\log\tau_\alpha(T) - \log\tau_\beta(T) \approx [1-\beta_K(T)]\log[\tau_\alpha(T)/t_c]. \qquad (12)$$

This relation predicts the separation of the JGβ relaxation from the α relaxation in glass-formers is proportional to $[1-\beta_K(T)] \equiv n(T)$ for any chosen value of $\tau_\alpha(T)$. All these properties of the JGβ relaxation are proven valid whenever it is resolved by experiments and simulations [11]. However, the JGβ relaxation in many polar glass-formers with larger β_K values [20] including glycerol is not resolved in dielectric spectroscopy, although the excess wing on the high frequency flank of the α-loss peak suggest its presence. The situation allowed Pabst et al. [193] and Böhmer et al.[194] to ignore the universal presence of the JGβ relaxation whether resolved or unresolved, and proposed their own interpretation of the dielectric spectra. They separate the dielectric loss into

View Article Online
DOI: 10.1039/D6MA00279J

Open Access Article. Published on 04 June 2026. Downloaded on 6/5/2026 12:04:33 AM.
This article is licensed under a Creative Commons Attribution 3.0 Unported Licence.

the two contributions. The slower and intense one with narrow frequency dispersion was attributed to come from the cross-correlation term but it is not the structural relaxation. They assumed the structural relaxation comes from the faster and less intense self-correlation term, as illustrated for glycerol by the lower inset in Fig.38a. It has the generic line shape as found by photon correlation spectroscopy (PCS) in different glass-formers,. The existence of the JGβ relaxation in glycerol as revealed by TDI contradicts the assertion[193,194] that the self-correlation term in dielectric loss spectrum is the structural α-relaxation and it has the generic shape as observed by PCS [163,164] (as shown by the lower inset in Fig.38a). The assertion ignores the presence of the JGβ relaxation now proven by TDI, and it overlaps the purported self-correlation term. Moreover, the TDI experiment on glycerol found the same spectra as observed by dielectric relaxation, i.e. the narrow and slow α-relaxation with βK =0.70 and accompanied by a weaker, broader and faster JGβ relaxation.

Propylene carbonate (PC) is another glass-former having its dielectric loss spectrum interpreted the same way as glycerol by Pabst et al.[193] and Böhmer et al.[194]. If one recalls from Fig.1b that the entire dielectric loss spectrum of PC is invariant to changes of T and P while $\tau_\alpha(T,P)$ is kept constant. This property has been explained by the CM in Section 3, where the loss spectrum is interpreted as composed of an intense α-loss peak and an unresolved JGβ relaxation (excess wing) This property has been explained by the CM in Section 3. It is unclear how Pabst et al.[193] and Böhmer et al[194] can explain the same property of PC.

The interpretation of dielectric data by Pabst et al.[193] and Böhmer et al[194] had been refuted by experiments and simulations in Refs.[11,196] by the present author, by Moch et al. [197,198], and by Richert[199,] , and the latest one is by Aresse-Igor [200]. It is pertinent to cite here the finding of Moch et al. [197] and their conclusion from it that dielectric spectroscopy is the rare molecular-level reorientation techniques that measures dynamical cooperativity directly and the frequency dispersion of the α-relaxation truthfully. None of these opposing papers were cited by Dyre and Ediger in their Perspective [201] published in 2026. Instead, they exclusively promote the generic line shape of the α-relaxation and the related generic linear-response losses proportional to $\omega^{1/2}$ at high frequencies. The assertion of a generic line shape observed by photon correlation spectroscopy for all glass-formers [163,164] was also contradicted by data published recently by Rössler and Becher [202] where they stated "While five systems virtually follow the generic relaxation [24,28] recently published by Blochowicz and coworkers (red crosses), three systems, namely, DMP, o-terphenyl, and salol, show significant departures. A Kohlrausch function interpolates the decay curves; the stretching parameter varies in the range β_K= 0.52–0.72 (Table I)." The references 24 and 28 in their statement quoted are Refs.[193,194] herein.

In Refs.[11,196], a reason was given for the narrow dielectric loss peak of polar molecules such as glycerol and propylene carbonate changing to approach the generic shape of the susceptibility $\chi''(\omega)$ when observed by light scattering[193,194] or mechanical shear loss modulus[201]. Using glycerol as an example, the much weaker dielectric strength of the JGβ relaxation ensures the dielectric loss peak is effectively contributed entirely by the α-relaxation. The fit by the KWW function with β_{KWW}=0.70 of the intense and narrow loss peak represents the α-relaxation is supported by TDI experiment [82]. The JGβ relaxation is unresolved and appears as an excess wing

Materials Advances Accepted Manuscript

View Article Online
DOI: 10.1039/D6MA00279J

on the high frequency side. On the other hand, when measured by light scattering or shear modulus, the relaxation strength of the JGβ relaxation is enhanced to make its contribution to $\chi''(\omega)$ comparable to that of the α-relaxation. Consequently, the $\chi''(\omega)$ on the high frequency side of the α-relaxation is broadened to resemble somewhat the generic shape [193,194], and at high frequencies $\chi''(\omega) \propto \omega^{\lambda}$ with λ having values near 0.5.[201]

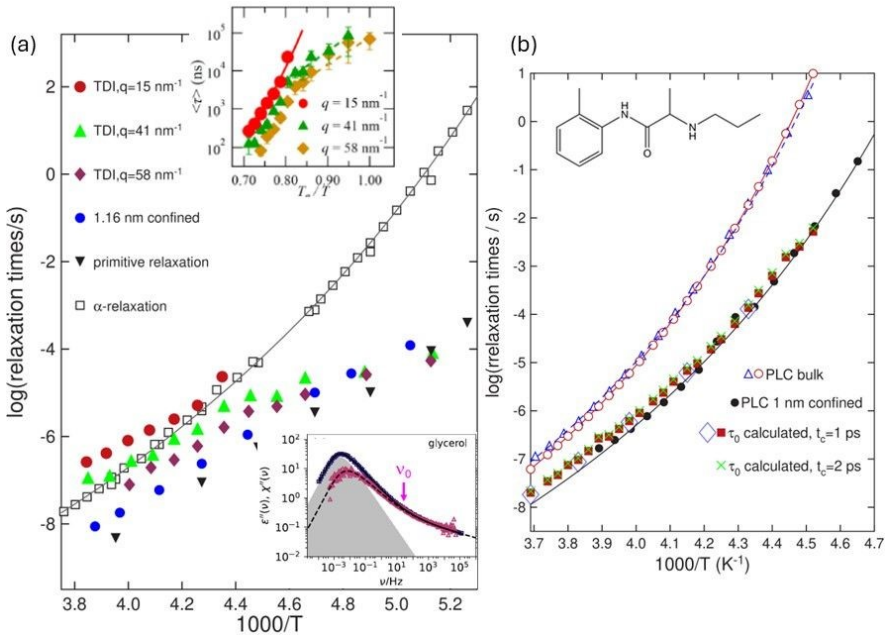

Fig. 38. (a) Arrhenius plot of relaxation times of glycerol: confined in ZIF-8 (blue circles); bulk glycerol (open squares) and the VFT fit; measured by TDI at three different q's; the primitive τ_0 (▼)[161]. The upper inset shows the TDI data [82], and reproduced with permission from APS. The lower inset from Ref.[194] was used therein to identify contribution of dipolar cross-correlation (shaded area) to ε"(ν) and compare with light-scattering data (purple), the cross-correlation contributions, and the dashed line obtained by subtracting the cross-correlation contribution from the ε"(ν) data.[193,194] The figure is adopted from Ref.[194] with permission from AIP. (b) Various relaxation times of bulk prilocaine and confined in 1 nm pores of molecular sieves explained quantitatively by the Coupling Model [191]. The figure is taken from Ref.[194], and reproduced with permission from PCCP.

6.3 Surface Diffusion of OTP, TPD, $Pd_{40}Cu_{30}Ni_{10}P_{20}$, ethylcyclohexane

Surface diffusion coefficients $D_S(T)$ of several molecular glass-formers including indomethacin (IMC), nifedipine (NIF), and ortho-terphenyl (OTP) [203,204,205] were measured at temperatures slightly above and mostly below the bulk glass transition temperature T_g using the method of surface-grating decay. The surface diffusion coefficients $D_S(T)$ are found to be many orders of magnitude larger than the bulk diffusion coefficients $D_V(T)$. The case of OTP [119,203] is presented

Open Access Article. Published on 04 June 2026. Downloaded on 6/5/2026 12:04:33 AM.
This article is licensed under a Creative Commons Attribution 3.0 Unported Licence.

Materials Advances Accepted Manuscript

View Article Online
DOI: 10.1039/D6MA00279J

Open Access Article. Published on 04 June 2026. Downloaded on 6/5/2026 12:04:33 AM.
This article is licensed under a Creative Commons Attribution 3.0 Unported Licence.

in Fig.39. By using the n=0.50 for OTP [206,207] together with the choice of $\tau_\alpha(T_g)=10^3$ s to define T_g, the CM Eq.(2) gives $\tau_\alpha(T_g)/\tau_0(T_g)=10^6$, which is in order of magnitude agreement with the experimentally observed surface diffusion enhancement $D_s(T_g)/D_v(T_g)$ in OTP as shown in Fig.39. The same quantitative success was accomplished for indomethacin [208] and *N*,*N'*-Bis(3-methylphenyl)-*N*,*N'*-diphenylbenzidine (TPD) [119].

Moreover in Fig.39 for OTP, the JGβ relaxation times $\tau_\beta(T)$ are in approximate agreement with $\tau_0(T)$ calculated from $\tau_\alpha(T)$. Above T_g, the shift of $\tau_0(T)$ with temperature is parallel to that of $D_s(T)$. Below T_g, the temperature dependence of $\tau_\beta(T)$ is approximately the same as $D_s(T)$, consistent with the prediction from the CM. There are other theories predicting surface diffusion is enhanced compared to the bulk. These include the Random First Order Transition (RFOT) Theory [55.56]. and the Elastically Collective Nonlinear Langevin Equation (ECNLE) theory [60]. However, no attempt has been made to apply these theories to compute either the surface diffusion coefficient or relaxation times for specific material to compare with experiments [125].

The surface diffusion coefficient $D_s(T)$ of the metallic glass, $Pd_{40}Cu_{30}Ni_{10}P_{20}$ was measured by the method of surface-grating decay [209]. $D_s(T_g)$ was found to be more than eight orders of magnitude larger than the bulk diffusion coefficient $D_v(T_g)$. The CM was applied [210] in a similar manner as in the case of OTP and TPD and predict correctly the large difference between $D_s(T_g)$ and $D_v(T_g)$ as shown in Fig.40. For details, see Ref.[210].

The JGβ relaxation in the molecular glass-former ethylcyclohexane (ECH) is located close to the α-relaxation and the two relaxations overlap [213,214,215]. Consequently, the frequency dispersion of the α-relaxation at temperatures above T_g is artificially broadened and the actual stretch exponent β_{KWW} of the Kohlrausch correlation function or coupling parameter n=(1-β_{KWW}) cannot be determined from the dielectric and mechanical spectra [216]. Nevertheless, the actual value of $n\approx$0.30 was deduced from dielectric data of the structurally close-related cyanocyclohexane (CNCH).[216] The calculated value of the primitive relaxation time $\tau_0(T)$ at T_g is consistent with the experimental JGβ relaxation times $\tau_\beta(T)$ near T_g from dielectric spectroscopy.[216] Below T_g the dielectric $\tau_\beta(T)$ is also compatible with the JGβ relaxation time $\tau_{ac}(T)$ from adiabatic calorimetry measurements by Ramos et al. [217] (see inset in Fig.41). Surface diffusion measurements performed on ECH by Tylinski et al. in Ref.[218] provide the surface diffusion times $\tau_{surface}(T)$. Unfortunately, the incorrect n value deduced from the fit of the artificially broadened dielectric α-loss peak in Refs. [211,212,213] was used in by Tylinski et al.[218] to test the CM prediction of $\tau_{surface}(T)\approx\tau_0(T)\approx\tau_\beta(T)$. The concocted CM prediction was found to contradict experimental result [218], but naturally this conclusion by the Tylinski et al. [218] is not real. It is manufactured by the use of the inappropriately inflated value of n in Ref. [218] This misunderstanding was rectified subsequently in Ref.[216] by using the suitable and justified value of n near 0.30, and approximate agreement of $\tau_{surface}(T)$ with the calculated $\tau_0(T)$, and the experimental $\tau_\beta(T)$ and $\tau_{ac}(T)$ are restored as shown in Fig.41. Reconciliation of the CM with the data of Tylinski et al.[218] also was made in the 2024 paper [125] in honor of the many outstanding experimental works of Ediger. In this paper, other misconception of the CM and its applications are resolved.

Materials Advances Accepted Manuscript

View Article Online
DOI: 10.1039/D6MA00279J

Whether it is diffusion of molecules or atoms at the surface discussed in this section or molecules and polymer confined in nanometer spaces discussed in Sections 6.1 and 6.2, the CM was able to account quantitatively the large change in dynamics from that of the bulk quantitatively for each case. To the best of my knowledge, the current theories [54,55,56,57,57,59,60,61,62] have not done so.

6.4 Surface diffusion of ultrastable, ordinary, and nano-thin film glasses of TPD.

Zhang et al. [219,220,221] investigated the effect of variations in bulk dynamics on the surface diffusion of the molecular glass, *N*,*N'*-Bis(3-methylphenyl)-*N*,*N*'-diphenylbenzidine (TPD) with its ordinary T_g =330 K. They measured $D_S(T)$ of ordinary glass (OG), ultrastable glass (SG), and 12 to 30 nm thin films of TPD. The three forms of TPD have many orders of magnitude differences in $\tau_\alpha(T)$, and different T_g values. However, $D_S(T)$ of these glasses are nearly identical at temperatures below the T_g of bulk OG. The remarkable results suggest that surface diffusion $D_S(T)$ is independent of the relaxation dynamics of the three forms of TPD. The dielectric spectra of bulk TPD above T_g were fitted by the KWW function to determine the value of 0.50 for (1-*n*).[119] The $\tau_0(T)$ calculated from $\tau_\alpha(T)$ in Ref.[119] shown in Fig.42 seems to be continuation of the Arrhenius dependence of the surface diffusion times $\tau_{surf}(T)$ below T_g deduced from $D_S(T)$. The good correspondence is another verification of surface $\tau_{surf}(T)$ and hence also $D_S(T)$ are determined by $\tau_0(T)$. Furthermore, the primitive relaxation time $\tau_0(T)$ of the CM is the same in OG, SG and nano-thin film, and $D_S(T)$ is determined by $\tau_0(T)$. From these facts, the CM [119] explain why $D_S(T)$ is the same in these three forms of TPD [219,220,221]. Except for the CM, no other theory has explained this remarkable finding of surface diffusion by the group led by Fakhraai.

Open Access Article. Published on 04 June 2026. Downloaded on 6/5/2026 12:04:33 AM.
This article is licensed under a Creative Commons Attribution 3.0 Unported Licence.

Materials Advances Accepted Manuscript

View Article Online
DOI: 10.1039/D6MA00279J

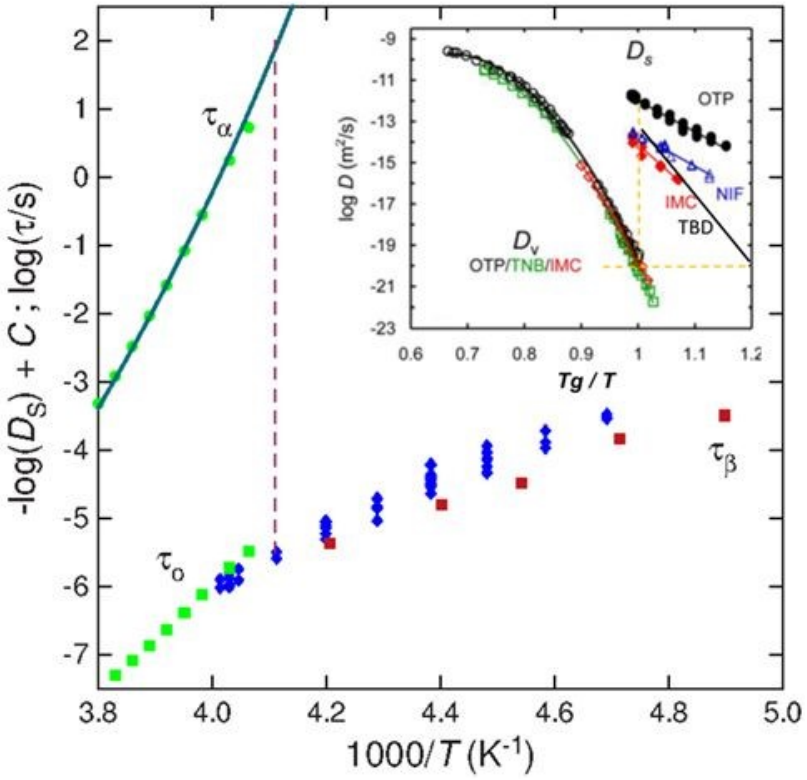

Fig. 39. Green closed circles and squares are the α-relaxation times $\tau_\alpha(T)$, and the primitive relaxation times $\tau_0(T)$ (calculated), and the red close squares are the β-relaxation times $\tau_\beta(T)$ of bulk OTP. The blue close diamonds represent -log $D_S(T) + C$ with C= -17.35 and the original data of $D_S(T)$ are from Ref.[203]. The inset showing $D_S(T)$ and $D_V(T)$ is reproduced from Ref.[203]. Added is the line, which is a fit of the $D_S(T)$ of the OG of TPD by the Arrhenius dependence. $D_S(T)$ data of SG and thin films are not included. Reproduced from *Phys. Chem. Chem. Phys.,* 2017, 19, 29905, Ref [119]. Available under a CC-BY 3.0 license. Copyright 2017 Ngai, K. L.; Paluch, M.; Rodriguez-Tinoco, C.

Open Access Article. Published on 04 June 2026. Downloaded on 6/5/2026 12:04:33 AM.
This article is licensed under a Creative Commons Attribution 3.0 Unported Licence.

Materials Advances Accepted Manuscript

View Article Online
DOI: 10.1039/D6MA00279J

Open Access Article. Published on 04 June 2026. Downloaded on 6/5/2026 12:04:33 AM.
This article is licensed under a Creative Commons Attribution 3.0 Unported Licence.

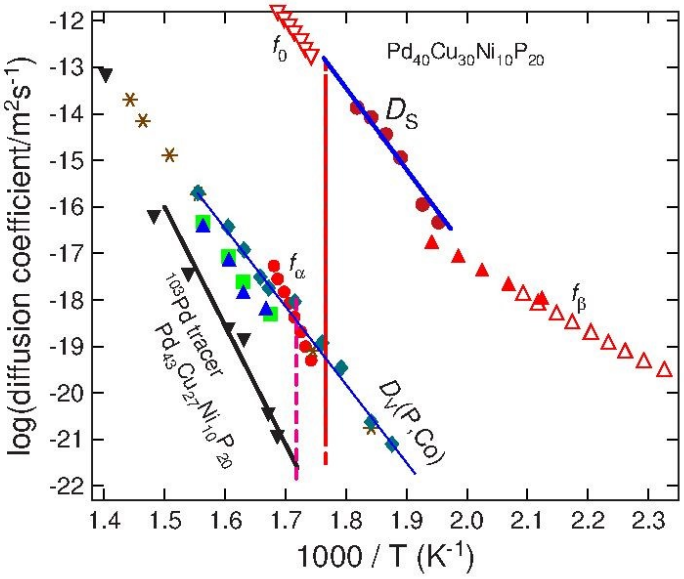

Fig. 40. Surface diffusion coefficients $D_s(T)$ of $Pd_{40}Cu_{30}Ni_{10}P_{20}$ (red close circles) and the fit to the Arrhenius T-dependence (blue line) from Cao et al.[209] Bulk tracer diffusion coefficients $D_{\mathrm{V}}^{\mathrm{Co}}$ of Co (pale blue close diamonds) of $Pd_{40}Cu_{30}Ni_{10}P_{20}$. The bulk tracer diffusion coefficients of $Pd_{43}Cu_{27}Ni_{10}P_{20}$, $D_{\mathrm{V}}^{\mathrm{Pd}}(T)$ of Pd (black close inverted triangles), $D_{\mathrm{V}}^{\mathrm{P}}$ of P (blue closed triangles), and $D_{\mathrm{V}}^{\mathrm{Co}}$ of Co (green closed squares). Open symbols represent the bulk tracer diffusion coefficients, $D_{\mathrm{V}}^{\mathrm{Pd}}(T)$ (purple open inverted triangles and the purple line), $D_{\mathrm{V}}^{\mathrm{P}}$ (open brown triangles), and $D_{\mathrm{V}}^{\mathrm{Co}}(T)$ (open green squares)) of $Pd_{43}Cu_{27}Ni_{10}P_{20}$ after temperatures are scaled by the ratio of the two glass transition temperatures (see text). The pale blue line placed near the data of $D_{\mathrm{V}}^{\mathrm{Co}}$ of Co (pale blue close diamonds) in $Pd_{40}Cu_{30}Ni_{10}P_{20}$ have exactly the same slope as the blue line above it, showing that $D_{\mathrm{V}}^{\mathrm{Co}} \approx D_{\mathrm{V}}^{\mathrm{P}}$ have the same activation energy as $D_s(T)$. The two vertical lines (from left to right) indicate the values of $1000/T$ for T=582 K and 566 K, the T_g of the two metallic glasses. The orange closed circles are the log of the α-loss peak frequencies, $\log f_\alpha$ obtained at temperatures above T_g=566 K, and the open orange triangles are the log of the β-loss peak frequencies, $\log f_\beta$, taken below T_g of $Pd_{40}Cu_{30}Ni_{10}P_{20}$ by Qiao et al. [211] The orange inverted triangles are the log of the primitive frequencies, $\log f_0$, calculate by Eq.2 with n=0.46. All $\log f_\alpha$, $\log f_\beta$, and $\log f_0$ are shifted vertically downward by the same amount such that the data of $\log(f_\alpha/\mathrm{Hz})$ at the lowest temperature corresponds to $\log(\tau_\alpha/\mathrm{s}) \approx 1.5$ as given in Ref.[105], while the bottom end of the vertical orange line corresponds to $\log(\tau_\alpha/\mathrm{s}) \approx 3.0$. The closed orange triangles are the β-loss peak frequencies of $Pd_{40}Cu_{30}Ni_{10}P_{20}$ from Yu et al. [212] and are shifted vertically downward to match those of Qiao et al. Figure taken from Ref.[210] and reproduced with the permission of Elsevier.

Materials Advances Accepted Manuscript

View Article Online
DOI: 10.1039/D6MA00279J

Open Access Article. Published on 04 June 2026. Downloaded on 6/5/2026 12:04:33 AM.
This article is licensed under a Creative Commons Attribution 3.0 Unported Licence.

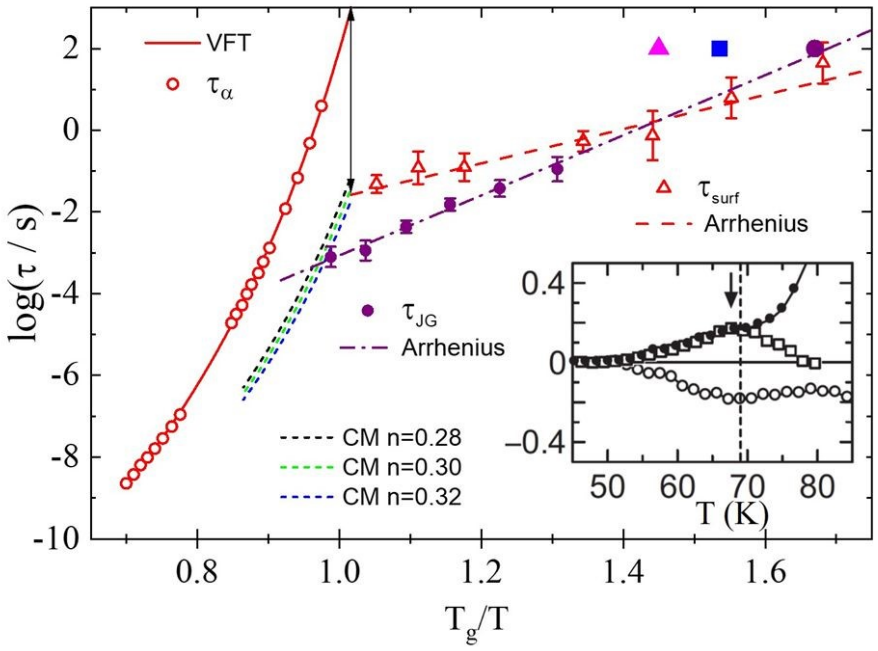

Fig. 41. Relaxation times τ_α (open circles) and $\tau_{surface}$ (open triangles) of ethylcyclohexane (ECH) plotted against T_g/T with T_g=100 K. The τ_α data were taken from Ref.[214] and the $\tau_{surface}$ data come from Ref.[218]. The solid line is the VFT fit of the temperature dependence of τ_α. The dashed line is the fit to $\tau_{surface}$ by Arrhenius dependence. The three dotted lines represent the calculated primitive relaxation times τ_0 with n=0.32, 0.30, and 0.28, and the differences between them are small. In addition, τ_{JG} (purple circles) taken from ref.[214] is plotted against T_g/T along with its Arrhenius fit (purple dash-dotted line). The large filled magenta triangle and purple circle respectively represent τ_{JG} ($T_{g\beta}$=69 K) ≈ τ_0($T_{g\beta}$=69 K) =100 s at $T_g/T_{g\beta}$=1.45 and τ_{JG}($T_{g\beta}$=60 K) ≈ τ_0($T_{g\beta}$=60 K) =100 s at $T_g/T_{g\beta}$=1.67. The blue square is similar adiabatic calorimetry result for *sec*-butylcyclohexane with T_g =129 K and $T_{g\beta}$=84 K. The inset show the heat-release/-absorption rates for bulk ECH within glassy state from adiabatic calorimetry measurements in Ref.[217]. The arrow locates 69 K. The solid and open circles represent respectively the data for the samples prepared by rapid (−5 K min^{-1}) and slow (−20 mK min^{-1}) precooling; with their smooth behaviors being portrayed by the respective solid lines. Open squares in some of the insets represent the data obtained in a sample prepared by rapid precooling with intermediate annealing at 80 K. Reproduced with permission from Ref.[216]. Copyright 2021 Elsevier.

Materials Advances Accepted Manuscript

View Article Online
DOI: 10.1039/D6MA00279J

Open Access Article. Published on 04 June 2026. Downloaded on 6/5/2026 12:04:33 AM.
This article is licensed under a Creative Commons Attribution 3.0 Unported Licence.

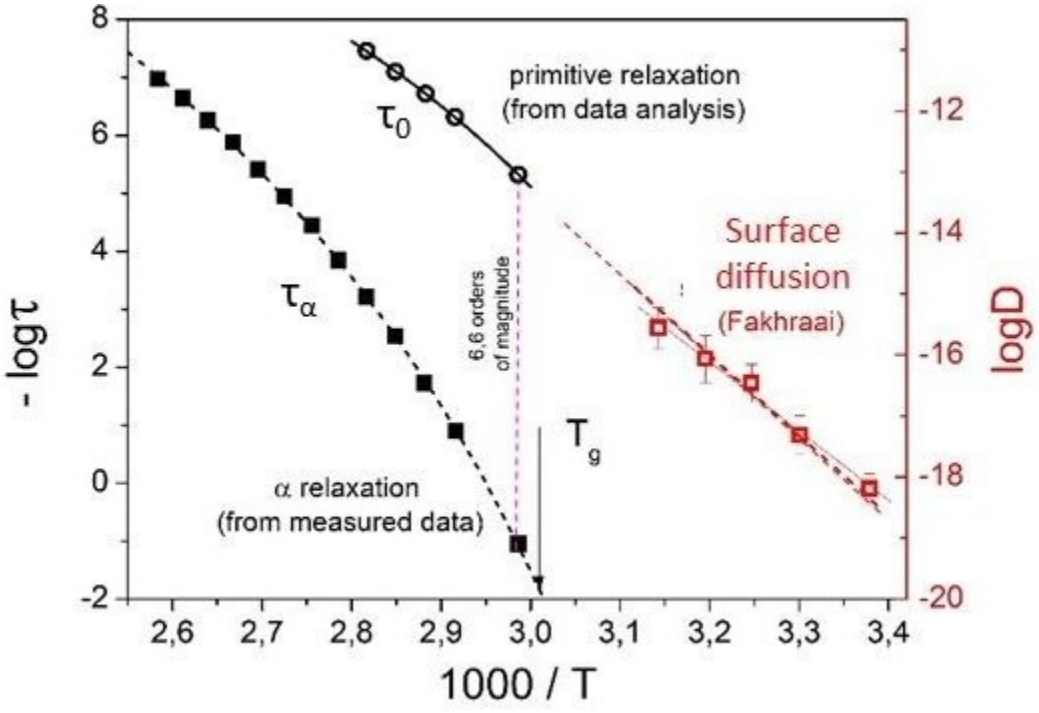

Fig. 42. A plot of the surface diffusion coefficient, D_s, data from Ref.[219] against 1000/T (open squares, left axis). Data is compared with bulk relaxation times τ_α (closed squares, left axis) from dielectric relaxation measurements (closed squares) from Ref.[220]. The primitive relaxation times τ_0 are calculated by the CM equation with β_K value determined from dielectric spectra. The relative shift in the data sets to enable them to be compared in the same plot is based on the empirical rule that the bulk diffusion coefficient at T_g is approximately 10^{-20} m^2 s^{-1}, and τ_α is approximately 100 s.[212] Error bars of surface diffusion coefficients were obtained from two repeating trials [219].

6.5 Ionic conductivity relaxation in yttria-stabilized zirconia thin films

To show the general applicability of the CM to account quantitatively for the enhanced surface diffusion of molecules and atoms observed experimentally, oxygen ion diffusion on the surface of the polycrystalline yttria-stabilized zirconia (YSZ) thin films is considered in conjunction with diffusion data in bulk YSZ. In thin films of YSZ with 10 mol% Y_2O_3 deposited on MgO substrates and thicknesses between 60 and 15 nm, Kosacki et al. [222] found enhanced oxygen ionic conductivity σ_{dc}. In the 15 nm film σ_{dc} is about 2 orders of magnitude higher than 2000 nm thick films at 673 K (see left panel of Fig. 43). Its activation energy is 0.62 eV, which is significantly lower than 1.09 eV of the 2000 nm thick film and 1.16 eV of the bulk samples (right panel). The σ_{dc} data of the 15 nm film were converted to relaxation times $\tau^*(T)$ in Ref.[223], and shown by purple closed squares lying above the dashed green line representing the primitive $\tau_{\sigma 0}(T)$ in the right panel of Fig. 43. These $\tau_{\sigma 0}(T)$ were calculated from $\tau_{\sigma\alpha}(T)$ of bulk YSZ by Eq.(2) with t_c =1 ps and the T-independent n value of 0.57 from the KWW fit of the electric modulus spectra of bulk YSZ [223]. The red arrows in the left and right panels indicates respectively the change in σ_{dc} and the

Materials Advances Accepted Manuscript

View Article Online
DOI: 10.1039/D6MA00279J

Open Access Article. Published on 04 June 2026. Downloaded on 6/5/2026 12:04:33 AM.
This article is licensed under a Creative Commons Attribution 3.0 Unported Licence.

corresponding change in $\tau_{\sigma\alpha}(T)$ at the same temperature. The purple closed squares of $\tau_{\sigma\alpha}(T)$ of the 15 nm film are in good agreement with the primitive $\tau_{\sigma 0}(T)$ of bulk YSZ represented by the green line. Thus, $\tau_{\sigma\alpha}(T)$ of oxygen ions in YSZ on the surface is reduced from the bulk value by orders of magnitude and become the same as the primitive conductivity relaxation time $\tau_{\sigma 0}(T)$,[11,223] in analogy to surface diffusion of molecules in Figs.39, 41 and 42, and of metallic alloy in Fig.40. For other applications of the CM to explain ionic conductivity relaxation dynamics in polycrystalline materials similar to YSZ, see Ref.[224].

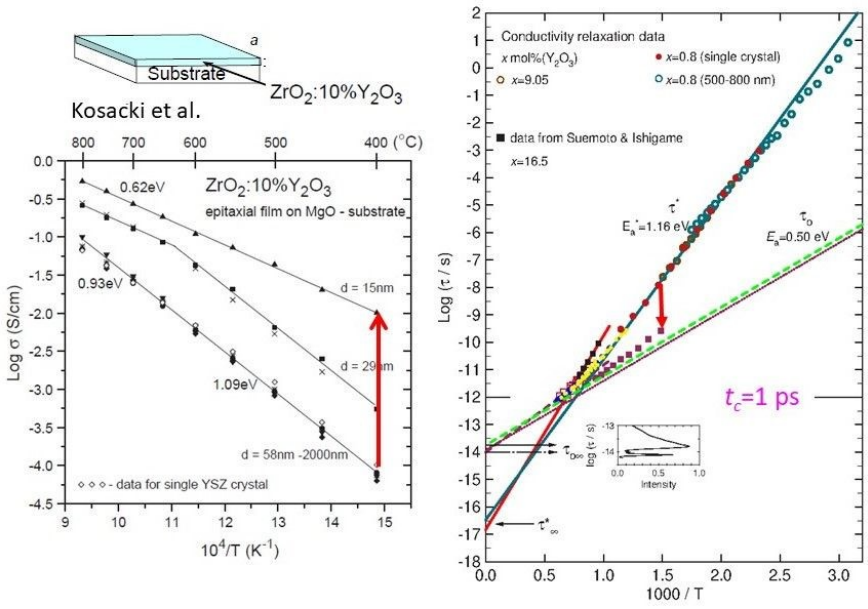

Fig. 43. (Left) Conductivity data of YSZ for different film thickness on MgO substrate [222]. (Right) The conductivity relaxation times $\tau^*(T)$ and quasielastic light scattering correlation time $\tau^*_{QELS}(T)$ in bulk YSZ samples. The pale blue and red solid lines are Arrhenius fits to the data of τ^* and τ^*_{QELS} respectively. The green broken line and the purple dotted line are the primitive $\tau_0(T)$ calculated from $\tau^*(T)$ by Eq.(2) with t_c=2 and 1 ps respectively. The data of the conductivity relaxation times, $\tau^*_S(T)$, of 15 nm YSZ thin film deposited on MgO are shown by closed purple squares located just above the green dashed line representing $\tau_0(T)$. For the other data, see Ref.[223]. Figures reproduced from Ref.[11] with permission from Elsevier.

7. Thermo-complexity and piezo-complexity of polymers

Amorphous polymers are glass-formers having the caged dynamics, JGβ relaxation and the α-relaxation and universal properties just like molecular materials as shown by examples in some Sections before. Each of the three processes have universal properties of its own and also interconnections which are as analogous to those of molecular glass-formers as shown present for PVAc, PMTS, PPGE, POB, selenium, polybutadiene, PMPS in Figs. 2, 5, 25, 34, 36, and 37 herein. Composed of long chains, polymers have relaxation processes involving part of the chain and entire chain of different length-scales. Naturally, the question that arises is whether the chain

Materials Advances Accepted Manuscript

View Article Online
DOI: 10.1039/D6MA00279J

Open Access Article. Published on 04 June 2026. Downloaded on 6/5/2026 12:04:33 AM.
This article is licensed under a Creative Commons Attribution 3.0 Unported Licence.

modes of polymers have universal relaxational and diffusional properties, and interconnectivity with those of the other processes related to glass transition. Another question is whether the CM is applicable to explain these chain modes related properties. Some answers are given as follows.

Conventional models of chain dynamics have the Rouse modes for low molecular weight unentangled polymers, and for entangled polymers there are additionally the plateau compliance leading to the terminal relaxation of coupled chains. From my collaboration with Don Plazek over three decades [225,226,227], we found the new chain mode with length-scale longer than the segmental α-relaxation but shorter than the Gaussian submolecule needed to form the Rouse modes.[225,226,227,228,229,230] We discovered it [229,230] called it the sub-Rouse (sR) mode to be distinguished from the Rouse modes, which are entropic and devoid of intermolecular coupling (*i.e.*, the primitive relaxation of the entangled terminal relaxation). Fig.44a show the shear compliance of polystyrene and the contributions from the α-process, the sR mode and the Rouse modes. The sR mode is intermolecularly coupled like the α-relaxation but to a lesser degree. From the general treatment of the CM, its correlation function is another KWW function, $\varphi_{sR}(t) = \exp[-(t/\tau_{sR})^{1-n_{sR}}]$, and the relaxation time $\tau_{sR}(T,P)$ is related to its primitive $\tau_{sR0}(T,P)$ and its coupling parameter $n_{sR}(T,P)$ by

$$\tau_{sR}(T,P) = [(t_c)^{-n_{sR}(T,P)}\tau_{sR0}(T,P)]^{1/[1-n_{sR}(T,P)]}. \quad (13)$$

Its primitive $\tau_{sR0}(T,P)$ is different from the primitive $\tau_0(T,P) \approx \tau_\beta(T,P)$ of the α-relaxation, but both are proportional to the same primitive friction factor $\zeta_0(T,P)$. Since $n_{sR}(T,P)$ is different from $n_\alpha(T,P)$, it follows that

$$\tau_{sR}(T,P) \propto [\zeta_0(T,P)]^{1/[1-n_{sR}(T,P)]} \quad (14)$$

has different T and P dependences than that of

$$\tau_\alpha(T,P) \propto [\zeta_0(T,P)]^{1/[1-n_\alpha(T,P)]}. \quad (15)$$

Also, $n_{sR}(T,P)$ is smaller than $n_\alpha(T,P)$ due to it involves longer length-scale. These are the basis of the CM explanation of the thermo-rheological complexity and piezo-rheological complexity observed in the glass-rubber transition zone of polymers. Although thermo-rheological complexity was discovered by shear compliance, stress relaxation, and photon correlation spectroscopic measurements [225,226,227,228,229,230], piezo-rheological complexity was observed in dielectric studies by Floudas and coworkers [231,232,233] and elucidated with the CM analysis in Ref.[227] as shown in Fig.44b for $\tau_{sR}(T,P)$ of the sub-Rouse mode compared with $\tau_\alpha(T,P)$ of a low molecular weight polyisoprene.

Another example of piezo-complexity and thermo-complexity of sub-Rouse and α relaxations is given in Figs.44d, 44e, and 44f. In Fig.44f, the left panel is from the associating poly(mercaptopropyl)methylsiloxane (PMMS) where α' stands for sub-Rouse [234], and the right panel is from PPG−OH and PPG−OCH_3.[235] Using precision shear mechanical spectroscopic tool, the sub-Rouse modes were observed in polystyrene (PS) with M_w = 21 kg/mol and M_w/M_n = 1.04, and poly(methylmethacylate) (PMMA) with M_w = 120 kg/mol and M_w/M_n = 1.8. PS and PMMA.

Materials Advances Accepted Manuscript

View Article Online
DOI: 10.1039/D6MA00279J

Open Access Article. Published on 04 June 2026. Downloaded on 6/5/2026 12:04:33 AM.
This article is licensed under a Creative Commons Attribution 3.0 Unported Licence.

[236] From their various properties determined, the sub-Rouse modes were shown to be intermolecularly coupled like the local segmental relaxation, albeit to a less degree with $n_{sR} < n_\alpha$.

Fig.44c shows the piezo complexity of $\tau_\alpha(T,P)$ with $\tau_{nm}(T,P)$, the terminal normal mode dielectric relaxation time of entangled PI chains in a high molecular weight. sample. The corresponding thermos-complexity was found earlier by dielectric relaxation in entangled PI by Adachi and Hirano [237]. Thermo-complexity of the α and terminal relaxations of entangled polymers was discovered for the first time in creep compliance measurements by Plazek [238,239,240,241,242]. This general property was first explained in a quantitative manner by the CM [168,226,227,243,244,245]. The CM has the equation relating $\tau_\eta(T,P)$, the terminal relaxation time of entangled polymers associated with viscosity η, to its primitive relaxation time, which is $\tau_R(T,P)$ of the Rouse model, and the entanglement coupling parameter n_η, given by

$$\tau_\eta(T) = [(\hat{t}_c)^{-n_\eta}\tau_R(T)]^{1/[1-n_\eta]}. \quad (16)$$

Here $(1\text{-}n_\eta)$ is the fractional exponent in $\varphi_\eta(t) = \exp[-(t/\tau_\eta)^{1-n_\eta}]$, the terminal correlation function of monodisperse polymers.

Here we recall some older data of entangled polymers not considered before, analyze them for the first time, and using the results to test the CM predictions. Figs.45c and 45d show the shear loss modulus $G''(\omega)$ of 1,2-PBD with M_w=80.1 kg/mol and 1,4-PBD with M_w=228 kg/mol respectively from Robertson et al. [246,247] and Palade et al. [248], and the fits by the Fourier transform of $\varphi_\eta(t)$ to determine the values of $(1\text{-}n_\eta) \approx 0.59$. By the way, $G''(\omega)$ in Fig.45c is similar to the $G''(\omega)$ data of the linear polyisoprene of M_w=357,000 with a partially resolved peak and the fit with n_η=0.40 by Bero and Roland [249]. On the other hand, the linear polyisoprene of M_w= 145,000 in also in Ref.[249] shows no peak at all, and the forced fit by Bero and Roland[249] yielded an unreliable value of n_η=0.35.

Eq.(16) together with the known mol. wt. and temperature dependence of the Rouse modes,

$$\tau_R(T,P) \propto M^2\zeta_0(T,P), \quad (17)$$

lead to the dependencies of τ_η given by

$$\tau_\eta(T,P,M) \propto M^{2/[1-n_\eta]}\zeta_0(T,P)^{1/[1-n_\eta]}. \quad (18)$$

Using the experimentally determined value of $(1\text{-}n_\eta) \approx 0.5$ from $G''(\omega)$ in Figs.45c and 45d as well as from other sources [245], the CM Eq.(17) predicts $\tau_\eta \propto M^{3.4}\zeta_0(T,P)^{1/0.59}$. The $M^{3.4}$-dependence of τ_η is in accord with that commonly found in the polybutadienes and other entangled polymers. On comparing $\tau_\eta(T,P) \propto \zeta_0(T,P)^{1/0.59}$ with $\tau_\alpha(T,P) \propto [\zeta_0(T,P)]^{1/[1-n_\alpha(T,P)]}$ of the α-relaxation, another prediction is [11,225,226,227]

$$\tau_\eta(T,P) = C[\tau_\alpha(T,P)]^{(1-n_\alpha)/(1-n_\eta)}. \quad (19)$$

Materials Advances Accepted Manuscript

View Article Online
DOI: 10.1039/D6MA00279J

Open Access Article. Published on 04 June 2026. Downloaded on 6/5/2026 12:04:33 AM.
This article is licensed under a Creative Commons Attribution 3.0 Unported Licence.

Robertson and coworkers [246,247] verified this CM prediction quantitatively in 1,4 and 1,2 polybutadienes (PBD) with M_w=38700 and 80100 g/mol respectively by shear modulus measurements over a wide temperature range by including the $\tau_\alpha(T)$ from dielectric measurements at shorter times than from mechanical measurements. The results are shown in Figs.38a and 38b for 1,4-PBD and 1,2-PBD. Earlier, the difference in temperature dependence between $\tau_\eta(T)$ and $\tau_\alpha(T)$ of atactic polypropylene was explained quantitatively in the same manner by the CM Eq.(19) in Ref.[250]. The difference in temperature and pressure dependence found in poly(methylphenyl siloxane) (PMPS) was explained in the same manner in Ref.[251].

The determination of the value of n_η from $G''(\omega)$ in Figs.45c and 45d is more reliable due to the terminal loss peak is partially resolved, and the mol. wt. of the polymers are monodisperse. This ideal condition is not always realized, and the true value of n_η cannot be obtained. This is the case of linear polyisoprene of M_w=145,000 measured by Bero and Roland [249], where $G''(\omega)$ shows no peak at all, and their forced KWW fit gave an arbitrary and unreliable value of n_η=0.35. Santangelo et al. [252] reexamined the $G''(\omega)$ with well resolved terminal loss peak in one of the 1,4-PBD samples with M_w=925,000 published by Colby et al. [253]. The $G''(\omega)$ data of Colby et al., and the KWW fit disregarding the low frequency part of the peak with n=0.21 by Santangelo et al. are shown in Fig.46b. In another paper by Colby et al. [254], they studied 1,4-PBD with mol. wt. ranging from 1×10^3 to 1.65×10^7 ($0.5 < M/M_e < 8000$) with M_e =1850 determined from the plateau modulus. Significant departures of η from the $M^{3.4}$-dependence were found beyond $M/M_e \sim 200$ with an approach to $M^{3.0}$-dependence. Having M/M_e=500, the M_w=925,000 sample in Fig.46b has deviated from the $M^{3.4}$-dependence [254], and hence n_η in Eq.(18) no longer has the value of 0.41. If the $M^{3.0}$-dependence holds instead, the n_η should have the value of 0.33 instead of 0.41 in Eq.(18). The same G"(ω) data of the M_w=925,000 sample in Fig.46b are replotted in Fig.46a. Represented by the two lines, the Fourier transforms of the KWW functions with n_η = 0.32 and 0.33 fit the G"(ω) data quite well.

Santangelo et al. considered also the $G''(\omega)$ of hydrogenated polybutadiene (HPB) of M_w = 95600, 150000, 174000, 202000, 212000, 359000, and 361000 most of which are from the thesis of Raju [255], but not published in a journal, and the status is unknown. The one published in Ref.[256] is HPB-350 with M_w=359000 and its $G''(\omega)$ solely is much narrower than the KWW fit with n_η=0.41 or 0.42 although the number of entanglements given by M/M_e is 300, the highest among the polymers included in Fig.47a, which is reproduced from Fig.1 of Ref.[256]. As remarked by Raju et al. [256] except for HPB-500 having M/M_e=300, the data of linear polymers with $M/M_e \geq 100$ converge to the limiting solid curve in Fig.47a. The latter is equivalent to the plot in Fig.47b of the universal G''/G_m'' vs ω/ω^m data for narrow-distribution linear chain polymers with $M/M_e \geq 100$ given by Raju et al. in their Table VII. The lines in Fig.47b are the KWW fit with n_η=0.40 and 0.41. Raju et al. suggested the exception of HPB-500 is caused by it having anomalous G' at low frequencies, time-temperature superposition violation in samples with long branches, and experimental difficulties in obtaining accurate values of G'' at high frequencies. Thus, the reliability of the HPB-500 data is questionable, and the deviation of its G'' from the universal shape should not be taken seriously.

Despite the difficulty of obtaining its exact value from $G''(\omega)$ in some cases, one should recognize the success of a single n_η in explaining both the M-dependence and the T dependence of $\tau_\eta(T,P)$ via Eqs.(18) and (19), as demonstrated by Robertson et al. [246] in 1,4 and 1,2 polybutadienes, and by others in aPP [250] and PMPS [251]. Equation (19) rewritten as $\tau_\alpha(T,P) = D$

Materials Advances Accepted Manuscript

View Article Online
DOI: 10.1039/D6MA00279J

$[\tau_\eta(T,P)]^{(1-n_\eta)/(1-n_\alpha)}$ was applied in Ref.[227] to the dielectric chain normal mode pressure dependence data of entangled polyisoprene of Floudas et al. [231,232] shown in Fig.44c. By using the experimental value of $n_\alpha(T,P)$=0.53, and n_η =0.41, the pressure dependence of $\tau_\alpha(T,P)$ in Fig.44c was predicted from that of $\tau_{nm}(T,P)$ standing for $\tau_\eta(T,P)$ herein by the ratio [1-$n_{nm}(T,P)$]/[1-$n_\alpha(T,P)$] = 0.59/0.47. As shown by the blue line in Fig.44c, the prediction is in agreement with experiment.

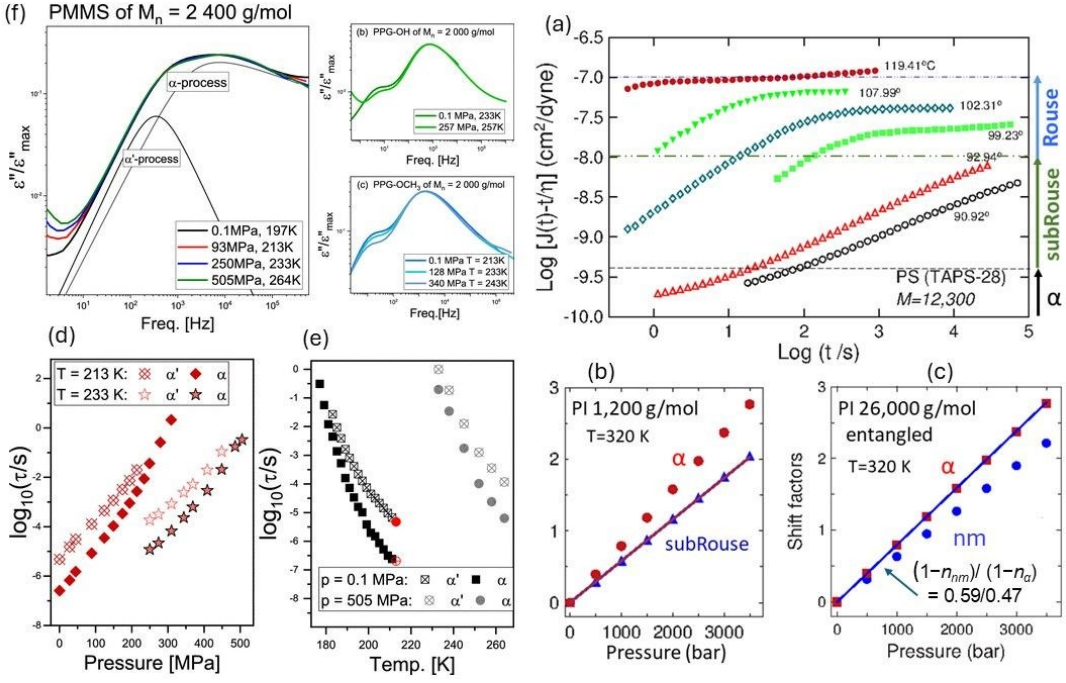

Fig. 44. (a) Shear compliance $J_r(t)$ of monodisperse PS with mol. wt. of 12,300 below M_c = 32,000. The contributions from the α, sub-Rouse, and Rouse are indicated. Data from Ref. [244] replotted. (b) and (c) Pressure dependences of the shift factors of the τ_α(squares) and the longest normal mode relaxation time (triangles) and (circles) for the unentangled PIP with M_n = 1200 g/mol, and the entangled PIP with M_n = 26000 g/mol at 320 K.[231,232] The blue line in (c) is the CM prediction. Data from Ref.[227] are replotted. (d) Piezo-complexity of PMMS where α' is sub-Rouse. (e) Thermo-complexity of PMMS. (f) Left panel: Comparison of the loss spectra obtained for PMMS at various T and P with the same τ_α. Right panel: Superposition of ε'' spectra for PPG−OH and PPG−OCH_3 with M_n=2000 g/mol at different T and P. Figures from Ref.[234] and Ref.[235] and reused with permission from ACS.

Open Access Article. Published on 04 June 2026. Downloaded on 6/5/2026 12:04:33 AM.
This article is licensed under a Creative Commons Attribution 3.0 Unported Licence.

Materials Advances Accepted Manuscript

View Article Online
DOI: 10.1039/D6MA00279J

Open Access Article. Published on 04 June 2026. Downloaded on 6/5/2026 12:04:33 AM.
This article is licensed under a Creative Commons Attribution 3.0 Unported Licence.

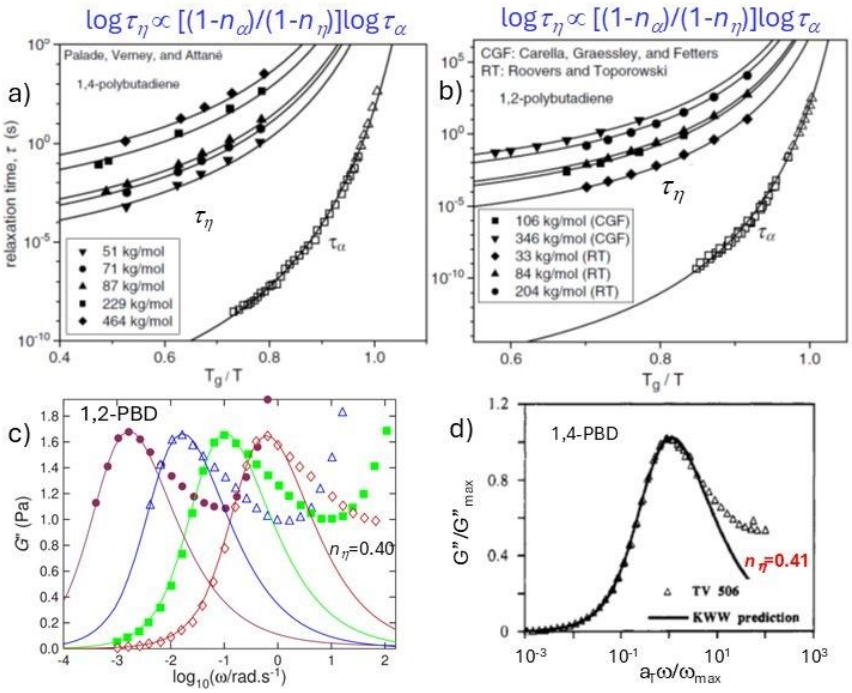

Fig. 45. (a) and (b) Relaxation times for α-relaxation (open symbols) and terminal flow (solid symbols) of 1,4-polybutadienes, at the indicated molecular weights. The line through $\tau_\alpha(T)$ is the VFTH fit, and the lines through $\tau_\eta(T)$ are CM fits. Figures reproduced from Ref.[246] with permission from Elsevier. (c) G'' for PBd-H with M_w=80.1 kg/mol within the plateau/terminal region. (d) Reduced terminal loss moduli plotted versus reduced frequency of 1,4-polybutadiene with M_w=210 kg/mol (open triangles). The line is the KWW fit with $(1\text{-}n_\eta) = 0.59$. Figure adopted from Ref.[247] with permission from ACS.

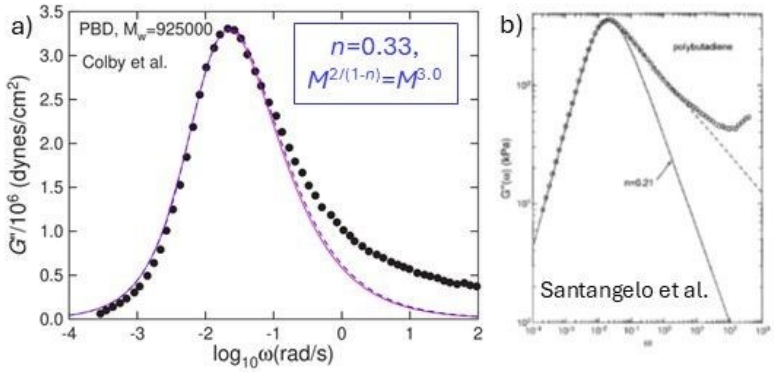

Fig. 46. (a) $G''(\omega)$ of 1,4-PBD with M_w=925,000 (filled circles) from Ref.[253] replotted. Continuous and broken lines are the KWW fits with n=0.32 and 0.33 respectively. (b) The same data in a log-log plot. The solid line is the KWW fit by Santangelo et al. [252] with n=0.21 by ignoring the data at higher frequencies. Figure taken from Ref.[252] and reused with permission from Elsevier.

Materials Advances Accepted Manuscript

View Article Online
DOI: 10.1039/D6MA00279J

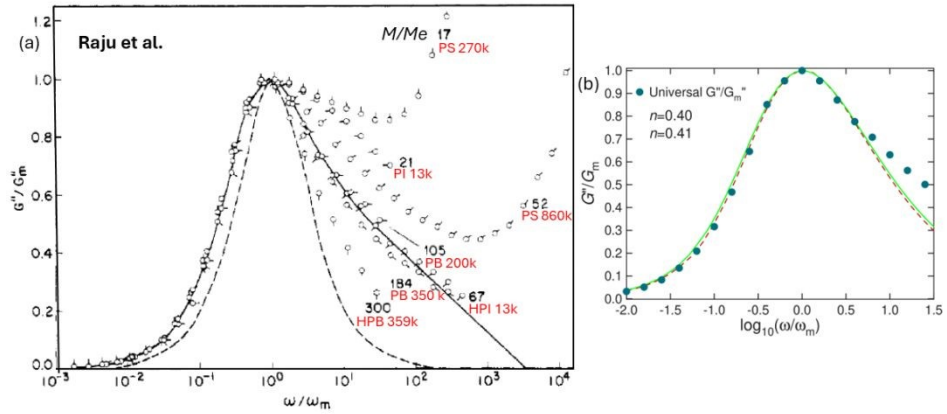

Fig. 47. (a) Reduced G'' for polystyrene; polybutadiene, hydrogenated polybutadiene; HPB-350; hydrogenated polyisoprene; HPI-1; polyisoprene, PI-1 with M/M_e shown. The solid curve represents the limiting behavior for long-chain ($M/M_e \sim 100$) linear polymers and the dashed line that of a single Maxwell element. Figure adapted from Ref.[256] and reused with permission from ACS. (b) Universal reduced dynamic loss modulus for narrow-distribution polymers (circles) given in Table VII of Ref.[256] plotted and KWW fits with n=0.40 and 0.41.

7.1 JGβ, α, Rouse modes, and entangled chains modes *all* in polyethylene oxide (PEO)

The universal properties in polymers are richer, involving the relations between the JGβ relaxation, the primitive relaxation, the structural α-relaxation, the Rouse modes, and the entangled chain modes. The equations representing the relations between the relaxation times of these processes are given by:

(*i*) $\tau_\beta(T) \approx \tau_0(T,P) \propto \zeta_0(T)$

(*ii*) $\tau_\alpha(T) \propto [t_c^{-n_\alpha}\tau_0(T)]^{1/[1-n_\alpha]}$ from crossover of primitive to α relaxation at $t_c \approx$ ps

(*iii*) $\tau_{\alpha,nano}(T) \approx \tau_0(T) \approx \tau_\beta(T)$

(*iv*) $\tau_\eta(T) = [(\hat{t}_c)^{-n_\eta}\tau_R(T)]^{1/[1-n_\eta]}$ from crossover of Rouse to entangled dynamics at $\hat{t}_c \approx ns$

(*v*) $\tau_R(T,M) \propto M^2\zeta_0(T)$

(*vi*) $\tau_\eta(T,M) \propto M^{2/[1-n_\eta]}\zeta_0(T)^{1/[1-n_\eta]}$.

In the figures given before, experimental data from different polymers are used to elucidate these five universal properties. It would be more impressive if all five are found in the *same* polymer. These are realized in the case of polyethyleneoxide (PEO). The paper published in 2025 [257] in response to dielectric relaxation data of Lunkenheimer and Loidl [258] published in the same year has demonstrate properties (*i*), (*ii*), and (*vi*) in PEO. The results are summarized in Fig.48, with

Open Access Article. Published on 04 June 2026. Downloaded on 6/5/2026 12:04:33 AM.
This article is licensed under a Creative Commons Attribution 3.0 Unported Licence.

Materials Advances Accepted Manuscript

View Article Online
DOI: 10.1039/D6MA00279J

Open Access Article. Published on 04 June 2026. Downloaded on 6/5/2026 12:04:33 AM.
This article is licensed under a Creative Commons Attribution 3.0 Unported Licence.

the detailed descriptions given in Ref.[257]. The other data included in Fig.38 are from Refs.[259,260,262,262]. The key to property (*ii*) is the crossover of primitive to α relaxation at $t_c \approx$ ps. It was observed by neutron scattering by Sakai, Maranas et al.[263] and the data was cited in Ref.[257]. Property (*iii*) of the drastic reduction of the segmental α-relaxation time $\tau_{\alpha,bulk}(T)$ of bulk PEO to become $\tau_0(T) \approx \tau_\beta(T)$ was observed by dielectric spectroscopy when it was transformed to ultrathin films with thickess ~ 1 nm confined within the galleries of hydrophilic silicates, sodium-montmorillonite (Na+MMT) [185,186].

On the other hand, the key to property (*iv*) is the crossover of Rouse dynamics to entangled chain dynamics at $\hat{t}_c$ of a few ns was not discussed in Ref.[257]. Herein, the neutron spin echo data $S(Q,t)/S(Q,0)$ of an entangled PEO with M_w = 81 kg/mol ($M_e \approx$2.2 kg/mol) at T = 400 K from Niedzwiedz et al.[264] presented in Fig.49. The symbols show the data measured for various Q values, and the lines are the fits with the single chain dynamic structure factor in the Rouse model simultaneously to all Q values. It can be seen that the Rouse model fits fail after 4 ns. The temperature dependence of the data changes to that of the entangled chains at $\hat{t}_c \approx$4 ns to verify property (*iv*) for PEO. The monomeric friction coefficient $\zeta_0(T)$ of Rouse modes from the fits were determined from the neutron spin echo data of the sample PEO with M_w = 81 kg/mol at four temperatures, and from neutron backscattering of PEO with M_w = 24 kg/mol at three temperatures [264]. After shifting $\zeta_0(T)$ by a constant, the adjusted values are shown in Fig.50 at the left bottom corner (black squares and red circles). There is good agreement of the adjusted $\zeta_0(T)$ with $\tau_0(T)$ in temperature dependence, and thus this is the first time property (*v*) is verified in PEO. The same $\zeta_0(T)$ is shifted upwards (also represented by black squares and red circles) in Fig.48 to compare its temperature dependence with the stronger temperature dependences of the terminal $\tau_\eta(T)$ of PEO from rheological data of Colby [261], and Zawada et al. [262]. The difference in the temperature dependences brought out more clearly in Fig.51 enables the test of the CM predictions from (*iv*) $\tau_\eta(T) = [(\hat{t}_c)^{-n_\eta}\tau_R(T)]^{1/[1-n_\eta]}$ and (*v*) $\tau_R(T,M) \propto M^2\zeta_0(T)$ combined, and with n_η=0.41 in accord with the $M^{2/(1-n_\eta)} = M^{3.4}$ dependence. The slopes of the two dashed lines are the temperature dependence of $\tau_R(T) \propto \zeta_0(T)$ predicted from that of the solid lines representing $\tau_\eta(T)$ after scaling by the factor of (1-*n*)=0.60. The agreement obtained verified the relations between $\tau_R(T)$ and $\tau_\eta(T)$.

The reptation based models [265,266,267] have long been established as the solution of the dynamics of entangled polymers. It is hard for any alternative theory including the CM [268] discussed in this Section 7 and Section 4.5, to gain attention. Nevertheless, the reader can see from the contents of this two Sections that the CM has more predictions than the reptation based models such as temperature dependence of the terminal relaxation time $\tau_\eta(T)$ and its relation to the different ones of $\tau_R(T)$ and $\tau_\alpha(T)$, and also in Refs.[1,269]. These predictions also explain [270] the activation energy and molecular weight dependence of cooperative tracer chains diffusion in highly entangled polymer melts in recent experiments [271,272].

Materials Advances Accepted Manuscript

View Article Online
DOI: 10.1039/D6MA00279J

Open Access Article. Published on 04 June 2026. Downloaded on 6/5/2026 12:04:33 AM.
This article is licensed under a Creative Commons Attribution 3.0 Unported Licence.

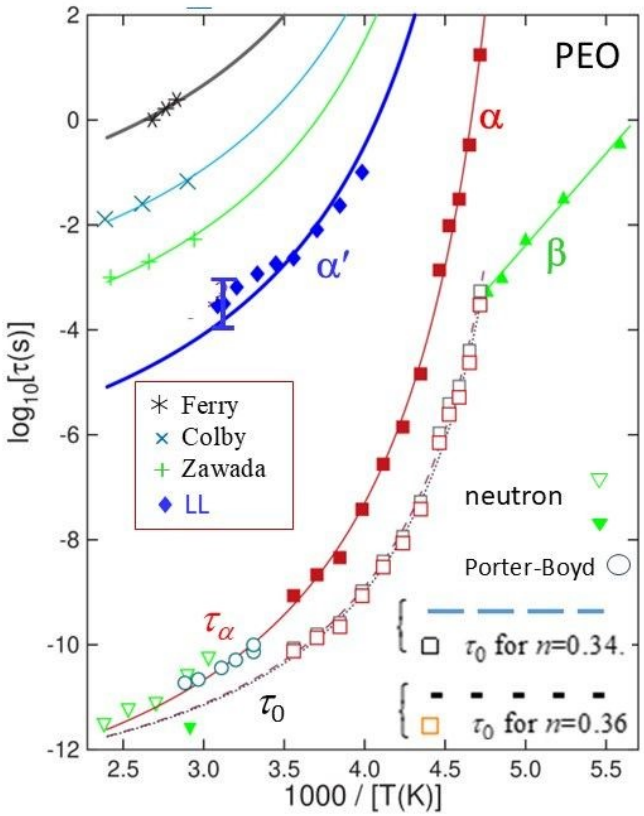

Fig. 48. Average dielectric relaxation times of three of the four processes, β, α, and α', detected in PEO as derived from the fits of the permittivity spectra by Lunkenheimer and Loidl (LL) [219] plotted within an Arrhenius representation (filled triangles, squares, and diamonds for $\tau_\beta(T)$, $\tau_\alpha(T)$, and $\tau_{\alpha'}(T)$ respectively). The red line is the fit of the $\tau_\alpha(T)$ data with the VFT equation performed by LL. The open circles are τ_α from the high frequency dielectric data of Porter and Boyd [260]. The open inverted triangles are $\tau_\alpha(T)$ of PEO from neutron scattering of Sakai et al. [259] The black open squares and black dotted line are the primitive relaxation times $\tau_0(T)$ calculated by using the CM eq 1 with $(1-n_\alpha)$=0.34 and $\tau_\alpha(T)$ represented by the filled squares and the VFT fit respectively. Similarly, the red open squares and red dashed line are $\tau_0(T)$ calculated by using the CM Eq. 2 with $(1-n_\alpha)$=0.36. The $*$, ×, and + are rheological data of the terminal $\tau_e(T)$ of PEO from Yin et al. [261], Colby [262], and Zawada et al. [263]. The published data of Yin et al. are reduced by three decades. The thicker blue line fitting the $\tau_{\alpha'}(T)$ data of LL is derived from eq 7 in Ref.[257] from the CM. The same applies to the three lines fitting the data of $*$, ×, and +. Figure taken from Ref.[257] and reused with permission from ACS.

Materials Advances Accepted Manuscript

View Article Online
DOI: 10.1039/D6MA00279J

Open Access Article. Published on 04 June 2026. Downloaded on 6/5/2026 12:04:33 AM.
This article is licensed under a Creative Commons Attribution 3.0 Unported Licence.

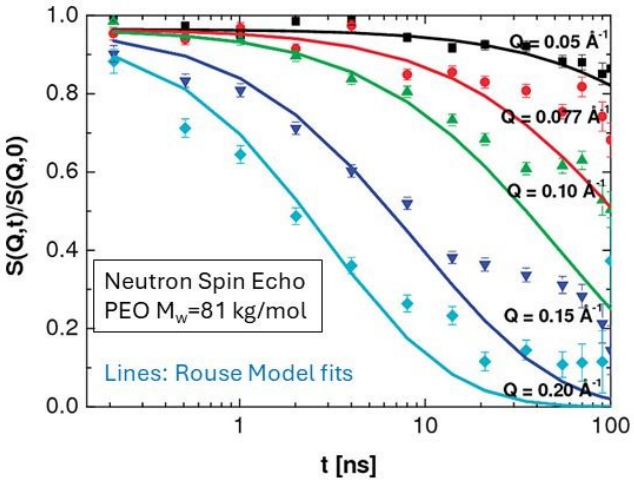

Fig. 49. NSE data of a PEO sample with Mw = 81 kg/mol at T = 400 K. The symbols show the data measured for various Q values. Solid lines represent a fit with the Rouse model simultaneously to all Q values. The data were fitted up to t = 10 ns and then extrapolated to observe the expected deviation from the Rouse behavior at longer times. Figure adopted from Ref. [264], and reused with permission from ACS.

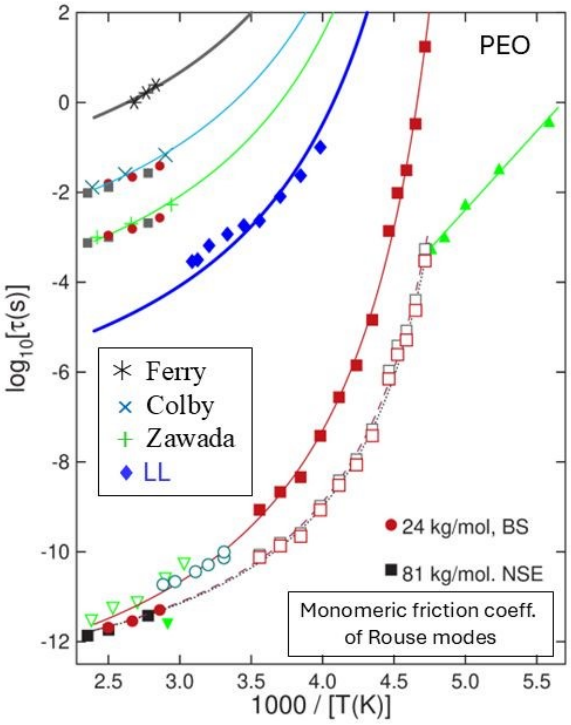

Fig. 50. Essentially the same as in Fig.48 except for the addition of the monomeric friction coefficient $\zeta_0(T)$ of the Rouse modes of two PEO with M_w = 81 and 24 kg/mol (black squares and red circles respectively) from neutron scattering from Niedzwiedz et al.[264] (bottom left corner) after shift by constant to compare with $\tau_0(T)$ in temperature dependence (dashed lines). Additional vertical shifts of the black squares and red circles are performed to show difference in temperature dependence with the terminal relaxation times $\tau_\eta(T)$ of entangled PEO from Colby [261], and Zawada et al. [262].

Materials Advances Accepted Manuscript

View Article Online
DOI: 10.1039/D6MA00279J

Open Access Article. Published on 04 June 2026. Downloaded on 6/5/2026 12:04:33 AM.
This article is licensed under a Creative Commons Attribution 3.0 Unported Licence.

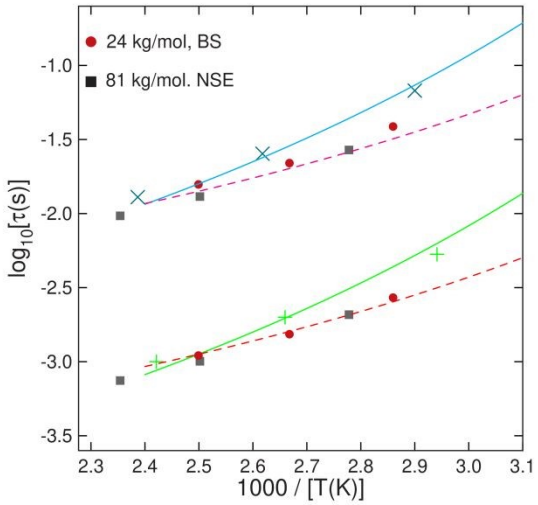

Fig. 51. The ×, and + are rheological data of the terminal $\tau_\eta(T)$ of PEO from Colby [261], and Zawada et al. [262], same as in Fig.48 and Fig.50 except for the addition of the monomeric friction coefficient $\zeta_0(T)$ of the Rouse modes of two PEO with M_w = 81 and 24 kg/mol (black squares and red circles respectively) from neutron scattering (Niedzwiedz et al.[264]) after a shift by constants to compare with the temperature dependence of the terminal relaxation times $\tau_\eta(T)$ of entangled PEO from Colby [261], and Zawada et al. [262]. The slopes of the dashed lines are predicted from that of the solid lines scaled by the factor of (1-n)=0.60 according the CM relation, $\tau_\eta(T) = [(\hat{t}_c)^{-n_\eta}\tau_R(T)]^{1/[1-n_\eta]}$.

8. *T-P invariance of the frequency dispersion of the sub-Rouse relaxation*

In polymers with too low mol. wt., the sub-Rouse (sR) $\tau_{sR}(T,P)$ is not much longer than $\tau_\alpha(T,P)$, and hence the former is not fully resolved from the latter. This is the case of PMMS with M_n=2400 g/mol [234] in Fig.44f. Nevertheless, both the dielectric loss from the unresolved sub-Rouse relaxation and the α-relaxation show perfect superposition at four different combinations of T and P. The same property was found from the sR mode and segmental α-process in PPG-OH and PPG-OCH_3 with 2000 mol. wt. [235]. The results in Fig.44f demonstrate the frequency dispersion of both the sub-Rouse and the α relaxations are T-P-invariant at constant $\tau_\alpha(T,P)$. In contrast, the sR relaxation is resolved in other low mol. wt. polymers by dielectric spectroscopy. Examples are PI with M_w=2.2 K (Fig.52a) [273], PPG4000 (Fig.52b) [274], poly(oxybutylene) (POB, Fig.52c) [275,276]. In all three figures, the frequency dispersion of the sR relaxation is invariant to changes of T and P at constant $\tau_{sR}(T,P)$.

The CM provide rationalization of the invariance property of the sR relaxation in the same manner as done for the α-relaxation. From Eq.(13) and at constant $\tau_{sR}(T,P)$, the right-hand-side requires $n_{sR}(T,P)$ and $\tau_{sR0}(T,P)$ individually to be invariant. This is because the two are different physical identities and no connection with each other, and hence they cannot vary in concert to maintain $\tau_{sR}(T,P)$ on the left-hand-side constant.

Materials Advances Accepted Manuscript

View Article Online
DOI: 10.1039/D6MA00279J

Open Access Article. Published on 04 June 2026. Downloaded on 6/5/2026 12:04:33 AM.
This article is licensed under a Creative Commons Attribution 3.0 Unported Licence.

Materials Advances Accepted Manuscript

However, the sR relaxation time $\tau_{sR}(T,P)$ is not exactly co-invariant with $\tau_\alpha(P,T)$. This fact was first observed by Floudas et al. [232] in polyisoprene with mol.wt.=1200 from $\tau_\alpha(T,P)$ having a stronger pressure dependence than $\tau_{sR}(T,P)$. This is confirmed by the slight increase in separation between $\tau_\alpha(P,T)$ and $\tau_{sR}(T,P)$ under pressure at the same $\tau_\alpha(T,P)$ in PI with M_w=2.5 k by Pawlus et al. [273] (see Fig.52a), and in POB by Casalini and Roland [277]. By contrast, in the case of the JGβ relaxation in Section 3, its relaxation time $\tau_\beta(P,T)$ is co-invariant with $\tau_\alpha(P,T)$, $n_\alpha(T,P)$, and $n_{sR}(T,P)$ to changing T and P. The difference comes from the primitive $\tau_{sR0}(T,P)$ of sR mode in Eq.(13) involves longer length-scale than the primitive $\tau_0(P,T) \approx \tau_\beta(P,T)$ of the local segmental α-relaxation, and they are not identical. Nevertheless, the T and P dependence of both $\tau_{sR0}(T,P)$ and $\tau_0(P,T) \approx \tau_\beta(P,T)$ are proportional to the same primitive friction factor $\zeta_0(T,P)$, and the larger $n_\alpha(T,P)$ in Eq.(2) than $n_{sR}(T,P)$ in Eq.(13) explains the stronger T and P dependences of $\tau_\alpha(P,T)$ than $\tau_{sR}(T,P)$.

Again, since $\tau_{sR0}(T,P)$ and $\tau_0(P,T)$ are proportional to the same primitive $\zeta_0(T,P)$, $\tau_\alpha(P,T)$ and $\tau_{sR}(T,P)$ can be scaled to become functions of TV^γ with the same γ, as shown in low and high mol. wt. PI and POB in Fig.53(a)-(c).

The dielectric spectra of the terminal relaxation in high mol. wt. *cis*-polyisoprene were obtained first by Adachi and coworkers [278,279], and by others [273,279,280]. Due to the dipoles, the global chain motion is observed as from contributions of the normal modes in dielectric spectrosopy. Although the global chain motion also induces slow viscoelastic relaxation, there is an important difference between the dielectric and viscoelastic properties observed by experiments. As pointed out in Ref.[273], dielectric spectroscopy probes the orientational correlation of two submolecules (entanglement segments) at different times while the viscoelastic measurements detect isochronally the orientational anisotropy of respective submolecules. Thus, the global chain motion manifested in dielectric $\varepsilon^*(\omega)$ is different from that in viscoelastic $G^*(\omega)$. The dielectric $\varepsilon''(\omega)$ of the terminal chain motion of PI with M_w=140,000 and 25,000 shown in Fig.54a and Fig.54b from Ref.[278] and Ref.[273] respectively have shapes different from $G''(\omega)$ in Figs.45, 46, and 47, and in the figures of Ref.[282]. The full-width at half-maximum of the former is less than that of the latter. The difference was rationalized in the reptation model by including of the dynamic tube dilation that increases the tube diameter [281,282]. Another rationalization by the CM is to include for terminal dielectric relaxation the lateral nature of the constraints by entanglements and its subsequent mitigation when the terminal time is reached [204,226]. Modified by inclusion of lateral constraint mitigation (LCM), the CM can explain the shape of the $\varepsilon''(\omega)$ loss peak quite well by result shown by the thick solid line in Fig.53a. The modified model can describe also the dielectric data of dilute polyisoprene probes in polybutadiene matrices and in networks [204,226].

Fig. 53b from the Pawlus et al. [273] shows the $\varepsilon''(\omega)$ loss peaks of PI with M_w=25,000 at two combinations of T and P. Despite the two having the same peak frequency, the shapes of the loss peaks are slightly different. Possible cause of the shape change is the LCM aspect in dielectric chain normal mode relaxation. The LCM can change on elevating pressure and temperature, and also differently for the various normal modes contributing to the $\varepsilon''(\omega)$ loss peak. The relation,

$$\tau_{nm}(T,P) \propto [\zeta_0(T,P)]^{1/[1-n_{nm}(T,P)]},$$

View Article Online
DOI: 10.1039/D6MA00279J

Open Access Article. Published on 04 June 2026. Downloaded on 6/5/2026 12:04:33 AM.
This article is licensed under a Creative Commons Attribution 3.0 Unported Licence.

holds with $n_{nm}(T,P)$=0.43 to obtain the $\tau_{nm} \propto M^{2/(1-n_{nm})} = M^{3.5}$ dependence for the entangled PI chains found by dielectric spectroscopy [278]. By comparing $\tau_{nm}(T,P) \propto [\zeta_0(T,P)]^{1/[1-0.43]}$ with $\tau_\alpha(T,P) \propto [\zeta_0(T,P)]^{1/[1-n_\alpha(T,P)]}$ using the experimental value of 0.54 for $n_\alpha(T,P)$ of entangled polyisoprene with M_w=25 K from Ref.[273], the dependence of $\tau_{nm}(T,P)$ in Fig.52d is predicted from that of $\tau_\alpha(T,P)$ by the ratio $[1-n_\alpha(T,P)]/[1-n_{nm}(T,P)]$=0.46/0.57. As shown by the thick black line in Fig.52d, the prediction is in accord with experiment. When the terminal relaxation of entangled polymer chains is characterized by viscosity, the temperature dependence of $\eta(T) \propto [\zeta_0(T)]^{1/[1-0.43]}$ is different from that of $\tau_\alpha(T) \propto [\zeta_0(T)]^{1/[1-n_\alpha]}$ if $[1-n_\alpha]$ is smaller than $[1-n_\eta]$=0.43. Like the PI 25k in Fig.52d, this is the case for atatic polypropylene with M_w=60 k as shown in Fig.55a, where $\tau_\alpha(T)$ and $1-n_\alpha$=0.36 was determined by photon-correlation [251], and the viscosity and its shift factor $a_{T\eta}$ by creep compliance measurements [283]. The CM prediction is the T-dependence of $\tau_\alpha(T)$ should be well described by $a_{T\eta}[1-n_\eta(T,P)]/[1-n_\alpha(T,P)]$. The prediction is verified in Fig.55a, and in Fig.53c for POB.

On the other hand, polyisobutylene (PIB) has a larger $(1-n_\alpha)$=0.45 [284] nearly the same as $[1-n_\eta]$=0.43. Therefore, $a_{T\eta}[1-n_\eta(T,P)]/[1-n_\alpha(T,P)]$ should have about the same temperature dependence as $a_{T\alpha}$ according to the CM. This is verified in Fig.55b by shear compliance data of PIB with M_w=78.5 k.[285]

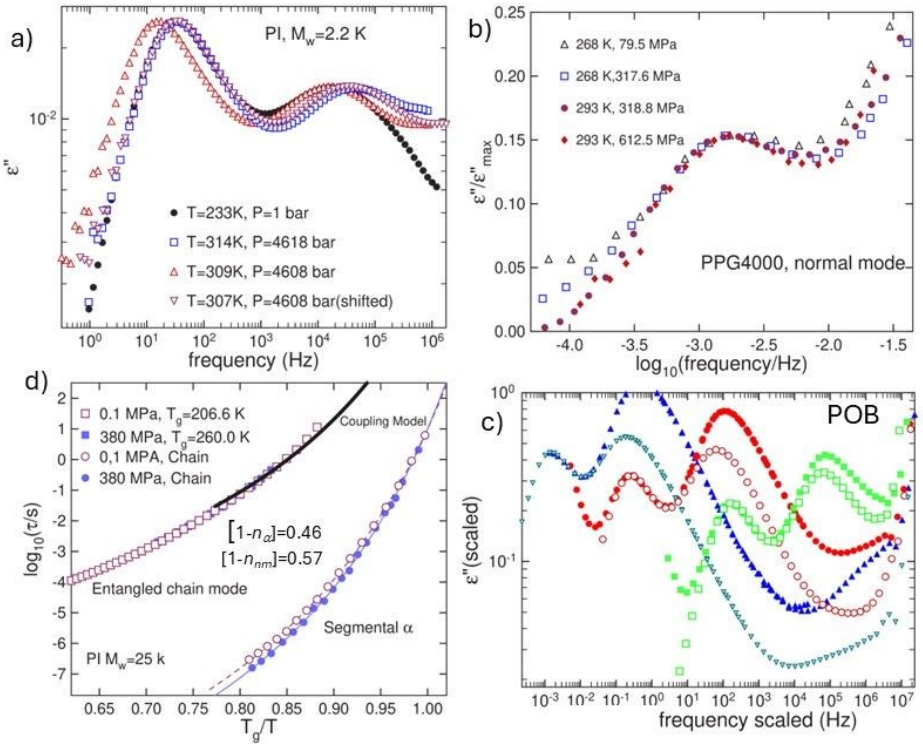

Fig. 52. *T-P* invariance of frequency dispersion of normal mode of low molecular weight PI (a) from Ref.[273]; PPG4000 (b) from Ref.[277]; and POB (c) from Ref.[277]. (d) Dielectric relaxation times as functions of T_g/T of the entangled chain terminal relaxation and the segmental α-relaxation PI

Materials Advances Accepted Manuscript

View Article Online
DOI: 10.1039/D6MA00279J

Open Access Article. Published on 04 June 2026. Downloaded on 6/5/2026 12:04:33 AM.
This article is licensed under a Creative Commons Attribution 3.0 Unported Licence.

with M_W= 25K for two different combinations of T and P from Ref.[273] The thick black line is predicted by the CM (see text).

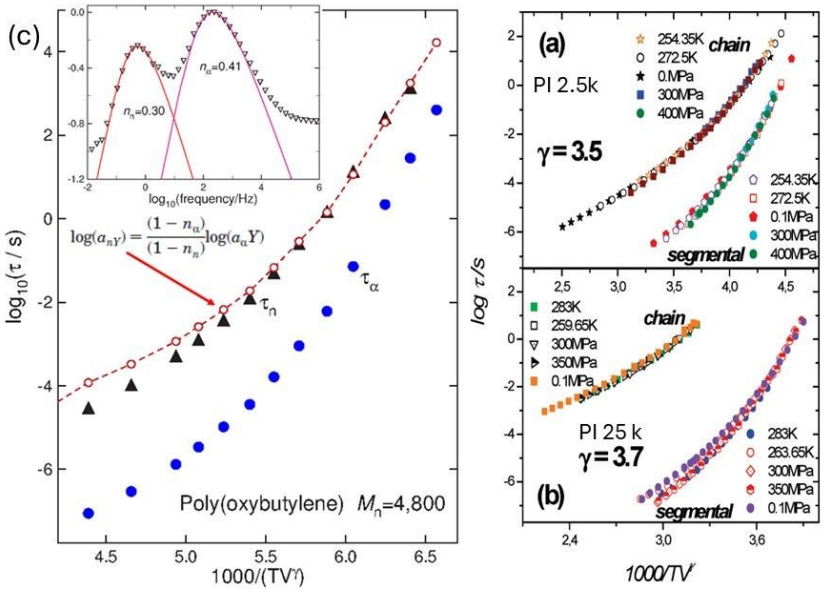

Fig. 53. TV^γ-scaling of $\tau_\alpha(T,P)$ and chain $\tau_n(T,P)$ for PI with mol. wt. (a) 2.5K and (b) 25K measured for different T and P conditions. Figure from Ref. [273] and reused with permission from ACS. (c) TV^γ-scaling of $\tau_\alpha(T,P)$ and chain $\tau_n(T,P)$ of POB with γ =2.65. Shift factors of the normal mode were calculated from $\tau_\alpha(T,P)$ using n_α =0.41 and n_n =0.30 (red circles). Inset: $\varepsilon''(f)$ of POB at T =246.6 K and P =201.4 MPa showing the normal mode and the segmental peak and the KWW fits with n_n =0.30 and n_α=0.41.

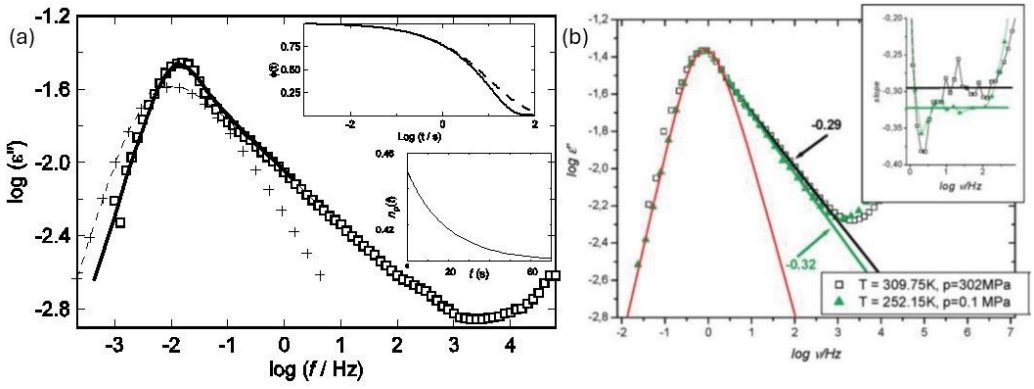

Fig. 54. (a) $\varepsilon''(\omega)$ data (□) of monodisperse entangled linear PI melts from Ref.[278]. The dashed curve is calculated by the original CM with n_p=0.45 summing over the first 4 modes, and only the first mode (+), and by the new CM that includes LCM with $n_p(t)$= (0.45-n_∞)exp(-t/τ_{LCM})+ n_∞ (solid curve). The lower inset shows the n_p(t) used in the calculation for the new CM. The upper inset shows the relaxation functions for the original CM (dashed curve) and the new CM with LCM for

Materials Advances Accepted Manuscript

View Article Online
DOI: 10.1039/D6MA00279J

p=1 mode only (solid curve). Figure taken from Ref.[226] and reused with permission from Elsevier. (b) Comparison of the spectral shape of terminal chain relaxation in PIP with M_W = 25K. Here the data at two different T and P combinations are superimposed on one curve. Lines depicted fits to the high frequency wings of this process at different conditions. Inset presents derivative analysis of the peak shape. Figure taken from Ref.[273] and reused with permission from ACS.

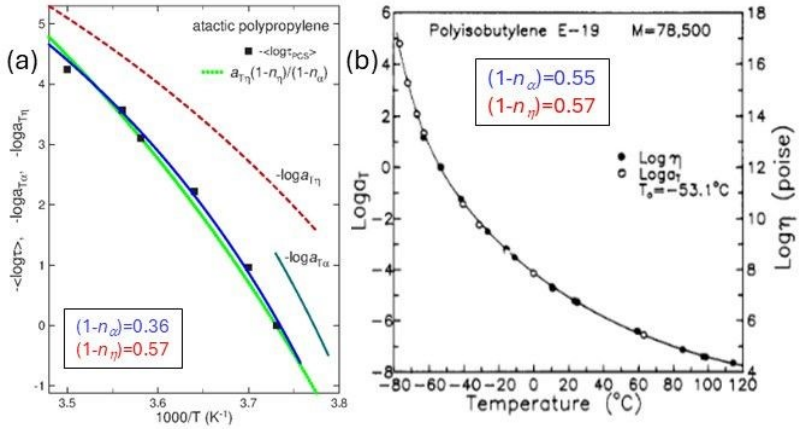

Fig. 55. (a) T-dependences of ($\log\tau$) from photon correlation studies (filled squares) and the time-scale shifts $a_{T\alpha}$ for the local segmental motion (shorter curve), and $a_{T\eta}$ for the viscosity (dashed red curve) from shear creep of a-polypropylene. The T-dependence of ($\log\tau$) obtained from the CM Eq.(19) is shown by the beaded green curve. (b) Comparison of the logarithm of the viscosity, η, and the temperature shift factors, a_T, obtained in the reduction of the recoverable compliance curves for PIB E-19, showing the same dependence from Ref.[285]. Figure reproduced from Ref.[11] with permission from Elsevier.

9. Data and alternative interpretations challenging the CM predictions?

As observed by a Reviewer, the present review presents experimental data almost exclusively as confirmations of the CM predictions. Therefore, the Reviewer requires the review to include a discussion of data that have challenged the CM and its results and predictions, and alternative interpretations or explanation of the same data. The requirement is complied with in the following subsections by revisiting the data, issues, and alternative interpretations raised by others to challenge the CM. In each case, experimental facts are provided to resolve the challenges.

9.1 Homogeneous or Heterogeneous Dynamics?

One challenge to the CM is related to the question of whether the structural α-relaxation is homogeneous or heterogeneous. The predictions from the CM related to various properties discussed in the present and past reviews are based on two equations (1) and (2), which have nothing to say whether the α-relaxation is homogeneous or heterogeneous. In 1990, the dynamics

Open Access Article. Published on 04 June 2026. Downloaded on 6/5/2026 12:04:33 AM.
This article is licensed under a Creative Commons Attribution 3.0 Unported Licence.

Materials Advances Accepted Manuscript

View Article Online
DOI: 10.1039/D6MA00279J

Open Access Article. Published on 04 June 2026. Downloaded on 6/5/2026 12:04:33 AM.
This article is licensed under a Creative Commons Attribution 3.0 Unported Licence.

of the α-relaxation in the CM is declared heterogeneous by the publication of an article [286] on the analogy with the heterogenous processes in the solution of the "Dining Philosophers Problem" of computer science [287]. The analogy gives a vivid demonstration that cooperative relaxation in the CM has to be dynamically heterogeneous and is the source of the nonexponentiality of the KWW correlation function. This was published a year before the seminal experimental work proving heterogeneous dynamics in the α-relaxation by Schmidt-Rohr and Spiess [288]. This 1990 publication is overlooked by Sillescu in his 1996 paper [289] by the statement: "Ngai and co-workers have discussed several different scenarios where stretched exponentials are obtained in homogeneous systems.". Fortunately, Sillescu corrected this mistaken view of the CM in a follow-up experimental paper with others [290] by citing the CM exclusively the 1990 paper on the dining philosophers problem [286]. Apparently, in his review published in 2000 [291], Ediger was not aware of the two papers [286,290] in making the statement: "Ngai recently used the coupling model to provide an alternate, homogeneous explanation for experimental observations of enhanced translational diffusion (79a)." This statement effectively labels the CM as a model for homogeneous dynamics, in spite of my paper [292] cited by him (Ref. 79a in his review) had explicitly made clear that the dynamics in the CM is heterogeneous.

9.2 Breakdown of Stokes-Einstein and Debye-Stokes-Einstein Relations

Breakdown of the Stokes-Einstein (SE) and the Debye-Stokes-Einstein (DSE) relations was found experimentally in different molecular glass-formers, including indomethacin [293], *tris*-naphthylbenzene [294], and ortho-terphenyl [295] over a range of temperatures down to T_g. In contrast to $D \propto \eta^{-1}$ given by the SE relation between diffusion coefficient D and viscosity η and to $D \propto \tau_\alpha{}^{-1}$ by the DSE relation, the fractional power relation of $D \propto \eta^{-\lambda}$ and $D \propto \tau_\alpha{}^{-\lambda}$ with $\lambda < 1$ were observed. The values of λ are 0.76, 0.77, and 0.80 for indomethacin, *tris*-naphthylbenzene and ortho-terphenyl respectively. Consequently, the measured D exceeds the value predicted by the SE relation by about two orders of magnitude at T_g. The spatially heterogeneous dynamics was used [292,293,294,295] to explain the breakdown of Debye-Stokes-Einstein and the Stokes-Einstein relations between diffusion and viscosity or relaxation time. It assumes regions of differing dynamics give rise to the Kohlrausch relaxation function of the structural α-relaxation in ensemble averaging. The decoupling between self-diffusion and rotation occurs because D and τ_c are averages over different moments of the distribution of relaxation times, with $D \propto <1/\tau>$ emphasizing fast dynamics, while $\tau_c \propto <\tau>$ is determined predominantly by the slowest molecules.

In order for the spatially heterogeneous explanation to be consistent with the observed monotonic increases of the products $D\eta$ and $D\tau_c$ as the temperature is lowered toward T_g, the breadth of the relaxation time distribution has to increase (or the Kohlrausch exponent β_K has to decrease) correspondingly. However, the dielectric spectra of *tris*naphthylbenzene (TNB) are characterized by a temperature independent width (e.g. β_K is constant and is equal to 0.50) from T_g=345 up to T_B≈417 K. [296]. Photon correlation spectroscopic [297] and NMR [298] measurements all indicate a temperature-independent distribution of relaxation times. Thus, the data of TNB are not consistent with the explanation based on spatial heterogeneities. The same was found in ortho-terphenyl by Richert [299] and sucrose benzoate by Rajian et al. [300]. These evidences from experiments as well as from simulations [301,302,303] led to the conclusion in Ref.[295] and Ref.[303] by Chakrabarti and Bagchi that spatial and dynamic heterogeneity of the structural relaxation cannot explain the breakdown of the Debye-Stokes-Einstein and Stokes-Einstein relations without modifications.

Materials Advances Accepted Manuscript

View Article Online
DOI: 10.1039/D6MA00279J

Open Access Article. Published on 04 June 2026. Downloaded on 6/5/2026 12:04:33 AM.
This article is licensed under a Creative Commons Attribution 3.0 Unported Licence.

The validity of the explanation by heterogeneity was taken back in the Perspective published in 2012 by Ediger and Harrowell[304] in statement: "The existence of spatially heterogeneous dynamics is the starting point for understanding why the "single time scale" proposal fails for translational diffusion while apparently working for other relaxation and transport processes. Initially, it was suggested that the difference in temperature dependence between diffusion and structural relaxation, for example, arose as a result of the difference in how the respective observables averaged over the distribution of time scales. This view is now seen as inconsistent with experiments[142, 144, 145] and simulations[148,149].". However, in the Perspective published in 2026 by Dyre and Ediger[62], apparently this standpoint is reversed. On the breakdown of SE and DSE relations, they stated: "It is generally understood as an effect of dynamic heterogeneity, the observation that the molecular dynamics always varies notably in space, at any given time, with some regions being slow and others fast[52,175–179].".

An alternative explanation [292] of the breakdown of the SE and DSE relations was proposed by the CM based on its Eq.2, now generalized to become $\tau_\mu = [t_c^{-n_\mu}\tau_{0\mu}]^{1/(1-n_\mu)}$. This form is applicable for different dynamic variables μ related to diffusion, rotation, and viscosity, and they have different coupling parameters n_μ. Applying these CM equations to the various μ, the one having a larger n_μ will bestow a longer and stronger temperature dependence for its relaxation time τ_μ, as demonstrated in ref.[49]. This is because the primitive relaxation times of all observables $\tau_{0\mu}$ should have comparable values and the same temperature dependence. This CM explanation applies straightforwardly when n_μ is independent of temperature from T_B down to T_g as found in experiments [296,297,298,299,300] and demonstrated in Ref.[304]. The CM was able in Ref.[292] to explain the empirical correlation found between the enhanced translation given by the product, $D\tau_c$, at T_g with the Kohlrausch non-exponentiality parameter β at T_g for probes in many different glass-formers.

Support of the CM explanation of the breakdown of the SE and DSE relations without assuming the value of n_D [302] came from molecular dynamics simulation of an equimolar mixture of interacting Gay-Berne ellipsoids of revolution and Lennard-Jones spheres along an isochore at a series of temperatures down to the deeply supercooled state by Chakrabarti and Bagchi [303]. Also known are the other coupling parameters n_1 and n_2 of the first and second rank single particle orientational time correlation functions, $C_1(t)$ and $C_2(t)$. The CM explanation is quantitative and the predictions compare well with the simulation data. For details, see Ref.[302].

9.3 Important to distinguish the JGβ relaxation from intramolecular secondary relaxation

The CM has the primitive relaxation, with relaxation time $\tau_0(T,P)$ related to the α-relaxation time $\tau_\alpha(T,P)$ by Eq.(2), is coupled to the α-relaxation in many properties. The primitive relaxation is the precursor of a special kind of secondary relaxation with relaxation time $\tau_\beta(T,P)$ also coupled to $\tau_\alpha(T,P)$ in properties, in accord with the prediction of the CM and as shown in various Sections of this review. This special kind of secondary relaxation is called the JGβ relaxation in order to distinguish those of intramolecular origin and having no relation to the α-relaxation in properties. The CM prediction of the properties of JGβ relaxation should not be applied when intramolecular secondary or non-JGβ relaxation is involved. The emphasis of the universal presence of the JGβ

Materials Advances Accepted Manuscript

View Article Online
DOI: 10.1039/D6MA00279J

Open Access Article. Published on 04 June 2026. Downloaded on 6/5/2026 12:04:33 AM.
This article is licensed under a Creative Commons Attribution 3.0 Unported Licence.

relaxation and the roles it plays is unique in the CM, and absent in conventional theory of glass transition including Adam and Gibbs [53] and free volume, as well as in current theories [54,55,56,57,58,59,60,61,62]. Thus, it is unsurprising that researchers unfamiliar with or unfavourable to the CM neglect the necessity to distinguish JGβ relaxation from the intramolecular secondary relaxation. They applied the CM prediction to non-JGβ relaxation, and naturally the prediction fails miserably. An example is the JGβ relaxation time $\tau_\beta(T)$ of toluene. Its value in ultrastable glass is longer than in ordinary glass[121] as shown before in Fig.2b. Like toluene, the JGβ relaxation of etoricoxib and telmisartan studied in Ref.[122] becomes *slower* in the USG than in OG. This behavior of JGβ relaxation has been explained by the CM in Ref.[119].

Studied also in Ref.[122] are the secondary relaxations in USG and OG glasses of β-D-maltose octa-acetate, carvedilol, and celecoxib. Known before from their properties in the supercooled liquid state, these secondary relaxations do not belong to the class of JGβ relaxations, and have no connection to the α relaxation in properties. Unsurprisingly, they behave differently from JGβ relaxation in β-D-maltose octa-acetate, carvedilol, and celecoxib by becoming *faster* in the USG than in the OG [122]. Unfortunately, Berthier and Ediger [58] did not recognize in reading Ref.122 that the secondary relaxation in β-D-maltose octa-acetate, carvedilol, and celecoxib are intramolecular in nature and not JGβ relaxations. The failure to distinguish non-JGβ secondary relaxation in β-D-maltose octa-acetate, carvedilol, and celecoxib from JGβ relaxation in toluene, etoricoxib and telmisartan led them to challenge the CM explanation [119].

9.4 Surface diffusion $\tau_{surface}(T)$ is agreement with $\tau_0(T) \approx \tau_\beta(T)$?

The CM was successful in explain quantitatively the diffusion coefficient at the surface of molecular glass-formers such as ortho-terphenyl, indomethacin, TPD, and metallic glass in Sections 6.3 and 6.4, and shown in Figs.39 and 40. The relaxation time at the surface $\tau_{surface}(T)$ should be close to the primitive relaxation time $\tau_0(T)$ calculated by the CM equation, $\tau_0 = t_c^n \tau_\alpha^{1-n}$ with t_c=2 ps for molecular liquids, or the JGβ relaxation time $\tau_\beta(T)$ from experiment. However, Tylinski et al.[218] questioned the CM explanation for ethylcyclohexane (ECH) by calculating $\tau_0(T)$ of ECH using the value of β_{KWW}=(1-n)=0.53 from the dielectric study by Mandanici et al. [213,214,215], and finding the $\tau_0(T)$ calculated is much shorter than $\tau_{surface}(T)$ for $T<T_g$. As demonstrated in Ref.[216] and described in Section of 6.3 and illustrated in Fig.41, the value β_{KWW}=(1-n)=0.53 used by Tylinski is obtained by fitting the dielectric α-loss peak broadened by the contribution from the JGβ relaxation. The actual β_{KWW} value of the α- relaxation is larger and close to 0.70 as discussed in Section 6.3. The calculated $\tau_0(T)$ with the corrected value of β_{KWW} are in good agreement with $\tau_{surface}(T)$ at $T=T_g$ (see Fig.41). The values of $\tau_\beta(T)$ determined from dielectric spectroscopy and by agreement with $\tau_0(T) \approx \tau_\beta(T)$ in ECH.

Tylinski et al. [218] measured also $\tau_{surface}(T)$ of the monohydroxy alcohol, 2-ethyl-1-hexanol (2E1H), and found $\tau_{surface}(T)$ is shorter than $\tau_0(T)$ calculated by the CM equation with β_{KWW}=(1-n)=0.53. This value of β_{KWW} is correct and close to value of 0.56 from another source [305]. However,

Materials Advances Accepted Manuscript

View Article Online
DOI: 10.1039/D6MA00279J

Open Access Article. Published on 04 June 2026. Downloaded on 6/5/2026 12:04:33 AM.
This article is licensed under a Creative Commons Attribution 3.0 Unported Licence.

Tylinski et al. should not compare the $\tau_{surface}(T)$ data of 2E1H with the CM and RFOT in their Fig.7 to show disagreement with the predictions. This is because 2E1H on the surface can form chains and clusters with other molecules below the surface by hydrogen bonds [306]. Hence the $\tau_{surface}(T)$ measured is unrelated to mobility on the surface per se.[307] Tylinski et al. knew this as evidenced by the statement: "Work by Chen et al. suggests that the ability to form intermolecular hydrogen bonds may limit the surface mobility and this would be consistent with the slower surface relaxation of 2-ethyl-1-hexanol.".

9.5 The $\chi''(\omega)$ of the α-relaxation has a generic line-shape with $\chi''(\omega) \propto \omega^{-1/2}$ ($\omega\tau_\alpha >> 1$)?

Probed by dielectric spectroscopy, many polar molecular liquids including glycerol, propylene glycol, and tributyl phosphate have intense and narrow dielectric loss, $\varepsilon''(\omega)$, peak identified with the structural α-relaxation in the CM. A weak excess wing on the high frequency flank is considered as contributed by the unresolved JGβ relaxation [11]. In contrast, the susceptibility spectra $\chi''(\omega)$ from depolarized dynamic light scattering (DDLS) or photon correlation spectroscopy (PCS) and ^{2}H NMR of the same polar molecules shows more or less the same generic line shape of many less polar molecules, with the high frequency slope near -0.5 in a log $\chi''(\omega)$ vs. logω plot [62,193,195]. This feature, and the fact that self-correlation is probed by DDLS and ^{2}H NMR, apparently led Pabst et al.[193] and Böhmer et al. [194] to believe that the intense and narrow dielectric loss $\varepsilon''(\omega)$ peak of polar molecules does not represent the true α-relaxation. They split the $\varepsilon''(\omega)$ spectrum into the sum of two contributions. The slower one is intense and Debye-like and is arbitrarily assigned as coming from dipolar cross-correlations. The faster and weaker one is assumed to have the generic line shape found by DDLS. It is assumed to come from dipolar self-correlations, i.e., orientational time autocorrelations of the single molecular dipoles, and it is identified as the true α-relaxation of polar molecules such as glycerol.

This generic line shape hypothesis for all molecules polar or not is the antithesis of the CM precepts and predictions. Probed by the same spectroscopies, the different intermolecular interactions present in molecules with widely different chemical composition and physical structures necessarily result in different values of the coupling parameter n=(1-β_{KWW}) in Eqs. (1) and (2). Hence, there is no generic line shape or the same β_{KWW} in the KWW relaxation function for all molecules in the CM. The universal presence of the JGβ relaxation is one of the key CM predictions. Its relaxation time τ_β is approximately the same as the primitive relaxation time τ_0 calculated with the value of n by Eq.(1). This prediction is verified in glass-formers whenever the JGβ relaxation is resolved and τ_β determined[11]. The intense and narrow dielectric loss peak of glycerol well fitted by the KWW function with β_{KWW}=0.70 is identified with the α-relaxation, and the weak excess wing on its high frequency side is considered as coming from the unresolved JGβ relaxation with its relaxation time τ_β approximately the same as the primitive τ_0 calculated by Eq.(2) as shown by the lower inset in Fig.38. The existence of the JGβ relaxation in glycerol was verified by Saito et al.[82] directly by quasielastic scattering experiments using time-domain interferometry (TDI). The α and JGβ relaxations were resolved in the TDI experiment, and

Materials Advances Accepted Manuscript

View Article Online
DOI: 10.1039/D6MA00279J

Open Access Article. Published on 04 June 2026. Downloaded on 6/5/2026 12:04:33 AM.
This article is licensed under a Creative Commons Attribution 3.0 Unported Licence.

confirmed is that the α-relaxation from TDI has β_{KWW} =0.70 as from dielectric relaxation (see Fig. 38). The JGβ relaxation times from TDI are [86] in good agreement with $\tau_0(T)$ as shown in Fig.38. These findings from TDI experiment cast serious doubt on the validity of decomposing $\varepsilon''(\omega)$ into the Debye-like cross-correlation term and the self-correlation term with the generic line shape. This is because the broad JGβ relaxation found by TDI cannot be ignored by Pabst et al.[193] and Böhmer et al. [194], and it is present in the $\varepsilon''(\omega)$ spectrum over the same frequency range as the purported self-correlation term.

The monohydroxy alcohols (MAs) including 1-propanol and 5-methyl-2-hexanol (5M2H) were studied by both dielectric spectroscopy and DDLS. These MAs have the molecules forming hydrogen-bonded supra-structures observed in the dielectric-loss spectrum as a slow and narrow Debye loss peak in $\varepsilon''(\omega)$. This process is unique to the MAS, and not present in glycerol or other polar molecules. Nevertheless, the Debye process is identified by Böhmer et al. [194] as from dipolar cross-correlation. This is questionable because the Debye process in the MAs is special and cannot be identified with the so called cross-correlation term in glycerol, propylene glycol, or other polar molecules. In other words, the cross-correlation term of the MAs has yet to be found in order to be consistent with the explanation given by Böhmer et al. [194] for the other polar molecules. After subtracting the extraneous Debye peak from $\varepsilon''(\omega)$, Gabriel et al.[308] and Böhmer et al.[194] found the remainder after subtraction in $\varepsilon''(\omega)$ is much less polar than glycerol or propylene glycol. The same is true for 1-propanol.[85,309] This remainder in $\varepsilon''(\omega)$ is the dielectric α-relaxation without question even though it has the same shape as $\chi''(\omega)$ of DDLS as shown in Fig.13b for 5M2H. However, one should not jump to assert it is from self-correlation without proof as done by Böhmer et al.[194] by the statement: "For monohydroxy alcohols, it is well established that the glass transition temperature determined using calorimetric techniques, as well as physical aging, is controlled by the characteristic relaxation time of the self-correlations instead of that of the Debye process [98,106,153–155]." Furthermore, Böhmer et al.[194] should not put the dielectric $\varepsilon''(\omega)$ of the MAs in the same category as glycerol, propylene glycol, and tributyl phosphate. Moreover, the remainder in $\varepsilon''(\omega)$ after subtraction has the same generic shape as $\chi''(\omega)$ from DDLS as shown in Fig.13b for 5M2H. Present also is the same resolved secondary relaxation in both the dielectric and DDLS spectra, which is identified as the JGβ relaxation by the fact of its relaxation time τ_β is approximately the same as the primitive τ_0 calculated by Eq.(2) , as well as the τ_β determined by TDI experiments [80,81,83] as shown in Ref. [85] for both 5M2H and 1-propanol and Fig.13a herein. The data of the MAs serve to demonstrate validity of the CM prediction of the relation between τ_α and $\tau_\beta \approx \tau_0$ given by Eq.2 in DDLS spectra of non-polar molecules, and also in dielectric spectra of non-polar molecules such as ortho-terphenyl[85] and toluene[310].

As discussed before in Section 6.2, the interpretation of dielectric data by Pabst et al.[193] and Böhmer et al[194] had been contested by Moch et al. [197,198], Richert[199], and Aresse-Igor [200]. Using physical aging and oscillatory shear rheology to directly access the structural relaxation of the polar tri-butyl phosphate, Moch et al.[197] revealed that the dielectric loss peak corresponds to

Materials Advances Accepted Manuscript

View Article Online
DOI: 10.1039/D6MA00279J

Open Access Article. Published on 04 June 2026. Downloaded on 6/5/2026 12:04:33 AM.
This article is licensed under a Creative Commons Attribution 3.0 Unported Licence.

collective equilibrium fluctuations govern the structural α-relaxation and is not the self-correlation term suggested by single-particle dynamics Pabst et al.[193] and Böhmer et al. [194]. The conclusion by Moch et al. is supported by dielectric study of the highly polar propylene glycol (β_{KWW} =0.81 and Δε=54.7) by Richert [199] in comparing directly the equilibrium fluctuations from 'structural' relaxation in the regime of linear response, with structural recovery by physical aging. Dielectric relaxation in equilibrium and recovery dynamics was observed to be identical. In contrast single-particle dynamics as seen by DDLS or PCS are about a factor of 20 faster than the collective counterpart seen by dielectric spectroscopy [198,311]. Richert's result confirms that structural recovery and aging is governed by all modes observed by dielectric spectroscopy, i.e., including cross correlations, and not only by single-particle dynamics observed by DDLS. Independently, another recent study of propylene glycol from linear and nonlinear dielectric experiments by Moch et al. [312] have also found that the dielectric relaxation times of PG are in agreement with calorimetry, found also for many glass-forming liquids from small-amplitude modulated calorimetry [312]. In view of these experimental results from Moch et al.[197] on tributyl phosphate and Richert [199] on propylene glycol. Böhmer et al. [194] made the statement: "First experiments on tributyl phosphate and propylene glycol suggest that in these systems the glass transition might instead be coupled to the relaxation time of cross-correlations.[124,156]" By this statement, they conceded that the dielectric α-loss peak (designated as the cross-correlation term by them) in these polar molecules are responsible for glass transition. The assertion of a generic line shape observed by photon correlation spectroscopy for all glass-formers [163,164] was also contradicted by data published recently by Rössler and Becher [202] where they found three systems, namely, DMP, o-terphenyl, and salol, show significant departures. Polychlorinated biphenyls also known as Aroclor is another highly polar glass-former having a narrow dielectric loss peak well fitted by the KWW function with β_{KWW} = 0.68 at 224 K, and 0.70 at 249.1 K.[196,313] Photon Correlation Spectroscopy (PCS) was performed by Rizos et al.[314] on Aroclor at temperatures near 249.1 K and higher. The value of β_{KWW} for PCS reported is 0.63 and temperature independent. Thus, unlike glycerol and TBP, the $\chi''(\omega)$ from self-correlation measured by PCS has the same narrow frequency dispersion as $\varepsilon''(\omega)$ far from the generic line shape and the $\chi''(\omega) \propto \omega^{-1/2}$ ($\omega\tau_\alpha >> 1$) expected. [62,194]

Böhmer et al. [194] did not consider the any aspect of the spectral shape of structural relaxation in polymers, although polymers belong to another important class of materials that are commonly obtained in the deeply supercooled liquid state like molecules. Therefore, the spectra of amorphous polymers obtained by photon correlation spectroscopy (PCS) should have the generic line shape. Had Böhmer et al. [194] considered the PCS data of the structural α-relaxation of amorphous polymers available, the results will show large deviations from the generic line shape and $\chi''(\omega) \propto \omega^{-1/2}$ ($\omega\tau_\alpha >> 1$) of molecular liquids. The PCS data of polymers were presented in terms of the time dependence of the correlation function $g(t)$. In most cases, $g(t)$ is well fitted by the KWW function, and the value of β_{KWW} at temperatures near T_g was determined. The value is 0.34 for polystyrene[315], 0,36 for poly(vinylacetate)[316], 0.38 for poly(ethyl acrylate)[317], 0.42 for poly(methyl acrylate)[318], 0.36 for atatic polypropylene[319], 0.52 for poly(methylphenyl siloxane)[320],

Materials Advances Accepted Manuscript

View Article Online
DOI: 10.1039/D6MA00279J

Open Access Article. Published on 04 June 2026. Downloaded on 6/5/2026 12:04:33 AM.
This article is licensed under a Creative Commons Attribution 3.0 Unported Licence.

0.56, for polyisobutylene[321], and 0.39 for poly(cyclohexy1 methacrylate)[322]. Authors of these publications all expressed that these β_{KWW} values characterize the structural α-relaxation of the polymers. From the large spread in the values of β_{KWW}, the generic line shape and $\chi''(\omega) \propto \omega^{-1/2}$ fail when applied to the structural relaxation of polymers. In defense of this problem, Böhmer et al. [194] cited the opinion of Dyre [323] that "Polymers are different". Dyre stated that "the low-frequency side of dielectric relaxation, frequency dependent shear and bulk modulus measurements in log-log plot has slope of 1 at sufficiently low frequencies, but this is not the case for polymers.". This statement by Dyre is not valid for the PCS data of polymers cited in Refs.[315-322] with $g(t)$ all well fitted by the KWW functions, and it is a fact from mathematics that the $\chi''(\omega)$ obtained by Fourier transform of the derivative of the KWW function has $\chi''(\omega) \propto \omega^{1.0}$ at sufficiently low frequencies. Williams and Watts themselves were the first ones to fit successfully the dielectric $\varepsilon''(\omega)$ from the α relaxation in polymers in a similar way by the KWW function[23,324,325]. Shown in Fig. S5 in Supplementary Materials are the KWW fits to $\varepsilon''(\omega)$ of poly(methylphenyl siloxane) [326] and poly(vinyl acetate) [327]. The purple and red lines in Fig. S(a) with slope exactly equal to 1 are drawn to demonstrate that the data as well as the KWW fit has slope unity at low frequencies. The $\varepsilon''(\omega)$ of poly(methyltolylsiloxane) (PMTS) shown in Fig.2b also has slope unity at low frequencies. If Dyre and Böhmer et al. [194] have the opportunity to learn that the universal properties of the α-relaxation and its precursors (JGβrelaxation and caged dynamics) in molecular glass-formers discussed in Sections 2, 3, 4, 5, and 6 are shared by the polymers, they will recognize that polymers are not different. The chain modes of polymers have properties connected with the α-relaxation as shown in Figs.44,45,48,50,51,52,53 and 55. Hence, one can say polymers are richer.

Böhmer et al. [194] was also concerned about polymers having other modes of relaxation. In practice, the only the JGβrelaxation and the slower chain modes at higher and lower frequencies may present a problem for the α-relaxation in polymer. Possible problem coming from the JGβ relaxation is common to both polymer and molecular liquids. It is of lesser concern in polymers because the JGβ and the α-relaxation are further apart in time/frequency in many polymers than molecular liquids because of the smaller β_{KWW} value in Eqs.(2) and (3) combined. The chain modes make insignificant contribution to the PCS correlation function $g(t)$ in the high molecular weight polymers studied in Refs.[315-322]. The KWW function fitting $g(t)$ is the relaxation function and the corresponding $\chi''(\omega)$ is the susceptibility of the α-relaxation.

10. Conclusions

Various amorphous materials have been studied for different purposes in physics, chemistry, biophysics, pharmaceutics, and material science and engineering in the past decades and continued to the present time. The materials studied can differ greatly in physical structures and chemical

Materials Advances Accepted Manuscript

View Article Online
DOI: 10.1039/D6MA00279J

Open Access Article. Published on 04 June 2026. Downloaded on 6/5/2026 12:04:33 AM.
This article is licensed under a Creative Commons Attribution 3.0 Unported Licence.

bonding and compositions and *a priori* there is no reason to expect the existence of some universal properties that are fundamental and sophisticated. Notwithstanding, my 1979 paper [1] suggested the existence of universal relaxation and diffusion dynamics governed by anharmonic interaction potentials in amorphous materials, which is reaffirmed by subsequent development of the theory now known as the Coupling Model [4-11]. The existence of universal or generic properties was promoted effectively by the eminent condensed matter physicist and Nobel-Prize winner, P.W. Anderson, by observing that "*Randomness and disorder could result in generic properties that are utterly different from those of merely somewhat impure regular materials*", cited by the editors of this themed collection on Amorphous Materials in their call for papers.

In the past few decades, advances in various spectroscopies enable measurements made over immense frequency range, at elevated pressures up to several GPa, and in configurations of nanometer size. These advances made possible the remarkable discoveries by experiments and simulations of several universal and fundamental properties of relaxation and diffusion in diverse types of materials studied in different disciplines. Some of the data available before 2022 together with the explanations by the Coupling Model were given in the extensive review [11] published in 2023. The research of dynamics and thermodynamics of amorphous materials since 2022 have yielded more data relevant to the universal or generic properties. These new developments are the focus of the present review to show consistency with the universal properties reviewed in the past. However, randomness and disorder or static and dynamics heterogeneity in amorphous materials are not sufficient or critical in generating these universal properties. Instead, it is the anharmonic interaction in an amorphous material which gives rise to the many-body dynamics characterized by the coupling parameter n of the Coupling Model. Importantly, the size of n determines the degree in the manifestation of each universal property in the amorphous material.

The interest of most researchers on relaxation and diffusion is limited to a few classes of amorphous materials, and may not care so much for universality of the properties. Nevertheless, the message conveyed by the present and the past reviews is clear that these universal properties are critical and impactful. It should draw special attention from all researchers in relaxation and diffusion of materials of many different classes, and the first order of business is the resolution and explanation of the universal properties. Inexplicably, this has not happened so far. The universal properties are put by the wayside while research continues and the results are interpreted unmindful of the properties. The impending danger of this current research trend is the interpretations of the results from current and past experiments may have contradicted already the universal properties. The situation is not helped by mainstream theories have either ignored these properties or offered no explanation so far, except from the Coupling Model. It is hoped by writing this review that the untenable current trend in research of relaxation and diffusion in complex materials will be rectified in the future.

Author contributions

Materials Advances Accepted Manuscript

View Article Online
DOI: 10.1039/D6MA00279J

Open Access Article. Published on 04 June 2026. Downloaded on 6/5/2026 12:04:33 AM.
This article is licensed under a Creative Commons Attribution 3.0 Unported Licence.

Materials Advances Accepted Manuscript

Conflicts of interest

I have no conflict of interest

Acknowledgements

I thank CNR-IPCF for my appointment as Ricercatore Associato con incarico di collaborazione Senior in 2025 and 2026.

References

1 K.L. Ngai, *Comment Solid State Phys*., 1979, **9**, 127.
2 R.G. Palmer, D.L. Stein, E. Abrahams and P.W. Anderson, *Phys.Rev.Lett*., 1984, **53**, 958.
3 P.W. Anderson, *Science*, 1995, **267**, 1609.
4 K.L. Ngai KL, S.L. Peng, and K.Y. Tsang, *Physica A,* 1992, **191**, 523-531.
5 K.Y. Tsang, and K.L. Ngai, *Phys Rev E* 1996, **54**, R3067.
6 K.Y. Tsang, and K.L. Ngai, *Phys Rev E* 1997, **56**, R17.
7 R.W. Rendell, *Phys Rev E* 1993, **48**, R17.
8 K.L. Ngai, and K.Y. Tsang, *Phys. Rev. E* 1999, **60**, 4511.
9 K.L. Ngai, *J. Phys. C* 2000, **12**, 6437.
10 K.L. Ngai, *Relaxation and Diffusion in Complex Systems*, Springer, New York, 2011.
11 K.L. Ngai, *Prog. Mater. Sci.* 2023, **139**, 101130.
12 K.L. Ngai, *J. Chem. Phys*. 1998, **109**, 6982.
13 K.L. Ngai, and M. Paluch, *J. Chem. Phys*. 2004, **120**, 857.
14 G.P. Johari and M. Goldstein, *J. Chem. Phys*., 1970, **53**, 2372.
15 G.P. Johari and M. Goldstein, *J. Chem. Phys*., 1972, **55**, 4245
16 G. P. Johari, Ann. N.Y. Acad. Sci. 1976, **279**, 117.
17 M. Goldstein, *J. Non-Cryst. Solids*, 2011, **357**, 249.
18 P. Bordat, F. Affouard, M. Descamps, and K.L. Ngai, *Phys. Rev. Lett*. 2004, **93**, 105502.
19 P. Bordat, F. Affouard, and M. Descamps, *J. Non-Cryst Solids* 2007, **353**, 3924.
20 M. Paluch, J. Knapik, Z. Wojnarowska, A. Grzybowski, and K. L. Ngai, *Phys. Rev. Lett*., 2016, **116**, 025702.
21 R. Kohlrausch, *Pogg. Ann. Phys. Chem*., 1854, **91**, 56.
22 R. Kohlrausch, *Pogg. Ann. Phys. Chem.*, 1854, **91**,179.
23 G. Williams and D.C. Watts, *Trans. Farad. Soc*., 1970, **66**, 80.
24 F. Kohlrausch, *Pogg. Ann. Phys. Chem.*, 1863, **119**, 337.
25 F. Kohlrausch, *Pogg. Ann. Phys. Chem*., 1866, **128**, 1, 207, 399.
26 F.S. Howell, R.A. Bose, P.B. Macedo, et al., *J. Phys. Chem*. 1974, **78**, 639.
27 K. L. Ngai, R. Casalini, S. Capaccioli, et al., *J. Phys. Chem. B,* 2005, **109**, 17356.
28 K. Adrjanowicz, K. Kaminski, M. Paluch, et al., *J. Chem. Phys*. 2012, **136**, 234509.
29 M. Romanini, M. Barrio, S. Capaccioli, R. Macovez, M. D. Ruiz-Martin and J. L. Tamarit, *J. Phys. Chem. C* 2016, **120**, 10614.
30 D. Heczko and E. Kaminska, *J. Non-Cryst. Solids*, 2026, **681**, 124061
31 P. Luo, Y. Zhai, P. Falus, V. Garcia Sakai, et al., *Nat. Commun*. 2022, **13**, 2092.
32. Y. Zhang, K. L. Ngai and Li-Min Wang, *J. Chem. Phys.*, 2025, **163**, 024509.

View Article Online
DOI: 10.1039/D6MA00279J

Open Access Article. Published on 04 June 2026. Downloaded on 6/5/2026 12:04:33 AM.
This article is licensed under a Creative Commons Attribution 3.0 Unported Licence.

33 G. F. Signorini, J. L. Barrat and M. L. Klein, *J. Chem. Phys*. 1990, **92**, 1294.
34 J. Baglioni, A. Martinelli, P. Sun, F. Dallari, L. Piemontese, M. Umair, F. Westermeier, M. Sprung and G. Monaco, *Newton*, 2026, **2**, 100338.
35 M. Umair, F. Dallari, J. Baglioni, A. Piarristeguy and G. Monaco, *Thermochimica Acta* 2025, **752**, 180067.
36 B. Rufflé and S. Longeville, *Scientific Highlights*, Laboratoire Léon Brillouin, CEA Saclay, 2004, 84.
37 G. C. Sosso, J. Colombo, J. Behler, E. Del Gado and M. Bernasconi, J. *Phys. Chem. B* 2014, **118**, 13621.
38 A. A. Pronin, M. V. Kondrin, A. G. Lyapin, V. V. Brazhkin, et al. *Phys. Rev. E* 2010, **81**, 041503.
39 M. Paluch, C. M. Roland, S. Pawlus, J. Zioło, K. L. Ngai, *Phys. Rev. Lett.* 2003, **91**, 115701.
40 K. Adrjanowicz, J. Pionteck and M. Paluch, *RSC Adv.* 2016, **6**, 49370.
41 K. Adrjanowicz, K. Kaminski, Z. Wojnarowska et al., *J. Phys. Chem. B* 2010, **114**, 6579.
42 M. Romanini, M. Barrio, R. Macovez, M. D. Ruiz-Martin, et al. *Sci. Rep*. 2017, **7**, 1346.
43 T. S. Ingebrigtsen, T. B. Schrøder, and J. C. Dyre, *Phys. Rev. X*, 2012, **2**, 011011.
44 H. W. Hansen et al., *Nat. Commun*. 2018, **9**, 518.
45 N. P. Bailey, U. R. Pedersen, N. Gnan, et al., *J. Chem. Phys*. 2009, **131**, 234504.
46 C. M. Roland, R. Casalini, R. Bergman, and J. Mattsson, *Phys. Rev. B*, 2008, **77**, 012201.
47 D. Fragiadakis and C. M. Roland, 2017, **147**, 084508.
48 Y-C Hu et al., *J. Chem. Phys*., 2016, **145**, 104503.
49 N. N. Ren, P. F. Guan and K. L. Ngai, *J. Chem. Phys*., 2021, **155**, 244502.
50 K. Kessairi, S. Capaccioli, et al., *J. Phys. Chem. B*, 2008, **112**, 4470.
51 M.S. Thayyil, K.L. Ngai, et al., *J.Non-Cryst.Solids,* 2015, **407**, 98.
52 D. Bedrov and G.D. Smith, *J. Non-Cryst. Solids*, 2011, **357**, 258.
53 G. Adam and J. H. Gibbs, *J. Chem. Phys*., 1965, **43**, 139.
54 W. Götze, *J. Phys. Condens. Matter*, 1999, **11**, A1.
55 J. D.Stevenson and P. G. Wolynes, *J. Phys. Chem. A* 2011, **115**, 3713.
56 V. Lubchenko and P. G. Wolynes, *Annu. Rev. Phys. Chem.* 2007, **58**, 235.
57 M. Mezard and G. Parisi, *J. Chem. Phys*. 1999, **11**, 1076.
58 L. Berthier and G. Biroli, *Rev. Mod. Phys*. 2011, **83**, 587.
59 L. Berthier and M. D. Ediger, *J. Chem. Phys.* 2020, **153**, No. 044501.
60 S. Mirigian and K. S. Schweizer, *J. Phys. Chem. Lett.* 2013, **4**, 3648. *J. Chem. Phys.* 2015, **143**, 244705.
61 J. C. Dyre, *J. Chem. Phys.* 2018, **149**, 210901.
62 J. C. Dyre and M. D. Ediger, *Nature Reviews Physics*, https://doi.org/10.1038/s42254-026-00940-x
63 G. Jarosz, M. Mierzwa, J. Ziolo, et al., *J. Phys. Chem. B*, 2011, **115**, 12709.
64 Z. Wojnarowska, A. Swiety-Pospiech, et al., *J. Chem. Phys*. 2012, **136**, 164507
65 M. Abkowitz, D. F. Pichan and J. M. Pochan, *J. Appl. Phys*. 1982, **53**, 4173.
66 S. Etienne, J. Y. Cavaille, J. Perez, et al., *Rev. Sci. Instrum*. 1982, **53**, 1261.
67 R. Böhmer and C.A. Angell*, Phys. Rev. B*. 1992, **45**, 10091.
68 R. Böhmer and C.A. Angell, *Phys. Rev. B*. 1993, **48**, 5857.
69 A. Zeidler, P. S. Salmon, D. A. J. Whittaker, K. J. Pizzey, et al., *Front. Mater*. 2017, **4**, 32.
70 K. L. Ngai and S. Capaccioli, *Phys. Rev. E* 2004, **69**, 031501.
71 A. Kudlik, C. Tschirwitz, S. Benkhof, et al., *Europhys. Lett*. 1997, **40**, 649.

Materials Advances Accepted Manuscript

View Article Online
DOI: 10.1039/D6MA00279J

Open Access Article. Published on 04 June 2026. Downloaded on 6/5/2026 12:04:33 AM.
This article is licensed under a Creative Commons Attribution 3.0 Unported Licence.

72 H. Yu, X. Shen, Z. Wang, L. Gu, W. Wang and H. Bai, *Phys. Rev. Lett*. 2012, **108,** 015504.
73 L. Hu and Y. Yue, *J. Phys. Chem. C* 2009, **113**, 15001.
74 P. Koštál, M. Včeláková and J. Málek, *J. Am. Ceram. Soc.* 2024, **107**, 844.
75 J. Málek and J. Shánělová, *J. Non-Cryst. Solids* 2005, **351**, 3458.
76 J. Thompson and K. Bailey, *J. Non-Cryst. Solids* 1978, **27**, 161.
77 M. Saito, R. Masuda, Y. Yoda and M. Seto, *Sci. Rep*. 2017, **7**, 12558.
78 M. Saito, S. Kitao, Y. Kobayashi, et al., *Phys. Rev. Lett*., 2012, **109**, 115705.
79 T. Kanaya, R. Inoue, M. Saito, et al., *J. Chem. Phys*., 2014, **140**, 144906.
80 F. Caporaletti, S. Capaccioli, S. Valenti, et al., *Sci. Rep*., 2019, **9**, 14319.
81 F. Caporaletti, S. Capaccioli, S. Valenti, et al., *Nat. Commun*., 2021, **12**, 1867.
82 M. Saito, M. Kurokuzu, Y. Yoda, and M. Seto, *Phys. Rev. E*, 2022, **105**, L012605.
83 F. Caporaletti, S. Capaccioli, D. Bessas, et al., *J. Mol. Liqu*. 2023, **383**, 122107.
84 M. Saito, T. Araki, Y. Onodera, K. Ohara, et al., *Acta Mater*., 2025, **284**, 120536.
85 K. L. Ngai, *Phys. Rev. E*, 2021,**104**, 015103.
86 K. L. Ngai, S. Capaccioli, P. Lunkenheimer et al., *Phys. Rev. E*, 2022, **105**, 054609.
87 K.L. Ngai and L-M Wang, *J. Phys. Chem. B*, 2019, **123**, 714.
88 K. L. Ngai, S. Capaccioli, M. Paluch and L. Wang, *Philos. Mag*. 2020, **100**, 2596.
89 Y. Yang and K. A. Nelson, *J. Chem. Phys*. 1996, **104**, 5429.
90 L.-T. Cheng, Y.-X. Yan and K. A. Nelson, *J. Chem. Phys*. 1989, **91**, 6052.
91 A. Pimenov, P. Lunkenheimer, et al. *Phys. Rev. E* 1996, **54**, 676.
92 E. A. Pavlatou, A. K. Rizos, G. N. Papatheodorou and G. Fytas, *J. Chem. Phys*. 1991, **94**, 224.
93 G. Li, W. M. Du, J. Hernandez and H. Z. Cummins, *Phys. Rev. E* 1993, **48**, 1192.
94 K.L. Ngai, *J. Phys. Chem. A* 2021, **125**, 13, 2759.
95 K.L. Ngai and G. Fytas, *Macromolecules* 2019, **52**, 8305.
96 G. P. Johari, A. Hallbrucker and E. Mayer, *J. Chem. Phys*.1991, **95**, 2955.
97 G. P. Johari, *J. Chem. Phys*. 2005, **122**, 144508.
98 K. Amann-Winkel, C. Gainaru,et al. *Proc. Natl. Acad. Sci. U. S. A*., 2013, **110**, 17720.
99 K. Amann-Winkel, R. Böhmer, C. Gainaru, et al., *Rev. Mod. Phys*., 2016, **88**, 011002.
100 L. J. Plaga, A. Raidt, V. Fuentes Landete, K. Amann-Winkel, et al., *J. Chem. Phys*. 2019, **150**, 244501.
101 K. Sasaki and Y. Suzuki, *J. Phys. Chem. Lett*. 2024, **15**, 11546.
102 M. Seidl, et al. *Phys. Rev. B,* 2011, **83**, 100201.
103 P.H. Handle, and T. Loerting, *Phys. Rev. B*, 2016, **93**, 064204.
104 P.H. Handle, M. Seidl and T. Loerting, *Phys. Rev. Lett*. 2012, **108**, 225901.
105 O. Mishima, *J. Chem. Phys.*2004, **121**, 3161.
106 M. S. Elsaesser, K. Winkel, E. Mayer and T. Loerting, *Phys.Chem.Chem.Phys*. 2010, **12**, 708.
107 K. L. Ngai. Y. Zhang, S. Capaccioli and Li-Min Wang, *J. Chem. Phys.*2026, **164**,044501.
108 M. Oguni, Y. Kanke and S. Namba, *AIP Conference Proceedings*, 2008, **982**, 34.
109 M. Oguni, S. Maruyama, K. Wakabayashi and A. Nagoe, *Chem. Asian. J*. 2007, **2**, 514.
110 S. Cerveny, *J. Phys. Chem. C,* 2010, **114**, 2604.
111 M. Sattig and M. Vogel, *J. Phys. Chem. Lett*., 2014, **5**, 174. 86.
112 K. L. Ngai, *Chemical Physics*, 2025, **595**, 112699.
113 K. L. Ngai, *Phys. Chem. Chem. Phys.*, 2024, **26**, 22083.
114 A. K. Murali, M. Paluch, et al. *J. Phys. Chem. Lett*., 2024, **15**, 3376.

Materials Advances Accepted Manuscript

View Article Online
DOI: 10.1039/D6MA00279J

Open Access Article. Published on 04 June 2026. Downloaded on 6/5/2026 12:04:33 AM.
This article is licensed under a Creative Commons Attribution 3.0 Unported Licence.

115 Z. Wojnarowska, S. Cheng, et al. *Nat. Commun*. 2022, **13,** 1342.
116 B. Yao, M. Paluch and Z. Wojnarowska, *Scientific Reports*, 2023, **13**, 3040.
117 B. Yao, M. Paluch, et al., *ACS Appl. Mater. Interfaces*, 2023, **15**, 39417.
118 Z. Wojnarowska, K. L. Ngai, and M. Paluch, *Phys Rev E* 2014, **90**, 062315.
119 K. L. Ngai, M. Paluch et al., *Phys. Chem. Chem. Phys*., 2017, **19**, 29905.
120 K. L. Ngai, M. Paluch, C. Rodriguez-Tinoco, *Phys. Chem. Chem. Phys.* 2018, **20**, 27342.
121 H. B. Yu, M. Tylinski, A. Guiseppi-Elie, et al., *Phys. Rev. Lett*., 2015, **115**, 185501.
122 C. Rodriguez-Tinoco, K. L. Ngai, et al. *Phys. Chem. Chem. Phys*., 2018, **20**, 21925.
123 X. Li, M. Wang, R. Liu, K. L. Ngai, Y. Tian, et al. *J. Chem. Phys*. 2015, **143**, 104505.
124 B. J. Kasting, M. S. Beasley, A. Guiseppi-Elie, et al. *J. Chem. Phys.* **2019,** *151*, 144502.
125 K. L. Ngai, *J. Phys. Chem. B* 2024, **128**, 10709.
126 K. L. Ngai, J. Habasaki, D. Prevosto, et al., *J. Chem. Phys*. 2012,**137**, 034511.
127 K.L. Ngai and M. Paluch, *J. Non-Cryst. Solids*, 2017, **478**, 1.
128 R. Casalini and C. M. Roland, 2013, **46**, 6364.
129 K. Kawai, T. Suzuki, M. Oguni, *Biophys. J*. 2006, **90**, 3732.
130 J. Bartoˇs, O. ˇSauˇsa, G.A. Schwartz, et al. *J. Chem. Phys*. 2011, **134**, 164507.
131 C. L. Wang, T. Hirade, F. H. J. Maurer, et al. *J. Chem. Phys*. 1998, **108**, 4654.
132 K. Kishimoto, H. Suga and S. Seki, S. *Bull. Chem. Soc. Jpn*. 1973, **46**, 3020.
133 T. Ichitsubo, E. Matsubara, et al., *Phys. Rev. Lett*, 2005, **95**, 245501.
134 J. Qiao, R. Casalini, J-M Pelletier and H. Kato, *J. Phys. Chem. B*, 2014, **118**, 3720.
135 K. L. Ngai, S. Capaccioli, D. Prevosto et al., *J. Phys. Chem. B*, 2015, **119**, 12502.
136 S. Capaccioli, K. L. Ngai and A. Paciaroni, *Chem. Phys*. 2025, **591**, 112543.
137 S. Capaccioli, K. L. Ngai, M. Shahin Thayyil, et al., *J. Phys. Chem. B*, 2015, **119**, 8800.
138 K. L. Ngai, S. Capaccioli, D. Prevosto, et al., *J. Phys. Chem. B*, 2015, **119**, 12519.
139 K. L. Ngai, M. Shahin Thayyil, and L.-M. Wang, *J. Mol. Liq*. 2017, **247**, 300.
140 U. Buchenau, and R. Zorn, *Europhys. Lett.,* 1992, **18**, 523.
141 U. Buchenau, R. Zorn and M.A. Ramos, *Phys. Rev. E*, 2014, **90**, 042312.
142 D. J. Plazek, *J. Non-Cryst. Solids,* 2007, **353**, 3783.
143 K. M. Bernatz, I. Echeverria, et al., *J. Non-Cryst. Solids*, 2002, **307–310**, 790.
144 M. Russina, F. Mezei, W. Miekeley, et al. *Physica B*, 1997, **234-236**, 421-423.
145 E. Weeks et al., *Science*, 2000, **287**, 627.
146 C. Donati, S.C. Glotzer, P.H. Poole, W. Kob, et al., *Phys. Rev. E*,1999, **60**. 3107.
147 K. L. Ngai, *J. Polym. Sci*. 2024, **62**, 174.
148 V. N. Novikov and A. Sokolov. *Nature (London*), 2004, **431**, 961.
149 V. N. Novikov, Y. Ding and A.P. Sokolov. *Phys. Rev. E*. 2005, **71**, 061501.
150 K. L. Ngai, L-M Wang, R. Liu, W.H. Wang. *J. Chem. Phys*. 2014, **140**, 044511.
151 K. L. Ngai, L-M Wang, R. Liu and W. H. Wang, *J. Molec. Liquids*, 2015, **205**, 37–41.
152 J. J. Lewandowski, W. H. Wang, and A. L. Greer, *Philos. Mag. Lett*. 2005, **85**, 77.
153 W. H. Wang, *Prog. Mater. Sci*. 2012, **57**, 487.
154 W. H. Wang, *Progr. Mater. Sci.* 2019, **106**,100561.
155 Z. Wang, K. L. Ngai and W. H. Wang, *J. Appl. Phys.* 2015, **118**, 034901.
156 T. Scopigno, G. Ruocco, F. Sette and G. Monaco. *Science*, 2003, **302**, 849.
157 U. Buchenau and A. Wischnewski. *Phys. Rev. B* 2004, **70**, 092201.
158 K. Niss and C. Alba-Simionesco. *Phys. Rev. B* 2006, **74**, 024205.
159 T. Scopigno, D. Cangialos and G. Ruocco, *Phys Rev B* 2004, **70**, 092201.
160 E. A. A. Pogna, C. Rodrıiguez-Tinoco, et al. *Sci. Rep*. 2013, **3**, 2518.

Materials Advances Accepted Manuscript

View Article Online
DOI: 10.1039/D6MA00279J

Open Access Article. Published on 04 June 2026. Downloaded on 6/5/2026 12:04:33 AM.
This article is licensed under a Creative Commons Attribution 3.0 Unported Licence.

161 S-X Peng, Y. Cheng, J. Pries, et al., *Sci. Adv.* 2020, **6**, eaay6726.
162 J. Pries, S. Wei, M. Wuttig and Pierre Lucas, *Adv. Mater.* 2019, **31**, 1900784.
163 A. N. Sreeram, A. K. Varshneya and D.R. Swiler, *J. Non-Cryst. Solids*, 1991, **128**, 294.
164 T. Rouxel. *J. Am. Ceram. Soc*. 2007, **90**, 3019.
165 Y. Gueguen, T. Rouxel, P. Gadaud, et al. *Phys. Rev. B*, 2011, **84**, 064201.
166 G.N. Greaves, A.L. Greer, R.S. Lakes, T. Rouxel. *Nat. Mater*. 2011, **10**, 823.
167 K. L. Ngai, *J. Polym. Sci*., 2024, **62**, 174.
168 K. L. Ngai, *Macromolecular Theory & Simulations*, 2024, **33**, 2400024.
169 K. L. Ngai, *J. Polym. Sci*., 2024, **62**, 2036.
170 K. L. Ngai, *Rubb. Chem. Tech*., 2024, **97**, 441.
171 K. L. Ngai, *Macromol. Theory Simul.* 2024, **33**, 2400021.
172 P. E. Rouse, *J. Chem. Phys.* 1953, **21**, 1272.
173 K. Hur, C. Jeong, R. G. Winkler, et al., *Macromolecules,* 2011**, 44**, 2311.
174 B. Kresse, M. Hofmann, A. F. Privalov, et al., *Macromolecules* 2015, **48**, 4491.
175 R. Meier, A. Herrmann, B. Kresse, et al., *ACS Macro Lett*. 2013, **2**, 96.
176 K.L. Ngai, et al., *Chem. Phys*., 2026, **602**, 113019.
177 K. Niss, C. Dalle-Ferrier, B. Frick, et al., *Phys. Rev. E*, 2010, **82**, 021508.
178 B. Frick and C. Alba-Simionesco, *Physica B*, 1999, **266**, 13.
179 S.A. Reinsberg, A. Heuer, et al., *J. Non-Cryst. Solids*, 2002, **307–310**, 208.
180 A. Schönhals, H. Goering, et al., *Colloid Polym. Sci*., 2004, **282**, 882.
181 A. Schönhals, H. Goering, Ch. Schick, et al., *Eur. Phys. J. E,* 2003,**12**,173.
182 A. Schönhals, H. Goering, et al., *J. Non-Cryst. Solids,* 2005, **351**, 2668.
183. S. H. Anastasiadis, K. Karatasos, et al., *Phys. Rev. Lett.*, 2000, **84**, 915.
184 K. L. Ngai, *Eur. Phys. J. E*, 2002, **8**, 225.
185 M. M. Elmahdy, K. Chrissopoulou, et al., *Macromolecules*, 2006, **39**, 5170.
186 K. L. Ngai*, J. Non-Cryst. Solids*, 2007, **353**, 4237.
187 D. Prevosto, S. Capaccioli and K. L. Ngai, *J. Chem. Phys*., 2014, **140**, 074903.
188 M. Uhl, J.K.H. Fischer, P. Sippel, et al., *J. Chem. Phys*., 2019, **150**, 024504.
189 G. N. Ruiz, et al., *Phys. Chem. Chem. Phys*., 2019, **21**, 15576.
190 K.L. Ngai, P. Lunkenheimer and A. Loidl, *Phys. Chem. Chem. Phys*., 2020, **22**, 507.
191 K.L. Ngai, Z. Wojnarowska, et al., *Phys. Chem. Chem. Phys*., 2020, **22**, 9257.
192 K.L. Ngai, P. Lunkenheimer, C. Leon, et al*., J. Chem. Phys*. 2001, **115**,1405.
193 T Pabst et al. *J. Phys. Chem. Lett*., 2021,**12**, 3685.
194 T. Böhmer et al. *J. Chem. Phys*., 2025, **162**, 120902.
195 U. Schneider, R. Brand, P. Lunkenheimer and A. Loidl, *Phys. Rev. Lett*. 2000, **84**, 5560.
196 K. L. Ngai, Z. Wojnarowska and M. Paluch, *Sci. Rep*., 2021, **11**, 22142.
197 K. Moch, P. Munzner, R. Böhmer, et al., *Phys. Rev. Lett*., 2022, **128**, 228001.
198 K. Moch, P. Munzner, C. Gainaru, et al., *J. Chem. Phys*., 2022, **157**, 231101.
199 R. Richert, *J. Chem. Phys*., 2022, **57**, 224501.
200 S. Arrese-Igor, *J. Chem. Phys.,* 2025, **162**, 114509.
201 J.C. Dyre and M.D. Ediger, Nature Rev. Phys., https://doi.org/10.1038/s42254-026-00940-x
202 E. A. Rössler, M. Becher, *J. Chem. Phys*., 2025, **163**, 054510.
203 L. Zhu, C. W. Brian, S. F. Swallen, et al., *Phys. Rev. Lett.,* 2011, **106**, 256103.
204 W. Zhang, C. W. Brian, L. Yu, *J. Phys. Chem. B*, 2015, **119**, 5071.
205 C.W. Brian and L. Yu, *J. Phys. Chem. A,* 2013, **117**, 13303.
206 C. Leon and K. L. Ngai, *J. Phys. Chem. B,* 1999, **103**, 4045–51.

Materials Advances Accepted Manuscript

View Article Online
DOI: 10.1039/D6MA00279J

Open Access Article. Published on 04 June 2026. Downloaded on 6/5/2026 12:04:33 AM.
This article is licensed under a Creative Commons Attribution 3.0 Unported Licence.

207 W. Steffen, A. Patkowski, et al. *Phys. Rev. E* 1994, **49**, 2992.
208 S. Capaccioli, K. L. Ngai, M. Paluch and D. Prevosto, *Phys. Rev. E* 2012**, 86**, 051503.
209 C. R. Cao, Y. M. Lu, H. Y. Bai and W. H. Wang, *Appl. Phys. Lett*., 2015, **107**, 141606.
210 K. L. Ngai, S. Capaccioli, C.R. Cao, et al., *J. Non-Cryst Solids*, 2017, **463**, 85.
211 J. Qiao, J.-M. Pelletier, R. Casalini, *J. Phys. Chem. B* 2013, **117**, 13658.
212 H. B. Yu, K. Samwer, Y. Wu and W. H. Wang, *Phys. Rev. Lett*. 2012, **109**, 095508.
213 A. Mandanici, W. Huang, M. Cutroni and R. Richert, *J. Chem. Phys.* 2008, **128**, 124505.
214 A. Mandanici, W. Huang, M. Cutroni and R. Richert, *Philos. Mag.* 2008, **88**, 3961.
215 A. Mandanici and M. Cutroni, *Mater. Sci. Eng. A* 2009, **521−522**, 279.
216 K. L. Ngai and S. Capaccioli, *J. Non-Cryst. Solids X* 2021, **11−12**, No. 100070.
217 S. L. L. M. Ramos, M. Ogino and M. Oguni, *J. Mol. Liq.* 2020, **311**, No. 113359.
218 M. Tylinski, M. S. Beasley, Y. Z. Chua, C. Schick M. D. Ediger, *J. Chem. Phys.* 2017, **146**, 203317.
219 Y. Zhang, R. Potter, W. Zhang and Z. Fakhraai, *Soft Matter,* 2016, **12**, 9115.
220 Y. Zhang and Z. Fakhraai, *Phys. Rev. Lett*. 2017, **118**, 066101.
221 Y. Zhang and Z. Fakhraai, *PNAS*, 2017,**114**, 4915.
222 I. Kosacki, C. M. Rouleau, P. F. Becher, et al., *Solid State Ion*., 2005, **176**,1319.
223 K. L. Ngai, J. Santamaria and C. Leon, *Eur. Phys. J. B,* 2013, **86**, 7.
224 C. León, J. Habasaki, and K. L. Ngai, *Z. Phys. Chem*. 2009, **223**, 1311.
225 K. L. Ngai and D.J. Plazek, *J. Rubber Chem.Technol. Rubber Rev*., 1995, **68**, 376.
226 K. L. Ngai, D. J. Plazek and R.W. Rendell, *Rheol. Acta*, 1997, **36**, 307.
227 K. L. Ngai and D. J. Plazek, *Macromolecules*, 2014, **47**, 8056.
228 D. J. Plazek, C. A. Bero, et al., *Colloid Polym. Sci*., 1994, **272**, 1430.
229 D. J. Plazek, I. C. Chay, K. L. Ngai and C. M. Roland, *Macromolecules,* 1995, **8**, 6432.
230 K. L. Ngai, D. J. Plazek and A. K. Rizos, *J. Polym. Sci. B,*1997, **35**, 599.
231 G. Floudas and T. Reisinger, *J. Chem. Phys*., 1999, **111**, 5201.
232 G. Floudas, C. Gravalides, T. Reisinger, et al., *J. Chem. Phys*. 1999, **111**, 9847.
233 G. Floudas, M. Paluch, A. Grzybowski and K.L. Ngai, *Molecular Dynamics of Glass-Forming Systems: Effects of Pressure*; Springer: Berlin, 2011.
234 S. Zimny, M. Tarnacka, E. Kamińska, et al., *Macromolecules*, 2022, **55**, 5581.
235 A.Talik, M. Tarnacka, A. Dzienia, et al., *Macromolecules*, 2019, **52**, 5658.
236 X. Wu, C. Liu, Z. Zhu, K. L. Ngai, et al., *Macromolecules* 2011, **44**, 3605.
237 K. Adachi and H. Hirano, *Macromolecules,* 1998, **31***,* 3958.
238 D. J. Plazek, *J. Phys. Chem.,*1965, **69**, 3480.
239 D. J. Plazek, *J. Polym. Sci., Part A-2*,1968, **6**, 621.
240 D. J. Plazek, *Polym. J.,*1980, **12**, 43.
241 D. J. Plazek, J. *Polym. Sci. Polym. Phys. Ed.,*1982, **20**, 729.
242 D, J. Plazek, *J. Rheol.,*1996, **40**, 987.
243 K. L. Ngai and D.J. Plazek, *J. Polym. Sci., Polym. Phys. Ed.,* 1986, **24**, 619.
244 K. L. Ngai, R. Rendell and D. Plazek, *J. de Physique IV Proc*.,1996, **06**, C8-555.
245 K. L. Ngai and D.J. Plazek, *J. Polym. Sci., Polym. Phys. Ed.* 1985, **23**, 2159.
246 C. G. Robertson and L. I. Palade, *J. Non-Cryst. Solids*, 2006, **352**, 342.
247 C.G. Robertson and C.M. Rademacher, *Macromolecule*s, 2004, **37**, 10009.
248 L.I. Palade, V. Verney and P. Attane´, *Macromolecules*, 1995, **28**, 7051.
249 C. A. Bero and C. M. Roland, *Macromolecules,* 1996**, 29***,* 1562.
250 G. Fytas and K. L. Ngai, *Macromolecules*, 1988, **21**, 804.

Materials Advances Accepted Manuscript

View Article Online
DOI: 10.1039/D6MA00279J

Open Access Article. Published on 04 June 2026. Downloaded on 6/5/2026 12:04:33 AM.
This article is licensed under a Creative Commons Attribution 3.0 Unported Licence.

251 K. L. Ngai and G. Fytas, *J. Polym. Sci. Polym. Phys. Ed*.,1986, **24**,1683.
252 P. G. Santangelo, K. L. Ngai and C. M. Roland, *Polymer*, 1998, **39**, 681.
253 R. H. Colby, L.J. Fetters, W. G. Funk et al., *Macromolecules,* 1991, **24**, 3873.
254 R. H. Colby, L.J. Fetters and W. W. Graessley, *Macromolecules,* 1987, **20**, 2226.
255 V. R. Raju, Ph.D. thesis, Northwestern University, Evanston, IL, 1980.
256 V. R. Raju, E. V. Menezes, G. Marin, et al. *Macromolecules*, 1981, **14**, 1668.
257 K.L. Ngai, Y. Zhang, Li-Min Wang, *Macromolecules* 2025, **58**, 14, 7178–7186
258 P. Lunkenheimer and A. Loidl, *Macromolecules* 2025, **58**, 3547−3553.
259 C. H. Porter and R. H. Boyd, *Macromolecules* 1971, **4**, 589.
260 T. P. Yin, S. E. Lovell and J. D. Ferry. *J. Phys. Chem.* 1961, **65**, 534.
261 R. H. Colby, *Polymer* 1989, **30**, 1275.
262 J. A. Zawada, C. M. Ylitalo, G. G. Fuller, et al. *Macromolecules* 1992, **25**, 2896.V. Garcia
263 Sakai, J. K. Maranas, I. Peral and J.R.D. Copley, *Macromolecules,* 2008, **41**, 3701.
264 K. Niedzwiedz, A. Wischnewski, et al. *Macromolecules* 2008, **41**, 4866.
265 M. Doi and S. F. Edwards, *The Theory of Polymer Dynamics*, Clarendon Press, Clarendon, Oxford, 1986.
266 T. P. Lodge, N. A. Rotstein and S. Prager, *Adv. Chem. Phys.* 1990, **74**, 1.
267 M. Kruteva, J. Allgaier, M. Monkenbusch, I. Hoffmann and D. Richter, *J. Rheol.* 2021, **65**, 713.
268 K. L. Ngai, *Macromol. Theory Simul.* 2024, **33**, 2400024,
269 G. B. McKenna, K. L. Ngai and D. J. Plazek, *Polymer* 1985, **26**, 1651.
270 K. L. Ngai, *J. Polym. Sci*. 2024, **62**, 2036.
271 M. Zamponi, et al. *J. Phys. Chem. B* 2008, **112**, 16220.
272 M. Kruteva et al. *Macromolecules* 2021**, 54**, 11384.
273 S. Pawlus, A.P. Sokolov, M. Paluch, et al., *Macromolecules*, 2010, **43**, 5845.
274 C. M. Roland, R. Casalini, et al., *J. Polym. Sci. Polym. Phys. Ed* 2004, **42**, 4313.
275 K. L. Ngai, R. Casalini, et al., *J. Phys. Chem. B,* 2005, **109**, 17356.
276 K. L. Ngai, R. Casalini and C. M. Roland, *Macromolecules,* 2005, **38**, 4363.
277 R. Casalini and C. M. Roland, *Macromolecules*, 2005, **38**, 1779.
278 K. Adachi, H. Yoshida, F. Fukui and T. Kotaka, *Macromolecules*, 1990, **23**, 3138.
279 K. Adachi and T. Kotaka, *Prog. Polym. Sci.*,1993, **18**, 585.
280 D. Boese and F. Kremer, *Macromolecules,* 1990, **23**, 829.
281 Y. Matsumiya, H. Watanabe and K. Osaki, *Macromolecules,* 2000, **33***,* 499.
282 H. Watanabe, Y. Matsumiya, K. Osaki, et al., *Macromolecules* 1998, **31***,* 7538.
283 D. L. Plazek and D. J. Plazek, *Macromolecules,* 1983*,* **16***,* 1469.
284 A. K. Rizos, T. Jian and K. L. Ngai, *Macromolecules,* 1995, **28**, 517.
285 D. J, Plazek, X. D. Zheng and K. L. Ngai, *Macromolecules,* 1992, **25**, 4920.
286 K. L. Ngai. R. W. Rendell, The Symmetric and Fully Distributed Solution to a Generalized Dining Philosophers Problem. In *Relaxation in Complex Systems and Related Topics*; Campbell, I. A.; Giovannella, C., Eds.; *Plenum Press*: New York, 1990; pp 309−316.
287 G. Kolata, Science, 1984, **223**, 917.
288 K. Schmidt-Rohr and H. W. Spiess, *Phys. Rev. Lett*. 1991, **66**, 3020.
289 H. Sillescu, *J. Chem. Phys*. 1996, **104**, 4877.
290 R. Böhmer, G. Hinze, G. Diezemann, B. Geil, H. Sillescu, *Europhys. Lett*. 1996, **36**, 55.
291 M. D. Ediger, *Annu. Rev. Phys. Chem*. 2000, **51**, 99.
292 K. L. Ngai, *J. Phys. Chem. B* 1999, **103**, 10684.

Materials Advances Accepted Manuscript

View Article Online
DOI: 10.1039/D6MA00279J

293 S. F. Swallen and M. D. Ediger, *Soft Matter* 2011, **7**, 10339.
294 S. F. Swallen, P. A. Bonvallet, et al. *Phys. Rev. Lett.* 2003, **90**, No. 015901.
295 M. K. Mapes, S. F. Swallen and M. D. Ediger. *J. Phys. Chem. B* 2006, **110**, 507.
296 R. Richert, K. Duvvuri and L. J. Duong, *J. Chem. Phys.* 2003, **118**, 1828.
297 X. R. Zhu and C. H. Wang, *J. Chem. Phys.* 1986, **84**, 6086.
298 K. Zemke, K. Schmidt-Rohr, J. H. Magill, et al., *Mol. Phys.* 1993, **80**, 1317.
299 R. Richert, *J. Chem. Phys.* 2005, **123**, 154502.
300 J. R. Rajian, W. Huang, R. Richert and E. L. Quitevis, *J. Chem. Phys.*2006, **124,** No.014510.
301 M. D. Ediger and P. Harrowell, *J. Chem. Phys.* 2012, **137**, No. 080901.
302 K. L. Ngai, *Philos. Mag.* 2007, **87**, 357.
303 D. Chakrabarti and B. Bagchi, *Phys. Rev. Lett.* 2006, **96**, No. 187801.
304 M. D. Ediger and P. Harrowell. *J. Chem. Phys*. 2012, **137**, 080901.
305 K. L. Ngai, S. Pawlus and M. Paluch, *Chem. Phys*.2020. **530**, 110617
306 R. Böhmer, C. Gainaru, and R. Richert, *Phys. Rep.* 2014, **545**, 125.
307 Y. Chen, W. Zhang and L. Yu, *Phys. Chem. B* 2016, 120, **32**, 8007.
308 J. Gabriel et al. *Phys. Rev. Lett*. 2018, **121**, 035501.
309 J. Gabriel et al. *J. Phys. Chem. B* 2017, **121**, 8847−8853.
310 S. Hensel-Bielówka, M. Paluch and K. L. Ngai, *J. Chem. Phys*. 2005, **123**, 014502.
311 T. Böhmer, J. P. Gabriel, R. Zeißler R, et al. *Phys. Chem. Chem. Phys*. 2022, **24**,18272
312 In C. Schick and V. Mathot editors. Fast scanning calorimetry. Springer International Publishing Switzerland; 2016. and references therein.
313 R. Casalini, M. Paluch and C. M. Roland, *J. Thermal Anal. Calorim.*2002, **69**, 947.
314 A. Rizos, G. Fytas, T. P. Lodge and K. L. Ngai, *J. Chem. Phys.* 1991, **95**, 2980.
315 C. P. Lindsey, G. D. Patterson and J. R. Stevens, *J. Polym. Sci.:Polym. Phys. Ed*. 1979, **17,**1547.
316 G. Fytas, C. H. Wang, G. Meier and E. W. Fischer, *Macromolecules*, 1985, **18**, 1492.
317 G. Fytas, A. Patkowski, G. Meier and Th. Dorfmüller, *Macromolecules* 1982, **15**, 870.
318 G. Fytas, A. Patkowski, G. Meier and Th. Dorfmüller *J. Chem. Phys*. 1984, **80**, 2214.
319 G. Fytas and K. L. Ngai, *Macromolecules*, 1988, **21**, 804.
320 D. Boese, *et al. Macromolecules* 1989, **22**, 4416.
321 A. Rizos, T. Jian and K. L. Ngai, *Macromolecules* 1995,**28**, 517.
322 G. Fytas, *Macromolecules* 1989, **22,** 211.
323 J. C. Dyre, *J. Phys.: Condens. Matter* 2007, **19**, 20510.
324 G. Williams and D. C. Watts, In NMR Basic Principles and Progress; Diehl, P., Fluck, E., Kosfeld, R., Eds.; Springer-Verlag: Berlin, 1971, **4**, 271.326
325 G. Williams, D. C. Watts, S. B. Dev and A. M. North. *Transactions of The Faraday Society*, 1971, **67**, 1323
326 M. Paluch, C. M. Roland and S. Pawlus. *J. Chem. Phys*. 2002, **116**, 10932.
327 R, W. Rendell, K. L. Ngai and S. Mashimo. *J. Chern. Phys*. 1987, **87**, 2359.

Open Access Article. Published on 04 June 2026. Downloaded on 6/5/2026 12:04:33 AM.
This article is licensed under a Creative Commons Attribution 3.0 Unported Licence.

Materials Advances Accepted Manuscript

View Article Online
DOI: 10.1039/D6MA00279J

Data availability

All the relevant data have been presented in the manuscript.

Open Access Article. Published on 04 June 2026. Downloaded on 6/5/2026 12:04:33 AM.
This article is licensed under a Creative Commons Attribution 3.0 Unported Licence.

Materials Advances Accepted Manuscript